Characterizing Dual-wettability Pore Network of Unconventional Rocks by Analyzing Water and Oil Imbibition Data

by

Yue Shi

A thesis submitted in partial fulfillment of the requirements for the degree of

Master of Science

in

Petroleum Engineering

Department of Civil & Environmental Engineering
University of Alberta

Abstract

Recent studies show that the pore network of unconventional rocks generally consists of inorganic and organic parts. The organic part has high wetting affinity towards the oleic phase but low wetting affinity towards the aqueous phase. In contrast, the inorganic part has high wetting affinity towards both oleic and aqueous phases. Separate characterization of the organic and inorganic pore networks is of great importance to understand the fluid storage and transport mechanisms, and to develop more accurate models for fluid flow in porous media. However, the traditional methods such as mercury injection capillary pressure (MICP) and CO_2/N_2 isotherm adsorption tests fail to characterize the dual-wettability pore network. As mercury is the non-wetting phase towards all the pores and CO_2 (or N_2) is the wetting phase towards all the pores, these techniques can only evaluate the total PSD (PSD_{tot}).

The objective of this study is to compute the oil-wet and water-wet pore size distributions (PSDs) of the unconventional rocks by analyzing the comparative oil and brine imbibition data. To achieve this objective, a modified analytical fractal model for co-current spontaneous imbibition is developed. In previous studies, spontaneous imbibition of wetting phase is considered as a piston-like displacement phenomenon which leads to similar rates of imbibition in pores with different diameters. However, imbibition rate of wetting phase is positively proportional to the square root of pore diameter based on Lucas-Washburn equation. Therefore, we extend the previous fractal models by assuming non-piston-like imbibition in pores with different diameters. In the proposed model, first the larger pores are filled by wetting phase, followed by smaller pores. Considering non-piston-like liquid imbibition, we use available imbibition data and propose a novel Imbibition Transient Analysis (ITA) to calculate PSD. We use the history matching technique to match the

experimental imbibition data with the proposed fractal model, and obtain the unknown parameters, such as fractal dimension (D_f) and minimum pore diameter (D_{min}), controlling imbibition profile. The determined parameters are then used to calculate PSD. The PSD of oil-wet pores (PSD_{oil}) is calculated by oil imbibition data and PSD of water-wet pores (PSD_{water}) is calculated by brine imbibition data. The PSD of water-repellant pores (PSD_{org}) is calculated by decoupling of PSD_{oil} and PSD_{water}.

On the basis of proposed non-piston-like fractal model, the minimum pore diameter (D_{min}) controls the equilibrated time in the spontaneous imbibition process. The calculated D_{min} from oil imbibition data is smaller than that from brine imbibition data, proving the assumptions about imbibition of oil in small organic pores that are not accessible for brine imbibition. Comparing PSD_{water} and $PSD_{water\text{-}repellant}$ shows that water-repellant pores are generally smaller than water-wet pores. This is in agreement with the results of scanning electron microscopy (SEM) and energy-dispersive x-ray spectroscopy (EDS) analyses that demonstrate the abundant number of nanopores within the organic matter with low wetting affinity towards water. Moreover, compared with the results of MICP test, PSD calculated by oil imbibition data can detect very small pores (< 3 nm) which are not accessible by mercury, especially for low-permeability rock samples. Thus, the proposed method in this study can complement the conventional MICP technique for a more comprehensive characterization of the pore network of unconventional tight rocks.

Preface

This thesis is original work by Yue Shi. Some parts of this research in chapter 1, 2 and 3 of this thesis have been published or presented as:

- Shi, Y., Yassin, M. R., & Dehghanpour, H. (2017). A Modified Model for Spontaneous Imbibition of Wetting Phase into Fractal Porous Media. Colloids and Surfaces A: Physicochemical and Engineering Aspects.

Dedication

This dissertation is dedicated to my dearest family, Mrs. Hongchun Fan, Mr. Wenli Shi and Miss. Yuwei Fan.

Acknowledgements

I wish to express my sincere appreciation from the bottom of my heart to my supervisor, Dr. Hassan Dehghanpour for his kind support, patient encouragement and insightful guidance throughout this study. This research would not have been possible without his help. I really enjoyed the years of studies and research under his supervision. His teachings and guidance will be with me through my whole career.

I would also like to thank Dr. Japan Trivedi and Dr. Alireza Nouri for being the member of examination committee of my MSc defense.

I would like to express my sincere gratitude to Mahmood Reza Yassin who gave me a lot of help and valuable suggestions. This dissertation could not have been completed without his help.

I would also like to thank my colleague and seniors, Mingxiang Xu, Yanmin Xu, Ali Habibi, Michael Tang and Yingkun Fu for their valuable assistance for my research.

I would acknowledge the Natural Sciences and Engineering Research Council of Canada (NSERC) and Nexen Energy ULC for providing the research funding for this study.

Finally, I would like to express my gratitude to my family and my girlfriend Yujia Guo for their endless understanding, support, encouragement and love during the past and future tough or easy times.

Table of Contents

List of Tables

List of Figures

Nomenclature

A_f Cross-sectional area of rock sample, L^2

A_o Effective pore area open to oil imbibition, L^2

A_P Total pore area in the cross section of rock sample, L^2

A_{Pu} Cross-sectional area of unit cell, L^2

A_w Effective pore area open to brine imbibition, L^2

D Pore diameter, L

D^* Threshold diameter, L

D_C Critical diameter, L

D_f Pore fractal dimension

D_{max} Maximum pore diameter, L

D_{min} Minimum pore diameter, L

D_s Mean diameter of particles, L

$f(D)$ Fractional number of pores

$F(D)$ Normalized pore volume

g Gravitational acceleration, Lt^{-2}

H Height of the rock sample, L

H^{eq} Equilibrated height of the liquid column inside a specific capillary, L

K Absolute permeability, L^2

L_f Tortuous length of liquid column, L

L_s Straight length of liquid column, L

m Imbibed mass in a single capillary at time t, M

m_i Imbibed mass in a single capillary at i^{th} time step, M

m^{eq} Equilibrated imbibed mass in a single capillary, M

M Imbibed mass in the capillaries with the diameter of D at time t, M

M_i Imbibed mass in the capillaries with the diameter of D at i^{th} time step, M

M_T Total imbibed mass in a bundle of capillaries, M

M_e^* Effective mobility of the wetting and non-wetting phase

M^{eq} Equilibrated imbibed mass in the capillaries with the diameter of D, M

n Incremental number of pores

N Cumulative number of pores in a unit cell

N_{exp} The number of experimental data point

N_f Cumulative number of pores in the cross section of rock sample

OF Objective function

S_{nwr} Residual saturation of the non-wetting phase

S_{wi} Initial water saturation

t Time, t

t_{eq} Equilibrated time, t

V_B Bulk volume of the rock sample, L^3

V_o Equilibrium imbibed volume of oil, L^3

V_T Total accessible pore volume, L^3

V_w Equilibrium imbibed volume of brine, L^3

ϕ Porosity

ϕ' Surface porosity

ϕ_a Wetting porosity

ϕ_a' Wetting surface porosity

ϕ_{ao} Wetting porosity for oil imbibition

ϕ'_{ao} Wetting surface porosity for oil imbibition

ϕ_{aw} Wetting porosity for brine imbibition

ϕ'_{aw} Wetting surface porosity for brine imbibition

θ Contact angle

μ Viscosity, $ML^{-1}t^{-1}$

ρ Density, ML^{-3}

σ Surface tension, Mt^{-2}

τ Average tortuosity of porous media

Abbreviations

BET	Brunauer, Emmett and Teller
EDS	Energy-Dispersive x-ray Spectroscopy
EMA	Effective Medium Approximation
GA	Genetic Algorithm
H-P	Hagen-Poiseuille
ITA	Imbibition Transient Analysis
LMT	Lower Montney
L-W	Lucas-Washburn
MICP	Mercury Injection Capillary Pressure
NGL	Natural Gas Liquid
NMR	Nuclear Magnetic Resonance
PSD	Pore Size Distribution
PSD_{oil}	Oil-wet Pore Size Distributions
PSD_{water}	Water-wet Pore Size Distributions
$PSD_{water\text{-}repellant}$	Water-repellant Pore Size Distribution
PSD_{MICP}	PSD obtained from MICP test
PSD_{tot}	Total Pore Size Distributions
PV	Pore Volume
PV_{oil}	Pore Volume of Oil-wet Pores
PV_{water}	Pore Volume of Water-wet Pores
$PV_{water\text{-}repellant}$	Pore Volume of Water-repellant Pores
SEM	Scanning Electron Microscope

TOC	Total Organic Carbon
TRA	Tight Rock Analysis
UMT	Upper Montney
WI_o	Wettability Index
Y-L	Young-Laplace

Chapter 1: Introduction

1.1. Backgrounds and Problem Statements

Unconventional resources, such as tight gas reservoirs, have received considerable attention in recent years with increasing demand for fossil fuels (Khlaifat et al. 2011; Cui et al. 2013). These resources are known for low porosity and ultra-low permeability (in the order of nanodarcy), which makes it challenging to produce oil and natural gas on a commercial scale. Thus, special completion and stimulation techniques such as hydraulic fracturing are required to enhance oil recovery from the unconventional reservoirs.

Hydraulic fracturing is one of the most successful completion techniques for increasing the hydrocarbon production from the unconventional reservoirs (Gidley 1989; Vengosh et al. 2014). Fractures networks are induced by pumping large quantities of fluids at high pressure into the formation. Consequently, an extensive surface area of the reservoir is exposed to the fracturing fluids after the fracturing operation. Moreover, special solvents, such as surfactant, can be added into the fracturing fluid to enhance oil recover from the unconventional resources (Hirasaki and Zhang 2004; Yarveicy and Haghtalab 2017). Understanding and modeling the fluid-rock interactions is of great importance to optimize the formulation of the fracturing fluid. These interactions may be associated with spontaneous imbibition, water adsorption and clay swelling (Dehghanpour et al. 2012).

Spontaneous imbibition of the wetting phase into the fractured tight reservoirs has received great attention due to the immense capillary pressure in the tight rocks. Imbibition is an immiscible displacement process, whereby the wetting fluid spontaneously imbibe into the porous media driven by capillary pressure and expel the non-wetting fluid (Schembre et al. 1998). This process is considered as a mechanism for fracturing fluid loss and possible formation damage. On the other hand, the imbibed fracturing fluid can displace the oil and enhance oil recovery. Extensive modeling and experimental studies have been carried out to understand the fluid-rock interactions as well as to characterize the properties of unconventional rocks.

Several analytical models have been proposed for relating the spontaneous imbibition process to capillary and hydrostatic pressures as well as other geometrical parameters. One of the pioneer models to analyze the spontaneous imbibition was proposed by Bell and Cameron (1906), who found a square root dependency of time for imbibed mass (or volume) of wetting liquid. On the basis of this work, Lucas (1918) and Washburn (1921) established most well-known solution, which describes the imbibition height and mass versus time follow the relation of square root of time in a cylindrical capillary as well as in porous media. To account for the complex pore structure of the porous media, Li and Zhao (2012) applied fractal theory for modeling spontaneous imbibition. Cai et al. (2012, 2014) furthered the fractal modeling study by considering hydrostatic pressure as well as different shapes of the pores.

The existing models simply assume the imbibition process in porous media as a piston-like displacement. However, non-piston-like imbibition process, which means the imbibition front is not uniform, has been experimentally visualized in the previous studies (Schembre et al. 1998, Gruener et al. 2012). By using an X-ray CT scanner, Schembre et al. (1998) showed the spontaneous imbibition of water into the Berea sandstone does not follow the piston-like displacement manner. Gruener et al. (2016) recorded spontaneous imbibition of n-alkanes into silica glass by using combined gravimetrical, optical, and neutron radiography measurements. The results also showed that the imbibition front is not piston-like. Thus, simply assuming piston-like imbibition may cause the erroneous modeling of spontaneous imbibition.

Beyond the modeling studies, laboratory experiments on spontaneous imbibition have also been carried out especially on unconventional rocks (Amott 1959; Chilingar and Yen 1983; Zhang and Austad 2006; Zhang et al. 2006; Odusina et al. 2011; Alotaibi et al. 2011; Dehghanpour et al. 2013; Dehghanpour et al. 2015; Yassin et al. 2017). Spontaneous imbibition together with nuclear magnetic resonance (NMR), and sessile drop are utilized to evaluate the wettability of unconventional rocks such as shales and tight sandstone (Dehghanpour et al. 2013; Lan et al. 2015; Yassin et al. 2016). Lan et al. (2015) conducted a series of comparative oil and brine spontaneous imbibition tests on the rock samples from a well drilled in the Montney tight-gas Formation. The results shows a significant higher oil uptake compared with brine, which indicates the strong affinity of the Montney rocks towards oil. Furthermore, Yassin et al. (2016) continued the

wettability study on Montney rocks by reviewing the results of SEM analysis, Mercury Injection Capillary Pressure (MICP) test, organic petrography, and tight rock analysis (TRA). On the basis of these analysis, the authors proposed the dual-wettability theory: the pore network of the Montey rocks generally consists of smaller hydrophobic organic pores and relatively larger hydrophilic inorganic pores.

Separate characterization of the water-wet and water-repellant pore networks is of great importance to understand the fluid storage and transport mechanisms and to develop more accurate models for fluid flow in porous media (Yassin et al. 2016; Zolfaghari et al. 2017). However, the traditional pore size distribution (PSD) methods such as MICP and N_2 (or CO_2) adsorption failed to characterize the dual-wettability pore network. Because mercury is non-wet towards all the pores and CO_2 (or N_2) is wet towards all the pores, these methods can only give the total PSD. Therefore, a new technique which allows the separate characterization of the dual-wettability pore network is demanded.

1.2. Objectives of Research

The specific objectives of this research are as follows:

(1) Develop a new fractal model for co-current spontaneous imbibition with considering non-piston-like displacement.

(2) Investigate the parameters controlling the imbibition process with the proposed fractal model.

(3) Analyze the comparative oil and brine imbibition data and explain the dual-wettability behavior of Montney rocks by using the proposed fractal model.

(4) Calculate pore size distribution (PSD) of water-wet and water-repellant pores based on the analysis of comparative oil and brine imbibition data.

1.3. Structure of Thesis

This thesis consists of five chapters.

Chapter 1 presents a brief overview of the research background and introduces the research gap and objectives of this study.

Chapter 2 provides a brief introduction to Montney tight-gas Formation as well as the literature review on fractal modeling of spontaneous imbibition and dual-wettability behavior. The pore size distribution techniques are also summarized.

Chapter 3 presents the proposed fractal model for co-current spontaneous imbibition of wetting phase into the porous media. We introduce the basic theory and assumptions for modelling and detailed derivation of the analytical and semi-analytical equations. We also introduce the computational procedure for application of the semi-analytical equation as well as the procedure for determining the unknown parameters. In the end, we compare the results of the proposed model with those of the previous model and conduct sensitivity analysis for investigating the effect of hydrostatic pressure, minimum pore diameter, and fractal dimension on the model outputs.

Chapter 4 presents the characterization of dual-wettability pore network based on the analysis of the comparative oil and brine imbibition data. We introduce the Imbibition Transient Analysis (ITA) method for calculating the pore size distribution (PSD) of water-wet and water-repellant pores by utilizing the proposed fractal model.

Chapter 5 summarizes the important findings and results of this research and provides recommendations for future studies.

Chapter 2: Literature Review

2.1 Overview of Montney Tight Gas Formation

The Montney Formation is located in the northeast of British Columbia, as shown in Fig. 2.1, south of Fort Nelson and spread into north Alberta past Grande Prairie (Nieto et al. 2009). It covers a large geographic area of approximately 130,000 km^2 with a typical thickness between 100 to 300 m (NEB et al. 2013). Montney sand is a Triassic-age siliclastic reservoir.

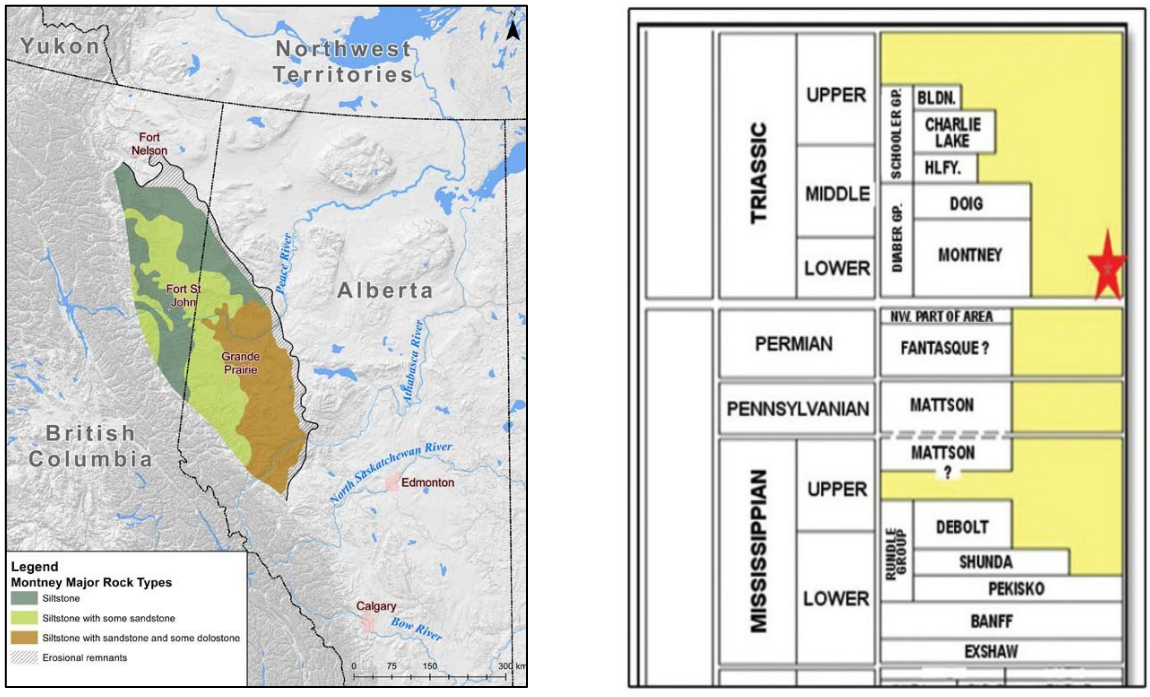

Fig 2.1: Location and depositional stratigraphy of Montney Formation. (Nieto et al. 2009; NEB et al. 2013)

Montney Formation represents a complex geological sequence. It has large deposits of gas shale and siltstone with poor permeability contain vast quantities of gas along the western edge (Fort St. John), tight gas and gas shale play in the center (Dawson Creek and Pouce Coupe areas), and the conventional gas (or oil) along the coarser eastern edge (Western Alberta Valleyview area) (Keneti and Wong 2011). Generally, Montney Formation is considered as a siltstone reservoir which composed of siltstone and dark grey shale. It has been classified into Upper Montney and

Lower Montney based on depth and different compositions. The Upper Montney contains light brown siltstone interlaminated with fine grained sandstone. The Lower Montney is characterized as dark grey, dolomitic siltstone with interbedded shales (Davies 1997).

The recent advance in horizontal drilling and multi-stage hydraulic fracturing have revolutionized the development of unconventional resources in Montney Formation. These techniques have enabled the economic production from low-porosity and low-permeability reservoirs in Montney Formation that were formerly uneconomic to produce with vertical wells (Johnson and Johnson 2012). Montney Formation's potential for marketable unconventional natural gas, natural gas liquid (NGL) and oil are estimated at 12,719 billion m^3 (449 Tcf), 2,308 million m^3 (14,521 million barrels) and 179 million m^3 (1,125 million barrels), respectively (NEB et al., 2013). The marketable unconventional petroleum estimate makes it one of the largest known gas resources in the world (NEB et al. 2013).

2.2 Modeling of Spontaneous Imbibition

In this section, we briefly review the Lucas-Washburn (L-W) equation (Lucas 1918; Washburn 1921) and its modification. Then we introduce the fractal theory and review the existing fractal models for spontaneous imbibition.

2.2.1 Lucas-Washburn (L-W) Equation and Its Modification

Combining the Laplace relation with Poiseuille's equation of laminar flow, Lucas (1918) and Washburn (1921) established the most well-known Lucas-Washburn (L-W) equation that the imbibition height and mass versus the time follow the relation of square root of time in cylindrical capillary and in porous media:

$$L_S = \sqrt{\frac{D\sigma cos\,\theta}{4\mu}}\, t^{\frac{1}{2}} \tag{2.1}$$

where L_S is the straight length of the liquid column; D is pore diameter; σ is surface or interfacial tension; θ is contact angle; μ is viscosity of wetting liquid and t is time.

Handy (1960) further correlated the imbibition rate (q) to the water saturation (S_w) based on the piston-like imbibition assumption

$$q = \sqrt{\frac{2A_f^2 P_C K \phi S_w t}{\mu}} \tag{2.2}$$

where A_f is the cross-sectional area of rock sample; P_C is the capillary pressure; K is permeability and ϕ is the porosity.

By considering the effect of tortuosity on the spontaneous imbibition, Lundblad and Bergman (1997) argued that the capillary radius should be replaced by effective radius r_e

$$L_S = \sqrt{\frac{r_e \sigma cos\,\theta}{2\mu}} t^{\frac{1}{2}} \tag{2.3}$$

Benavente et al. (2002) modified the L-W equation by introducing various corrections relating to the microstructure of the rocks, such as pore shape and applying effective medium approximation (EMA) to calculate the effective radius.

$$L_S = \phi \sqrt{\frac{r_e \delta \sigma cos\theta}{2\mu\tau}} t^{\frac{1}{2}} \tag{2.4}$$

where τ is tortuosity and δ is the pore shape factor that accounting for 'roundness'.

2.2.2 Fractal Theory and Fractal Models for Spontaneous Imbibition

'Fractal' was introduced by Mandelbrot (1983) from a Latin word meaning 'to create irregular fragment'. The most important feature of a fractal object is its 'degree of irregularity', which is independent of scale (Wheatcraft and Tyler 1988). In other words, a small part of a fractal object is similar to the whole object. This feature of the fractal object is called self-similarity (Mandelbrot 1967).

Since the introduction of fractal theory by Manderbrot (1967), a great deal of experimental studies have been carried out to investigate the fractal pore structure of porous media. Katz and Thompson (1985) proved the fractal geometry of pores in sandstones by measuring fractal parameters using scanning electron microscope (SEM). After that, several researchers (Jacquin and Adler 1987; Hansen and Skjeltorp 1988; Krohn 1988a; Wheatcraft and Tyler 1988; Adler and Thovert 1993; Perfect and Kay 1995) conducted experimental and theoretical studies on fractal characteristics of

sedimentary rocks such as sandstones, shales, and carbonates. Most of sedimentary rocks have been found to have fractal pore structure. On the basis of fractal theory (Mandelbrot 1967), the number of pores with a particular diameter is a function of (1) pore diameter and (2) fractal dimension.

Fractal theory have been widely used for characterizing the complex pore structure of sedimentary rocks and describing fluid flow in porous media. Krohn (1988b) studied the fractal behavior of sandstone samples by analyzing scanning electron microscope (SEM) images of pores. Liu et al. (2015) investigated fractal characteristics of organic-rich shales by analyzing nitrogen adsorption/desorption tests. Fractal theory has been successfully applied to model rock properties such as rock surface roughness (Majumdar and Bhushan 1990; Power and Tullis 1991; Xie et al. 1997), porosity (Hamm and Bidaux 1996; Pia and Sanna 2013), permeability (Pape et al. 1999; Li and Logan 2001; Yu and Cheng 2002; Xu and Yu 2008; Cai et al. 2012; Cai et al. 2015), and tortuosity (Yu 2005; Cai et al. 2012). Several modeling studies on capillary pressure (Li and Horne 2006; Li 2010a, b) have also been performed based on fractal theory.

In one of the early studies, Li and Zhao (2012) applied the fractal theory for modeling the production rate (q) by spontaneous imbibition.

$$q = (D_f - 2)\sqrt{2(1 - S_{wi} - S_{nwr})\frac{P_C}{\phi H^2}M_e^* t^{-(3-D_f)}} \tag{2.5}$$

where D_f is fractal dimension; S_{wi} and S_{nwr} are initial water saturation and residual saturation of the non-wetting phase; H is the height of the rock sample sample; M_e* is the effective mobility of the wetting and non-wetting phase.

Cai et al. (2012) considered the porous media as a bundle of tortuous capillaries, and developed an analytical fractal model to analyze spontaneous imbibition under the consideration of gravity effect, as shown in Eq. (2.6)

$$M(t) = \frac{a}{b}\left\{1 + W\left(-e^{-1-\left(\frac{b^2}{a}\right)t}\right)\right\} \tag{2.6}$$

where

$$a = \frac{\sigma cos\theta (2 - D_f) D_{max} (A_f * \phi * \rho)^2}{8\mu\tau^2 (3 - D_f) \left[1 - \left(\frac{D_{min}}{D_{max}}\right)^{2-D_f}\right]} \quad (2.7)$$

$$b = \frac{A_f \rho^2 g (2 - D_f) \phi D_{max}^2}{32\mu\tau^2 (4 - D_f) \left[1 - \left(\frac{D_{min}}{D_{max}}\right)^{2-D_f}\right]} \quad (2.8)$$

$$\mathrm{W(x)} = \frac{2ex - 10.7036 + 7.56859\sqrt{2 + 2ex}}{12.7036 + 5.13501\sqrt{2 + 2ex}} \quad (2.9)$$

Here, D_{max} and D_{min} are the maximum and minimum pore diameters, respectively; ρ is the density and g is the gravitational acceleration. Cai et al. (2014) further extended their work by considering different shapes of the pores and developed a more generalized fractal model.

The authors assumed piston-like displacement in modeling the imbibition process, and considered capillary and hydrostatic pressures as driving and deterrent forces, respectively. In other words, the height of liquid column inside capillaries with different diameters is assumed to be similar at a certain time. This assumption may be acceptable for the materials with highly interconnected pores such as paper and unconsolidated sand (Sadjadi and Rieger 2013). Because the pores in such porous media have small length-to-width ratio and the highly interconnected pore network can smooth the imbibition front. However, the pore network of sedimentary rocks contains elongated pores with limited connectivity (Sahimi 1993; Gelb and Gubbins 1998; Yi et al. 2000; Gruener et al. 2012). Due to the limited connectivity between pores, the spontaneous imbibition of wetting fluid into the elongated pores can be considered as laminar flow by following Lucas-Washburn (L-W) equation (Lucas 1918; Washburn 1921). On the basis of the L-W equation, the imbibition rate of a certain wetting phase is positively proportional to the square root of pore diameter. As different elongated pores have different imbibition rates, imbibition process is not piston-like and imbibition front is not smooth, which has been experimentally visualized in the previous studies (Schembre et al. 1998; Gruener et al. 2012). In this thesis, we modify the previous piston-like imbibition model (Cai et al. 2012) by considering non-piston-like displacement in the elongated pores with limited connectivity.

2.3 Previous Studies on Dual-Wettability Behavior

In this section, we review the previous studies on the dual-wettability behavior of unconventional rocks including Montney tight rock and Duverney shales.

Lan et al. (2015) performed a series of tests to measure and compare spontaneous imbibition of oil and brine for the rock samples from different depths of a well drilled in the Montney tight-gas Formation. The rock sample was initially saturated with air and then the bottom face of the plug was exposed to oil or brine. As oil or brine was imbibed into rock sample, the mass gain was recorded periodically. Figs. 2.2a-b compare the normalized imbibed volume of oil and brine for the upper Montney (UMT) and the lower Montney (LMT) rock samples, respectively. Normalized imbibed volume is calculated by dividing the imbibed volume by the effective pore volume of the rock sample. The equilibrated imbibed volume of oil is significantly higher than that of brine. In some plugs, even more than 80% of effective pore volume is invaded by oil. Lan et al. (2015) explained the strong wetting affinity of the Montney samples towards oil by the presence of the brine-repellant pores within or coated by solid bitumen and pyrobitumen.

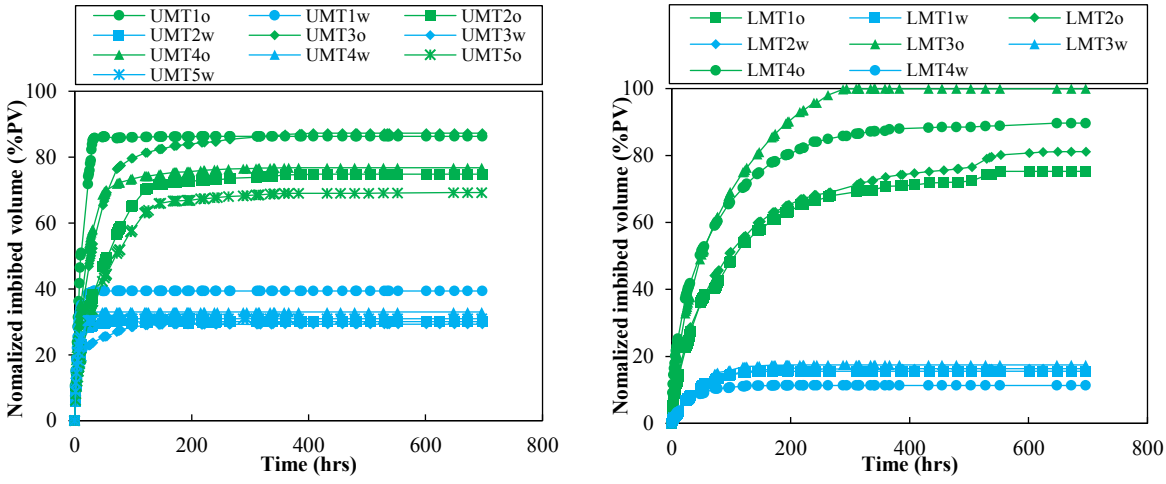

(a) **(b)**

Fig. 2.2 Comparative spontaneous imbibition tests of oil and brine into the rock samples from (a) the upper Montney (UMT) and (b) the lower Montney (LMT) Formations (Lan et al. 2015).

Yassin et al. (2016) extended the wettability study on Montney rock samples by reviewing the results of SEM analysis (as shown in Fig. 2.3, MICP test, organic petrography, and tight rock

analysis (TRA). On the basis of these analyses, the authors proposed the dual-wettability theory: (1) nanopores within solid bitumen/pyrobitumen that are strongly hydrophobic with no or negligible wetting affinity towards the aqueous phase and (2) micropores bordered by inorganic minerals that are hydrophilic with strong wetting affinity towards the aqueous phase. Yassin et al. (Yassin et al. 2017) further conducted spontaneous imbibition tests on rock samples from the Duvernay shale formation and observed the similar dual-wettability behavior. SEM/EDS analyses demonstrated abundant number of small nanopores within the organic matter. The hydrophobic organic nanopores also supports the late equilibrium of oil compared with brine in the imbibition tests. Yassin et al. (2016) also validated this hypothesis by comparing the proposed dual-wettability model with the measured gas relative permeability data.

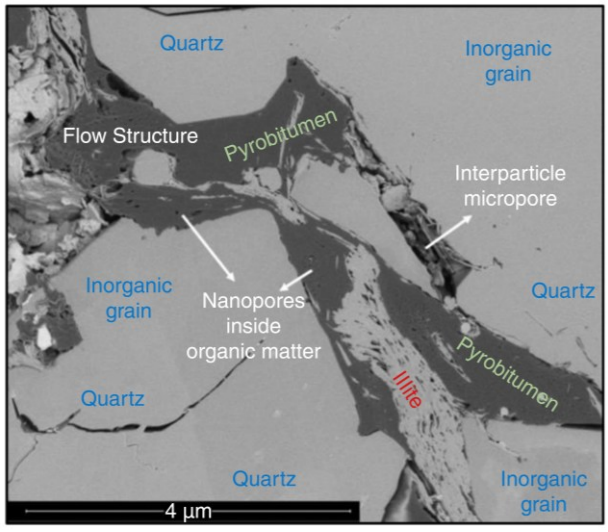

Fig. 2.3 FIB/SEM images of one Montney sample from the dry-gas window (Yassin et al. 2016)

Yassin et al. (2017) also conducted spontaneous imbibition tests of nine twin rock samples from five wells drilled in the Duvernay formation and observed similar results. The authors defined oil wettability index (WI_o) based on the equilibrium imbibed volume of oil and brine. The results showed that the samples with higher TOC content and effective porosity have higher WI_o. Positive correlations of WI_o with TOC content and effective porosity suggested that the majority of hydrophobic connected pores exist in the organic part of the rock.

Zolfaghari et al. (2017) performed a series of adsorption tests to characterize the dual-wettability pore network of gas-shale plugs from the Horn River Basin. The authors used water and N_2 to get

inorganic and total pore size distributions, respectively. The PSD of hydrophobic organic pores (PSD_{org}) was calculated by subtracting PSD of inorganic pores from total PSD. In this study, we propose a new technique to characteraize the dual-wettability pore network by the comparative analysis of the oil and brine imbibition data.

2.4 Pore Size Distribution Techniques

Different techniques have been applied to investigate the pore size distribution (PSD) of unconventional reservoir rocks. These techniques are generally characterized as radiation methods and fluid invasion methods (Bustin et al. 2008; Clarkson et al. 2012).

2.5.1 Radiation Method

Radiation methods mainly consist of scanning electron microscope (SEM) and nuclear magnetic resonance (NMR). SEM analysis is one of the radiation techniques which has been widely utilized to investigate the pore network of reservoir rocks (Pittman 1972; Hurst and Nadeau 1995; Bustin et al. 2008; Wang et al. 2014; Saraji and Piri 2015). However, some nanopores (< 2 nm) are hard to be detected by SEM images due to the resolution limitations (Bustin et al. 2008; Curtis et al. 2011; Clarkson et al. 2012).

NMR is another radiation technique with the advantage of detecting both connected and isolated pores. However, converting NMR spectrum to pore size distribution needs the accurate estimation of some parameters such as total pore surface area of the rock sample (Sigal 2015; Liu et al. 2017).

2.5.2 Fluid Invasion Method

Besides radiation methods, fluid invasion methods are also used for PSD determination. Mercury injection capillary pressure (MICP) test (Smith 1966; Berg 1975) is one of commonly used fluid invasion methods for pore-throat size distribution. During MICP test, mercury intrudes into the pore-throats by successive pressure increments. However, MICP fails to give the PSD of nanopores in unconventional tight rocks as extremely high pressure (> 400 MPa) is required (Al Hinai et al. 2014; Yassin et al. 2016; Zolfaghari et al. 2017). Furthermore, applying high pressures in MICP test may compress and even damage the pore system (Clarkson et al. 2012; Labani et al. 2013).

CO_2/N_2 isotherm adsorption is another fluid invasion method for measuring the PSD (Clarkson et al. 2012). Brunauer, Emmett and Teller (BET) equation is widely used to calculate the PSD from CO_2 and N_2 adsorption data (Clarkson et al. 2012; Zolfaghari et al. 2017). Compared with MICP test, isotherm adsorption can detect smaller nanopores. However, isotherm adsorption is low pressure technique and cannot be used to simulate reservoir condition (high pressure and high temperature) (Clarkson et al. 2012).

Spontaneous imbibition is also an important fluid invasion method for characterizing the properties of unconventional rocks (Dehghanpour et al. 2013; Xu and Dehghanpour 2014; Dehghanpour et al. 2015; Ghanbari and Dehghanpour 2015, 2016; Habibi et al. 2016). In this study, we propose a new technique to calculate the PSD based on the spontaneous imbibition data.

Chapter 3: Modified Fractal Model for Co-Current Spontaneous Imbibition

3.1 Introduction

In this chapter, we extend the previous model by assuming non-piston-like imbibition in capillaries with different diameters. In our model, first the larger capillaries are filled by wetting phase, followed by smaller capillaries. We develop an analytical equation without considering hydrostatic pressure and a semi-analytical equation with considering hydrostatic pressure. We can apply actual boundary conditions in the proposed model, while the previous piston-like models are only valid before the wetting phase reaches the top of the porous media in co-current spontaneous imbibition test. Moreover, the proposed model can be used to determine the minimum pore diameter of rock sample according to the equilibrium time in spontaneous imbibition tests.

3.2 Basic Theory and Assumptions

In this study, we model co-current spontaneous imbibition of a wetting phase into a porous media with fractal pore structure. The schematic view of co-current spontaneous imbibition test is shown in Fig. 3.1a. The rock sample is initially saturated with air (initial water saturation, S_{wi}=0) and only the bottom face of the rock sample is exposed to the wetting phase. The theory and assumptions for modeling of this process are summarized as follows:

a. The pore structure of the rock is assumed to be a bundle of tortuous capillaries with different diameters as shown in Fig. 3.1b.

b. All capillaries are exposed to liquid at the bottom of the sample, and are continuously extended to the top of the rock sample without any interconnection.

c. The diameter of a single capillary is constant along the height of the rock sample.

d. The liquid imbibition in a certain capillary stops right after reaching the top of the rock sample.

e. The driving mechanism for liquid imbibition is capillary pressure and we do not consider other driving mechanisms such as water adsorption by clay minerals (Bernard 1967), osmotic effect

(Chenevert 1989; Neuzil 2000; Bai et al. 2008; Chen et al. 2010), or electrical double layer expansion (Holmbergc et al. 2002; Nasralla and Nasr-El-Din 2014).

f. The pore size distribution (PSD) of capillaries is constant during the time course of imbibition process and we neglect the pore size alterations that may be induced by clay swelling.

g. We neglect air trapping during liquid imbibition in a single capillary. In other words, liquid saturation is 100% behind the liquid front for a single capillary.

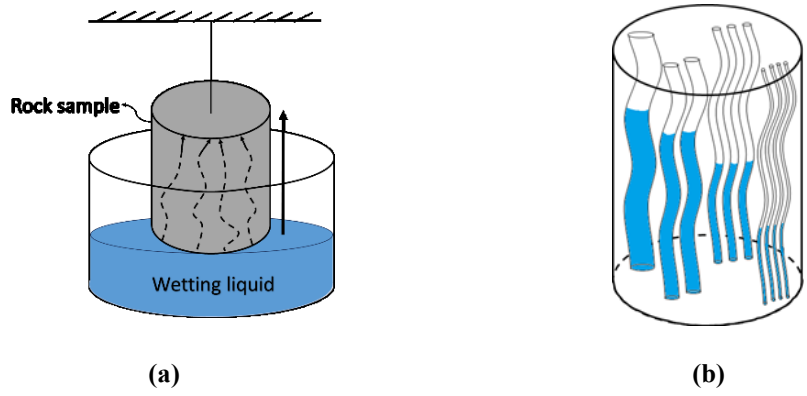

Fig. 3.1 (a) Schematic view of co-current spontaneous imbibition test. (b) Schematic view of a bundle of tortuous capillaries for modeling co-current spontaneous imbibition.

3.3 Model Derivation

We divide the model derivation into two steps. In the first step, we start the derivation of spontaneous imbibition model in a single capillary. We review the previous equations developed by Cai and Yu (2011) without considering hydrostatic pressure, and propose a new equation with considering hydrostatic pressure. In the second step, we extend single capillary equations for simulating spontaneous imbibition in a bundle of capillaries with different diameters.

3.3.1 Spontaneous Imbibition in A Single Tortuous Capillary

The imbibition of a Newtonian fluid through a vertical capillary follows the Hagen-Poiseuille's (H-P) law (Poiseuille 1844)

$$\frac{d(L_f)}{dt} = \frac{D^2}{32\mu L_f}\left(\frac{4\sigma cos\theta}{D} - \rho g L_s\right) \tag{3.1}$$

where L_f and L_s are tortuous and straight heights of the liquid column inside a capillary, respectively; D is the capillary diameter, $4\sigma\, cos(\theta)\,/D$ is the capillary pressure term from Young-Laplace (Y-L) equation (Young 1805; Gauss 1830), which is the driving force for imbibition of wetting phase, σ is air-liquid surface tension, θ is contact angle, μ is the liquid viscosity, and $\rho g L_s$ is hydrostatic pressure of the liquid column inside the capillary. Hydrostatic pressure is in opposite direction of capillary pressure as shown by negative sign ($-\rho g L_s$) in Eq. (3.1). The tortuosity (τ) of a single capillary is defined as the ratio of the tortuous height over straight height (Bear 2013) as

$$L_f = \tau L_s \tag{3.2}$$

In order to compare our proposed model with previous one (Cai et al. 2012), we similarly assume a constant value of tortuosity for all pores regardless of pore diameter. However, the tortuosity can highly vary from one pore to another pore due to the variation of pore size. On the basis of the fractal theory, the tortuosity is a function of (1) pore diameter and (2) pore length (Cai and Yu 2011; Schopf et al. 2017).

Inserting Eq. (3.2) into Eq. (3.1) and rearranging Eq. (3.1) yields

$$L_s dL_s = (\frac{D\sigma\, cos\theta}{8\mu\tau^2} - \frac{\rho g L_s D^2}{32\mu\tau^2})dt \tag{3.3}$$

When hydrostatic pressure is negligible compared with capillary pressure, the second term in the bracket of Eq. (3.3) can be eliminated and Eq. (3.3) is solved by analytical integration

$$L_s = \sqrt{\frac{D\sigma\cos\theta}{4\mu\tau^2}}\sqrt{t} \tag{3.4}$$

Eq. (3.4) is similar to Lucas-Washburn equation (Lucas 1918; Washburn 1921) except the tortuosity term. The imbibed mass of wetting phase can be expressed as (Cai and Yu 2011)

$$m = \frac{\rho\pi}{8}\sqrt{\frac{D^5\sigma cos\theta}{\mu}}\sqrt{t} \tag{3.5}$$

When hydrostatic pressure term cannot be neglected in Eq. (3.3), L_s in hydrostatic pressure term is not a constant value and varies with time. Thus, we use a numerical method to solve Eq. (3.3).

The height of liquid column increases from $L_{s,i-1}$ to $L_{s,i}$ as imbibition proceeds from t_{i-1} to t_i. t_i and t_{i-1} represent the current and previous time steps, respectively. We can assume that the hydrostatic pressure of liquid column is equal to $\rho g L_{s,i-1}$ for a small time interval (*dt*). In other words, hydrostatic pressure is assumed to be constant as the height of liquid column increases from $L_{s,i-1}$ to $L_{s,i}$. The error corresponding to this approximation is negligible if *dt* is small enough. Integrating Eq. (3.3) from (*i-1*)th to *i*th time step gives

$$\int_{L_{s,i-1}}^{L_{s,i}} L_s dL_s = \int_{t_{i-1}}^{t_i} \left(\frac{D\sigma\cos\theta}{8\mu\tau^2} - \frac{\rho g L_{s,i-1} D^2}{32\mu\tau^2}\right) dt \tag{3.6}$$

After rearranging Eq. (3.6) we have

$$L_{s,i} = \left[{L_{s,i-1}}^2 + \left(\frac{D\sigma\cos\theta}{4\mu\tau^2} - \frac{\rho g L_{s,i-1} D^2}{16\mu\tau^2}\right)(t_i - t_{i-1}) \right]^{\frac{1}{2}} \tag{3.7}$$

where $L_{s,i}$=0 for *i*=1. The first time step (*i*=1) represents the start of imbibition when the bottom of capillary just touches the liquid. At this time, the height of liquid column ($L_{s,i}$) is zero. As imbibition proceeds, $L_{s,i}$ and $L_{s,i-1}$ represent the straight height of liquid column at *i*th and (*i-1*)th time steps, respectively. So, the straight height of liquid column at any time step ($L_{s,i}$) can be calculated by Eq. (3.7). The imbibed mass of liquid (m_i) at *i*th time step is expressed as

$$m_i = \frac{\pi D^2 \rho}{4} \left[(L_{s,i-1}\tau)^2 + \left(\frac{D\sigma\cos\theta}{4\mu} - \frac{\rho g L_{s,i-1} D^2}{16\mu}\right)(t_i - t_{i-1}) \right]^{\frac{1}{2}} \tag{3.8}$$

Eqs. (3.4) and (3.7) indicate that the larger the diameter of capillary (*D*), the faster the liquid fills the capillary. Faster liquid imbibition in larger capillaries is also qualitatively illustrated in Fig. 3.1b. Faster liquid imbibition in larger capillaries is explained by the fact that despite lower driving capillary pressure in larger capillaries, the permeability (conductivity) is higher in larger capillaries.

3.3.2 Spontaneous Imbibition in Porous Media

In this part, we consider the porous media as an idealized bundle of tortuous capillaries with different diameters. We extend Eqs. (3.4) and (3.7) for simulating co-current spontaneous imbibition in a bundle of capillaries. On the basis of fractal theory (Mandelbrot 1967), the number

of pores with a particular diameter is a function of (1) pore diameter (D) and (2) fractal dimension (D_f). On the basis of the previous studies regarding cumulative size distribution of fractals (Krohn 1988b; Majumdar and Bhushan 1990), Yu and Cheng (Yu and Cheng 2002) argued that the distribution of pores in a self-similar unit should follow the fractal scaling law

$$N(\geq D) = (\frac{D_{max}}{D})^{D_f} \tag{3.9}$$

On the basis of Eq. (3.9), the number of small pores is higher than that of large pores. Rieu and Perrier (Rieu and Perrier 1998) established a fractal model for pore size distribution based on the Sierpinski carpet (Fig. 3.2). They used white and gray color to present pores and rock matrix, respectively. As shown in Fig. 3.2, the number of pores (N) increases with reducing pore diameter (D), which was qualitatively illustrated in Fig. 3.1b.

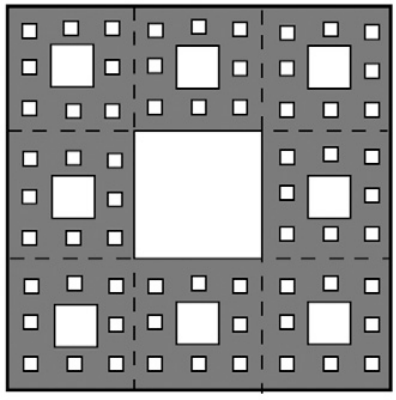

Fig. 3.2. Construction of the Sierpinski carpet (Yu, Cai, and Zou 2009). White and gray colors present pores and rock matrix, respectively. The number of pores (*N*) increases as pore diameter (*D*) decreases.

Total pore area in the unit cell (A_{Pu}) is calculated by (Wu and Yu 2007)

$$A_{Pu} = -\int_{D_{min}}^{D_{max}} \frac{\pi D^2}{4} dN \tag{3.10}$$

where D_{min} is the minimum pore diameter. Differentiating both sides of Eq. (3.9) with respect to N and D, and then inserting dN into Eq. (3.10) gives (Wu and Yu 2007)

$$A_{Pu} = \frac{\pi}{4}\frac{D_f}{2-D_f} D_{max}^2 \left[1 - (\frac{D_{min}}{D_{max}})^{2-D_f}\right] \tag{3.11}$$

The number of capillaries with diameter larger than D in the rock sample (N_f) is obtained by (Wu and Yu 2007, Yu et al. 2009)

$$N_f(\geq D) = \frac{A_f \times \phi'}{A_{pu}} N(\geq D) = \frac{4A_f}{\pi D_{max}^{2-D_f}} \frac{2-D_f}{D_f} \frac{\phi'}{1-\left(\frac{D_{min}}{D_{max}}\right)^{2-D_f}} D^{-Df} \tag{3.12}$$

where A_f is the total cross-sectional area of rock sample. We name ϕ' as 'surface porosity', which is the ratio of pore area to cross-sectional area of rock sample. It is worth mentioning that porosity (ϕ) was used instead of ϕ' in previous studies (Cai et al. 2012; Wu and Yu 2007) in Eq. (3.12). However, for a bundle of tortuous capillaries as shown in Fig. 3.3, ϕ' and ϕ should follow

$$\phi = \frac{V_P}{V} = \frac{A_P \tau L_s}{A_f L_s} = \phi' \tau \tag{3.13}$$

where V_P and V are the volume of pores and rock sample, respectively. A_p is total pore area in the cross section of the rock sample. ϕ is equal to ϕ' only when the capillaries are assumed straight ($\tau = 1$). As we consider tortuous capillaries in this study, surface porosity ϕ' should be used in Eq. (3.12). Schopf et al. (Schopf et al. 2017) also took this correlation into the consideration when developing a model for imbibition into highly porous layers of aggregated particles.

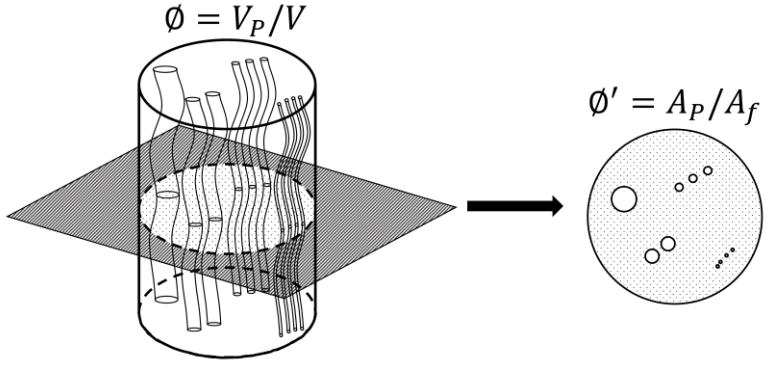

Fig. 3.3. Schematic illustration of the relationship between ϕ and ϕ'.

3.3.2.1 Spontaneous Imbibition in Fractal Porous Media without Considering Hydrostatic Pressure

In this section, we model spontaneous imbibition in a bundle of capillaries with ignoring hydrostatic pressure term. By differentiating Eq. (3.12) with respect to D, we can calculate the

incremental number of capillaries ($n(D)$) with diameters in the range of D to $D+dD$ (Cai, Hu, et al. 2012)

$$n(D) = -dN_f = \frac{4A_f}{\pi D_{max}^{2-D_f}} \frac{(2-D_f)\phi'}{1-\left(\frac{D_{min}}{D_{max}}\right)^{2-D_f}} D^{-(D_f+1)} dD \tag{3.14}$$

Eq. (3.14) implies that the number of capillaries decreases with increasing of pore size and $dN_f < 0$ (Yu et al. 2009). By multiplying the imbibed mass in a single capillary ((m) in Eq. (3.5)) by incremental number of pores ($n(D)$), we can calculate the total imbibed mass of liquid in the capillaries with diameter D

$$M(D) = m \cdot n(D) = \frac{A_f \rho}{2D_{max}^{2-D_f}} \frac{(2-D_f)\phi'}{1-\left(\frac{D_{min}}{D_{max}}\right)^{2-D_f}} \sqrt{\frac{\sigma cos\theta}{\mu}} \sqrt{t} D^{1.5-D_f} dD \tag{3.15}$$

The total imbibed volume of liquid can be calculated through dividing Eq. (3.15) by the liquid density. Eq. (3.15) is valid when the imbibed liquid front has not reached top of the capillary. When liquid reaches top of the capillary with diameter of D, imbibition stops and the total imbibed mass is considered as equilibrated mass

$$m^{eq}(D) = \frac{\pi D^2}{4} \rho \tau H \tag{3.16}$$

Here, m^{eq} is the equilibrated mass of liquid in one capillary with diameter of D, H is the height of the rock sample, and (τH) is the actual tortuous height of the capillary based on Eq. (3.2). The equilibrated imbibed mass (M^{eq}) in the capillaries with diameter of D is calculated by

$$M^{eq}(D) = m^{eq} \cdot n(D) = \frac{A_f H \phi \rho}{D_{max}^{2-D_f}} \frac{(2-D_f)}{1-\left(\frac{D_{min}}{D_{max}}\right)^{2-D_f}} D^{1-D_f} dD \tag{3.17}$$

Finally, the total imbibed mass of liquid inside all the capillaries (M_T) at time t is calculated by integrating $M(D)$ and $M^{eq}(D)$ from D_{min} to D_C and from D_C to D_{max}, respectively

$$M_T = \int_{D_{min}}^{D_C} M(D) + \int_{D_C}^{D_{max}} M^{eq}(D) \tag{3.18}$$

where critical diameter D_C is the diameter of the capillaries that are just filled by liquid at time *t*. On the basis of Eq. (3.7), larger capillaries are filled faster than smaller capillaries. Therefore, any capillary with diameter larger than D_c is already filled with liquid at time *t*. D_c is a time-dependent parameter and decreases with time. The total imbibed mass of liquid (M_T) can be analytically obtained by substituting Eqs. (3.15) and (3.17) into Eq. (3.18)

$$M_T = \frac{A_f \rho}{2D_{max}^{2-D_f}} \frac{\phi'}{1-\left(\frac{D_{min}}{D_{max}}\right)^{2-D_f}} \sqrt{\frac{\sigma cos\theta}{\mu}} \left(\frac{2-D_f}{2.5-D_f}\right) \left[D_C^{2.5-D_f} - D_{min}^{2.5-D_f}\right] \sqrt{t} + \frac{A_f \rho H}{D_{max}^{2-D_f}} \frac{\phi}{1-\left(\frac{D_{min}}{D_{max}}\right)^{2-D_f}} \left[D_{max}^{2-D_f} - D_C^{2-D_f}\right] \tag{3.19}$$

Eq. (3.19) is the analytical equation for spontaneous imbibition of wetting phase into a bundle of capillaries without considering the hydrostatic pressure term. D_C can be analytically solved by rearranging Eq. (3.4)

$$D_C = \frac{4\mu\tau^2 H^2}{\sigma cos\theta t} \tag{3.20}$$

It should be mentioned that D_C in Eq. (3.20) should lie in the range of D_{min} to D_{max}. However, D_C calculated by Eq. (3.20) might not be in this range for two special cases. The first case occurs at the initial imbibition period when even the largest capillaries are not filled completely and are still imbibing liquid. If we use Eq. (3.20) to calculate D_C, D_C can be even larger than D_{max}. For this case, we should set D_c=D_{max} and Eq. (3.19) becomes

$$M_T = \int_{D_{min}}^{D_{max}} M_i(D) = \frac{A_f \rho}{2D_{max}^{2-D_f}} \frac{\phi'}{1-\left(\frac{D_{min}}{D_{max}}\right)^{2-D_f}} \sqrt{\frac{\sigma cos\theta}{\mu}} \left(\frac{2-D_f}{2.5-D_f}\right) \left[D_{max}^{2.5-D_f} - D_{min}^{2.5-D_f}\right] \sqrt{t} \tag{3.21}$$

The second case happens at the late imbibition period when all the capillaries are already filled with the liquid. For this case, even the smallest capillaries (D_{min}) already stopped imbibing liquid.

Therefore, if we calculate D_c by Eq. (3.20), the value of D_C will be smaller than D_{min}. Set D_c=D_{min} and Eq. (3.19) becomes

$$M_T = \int_{D_{min}}^{D_{max}} M^{eq}(D) = \frac{A_f \rho H}{D_{max}^{2-D_f}} \frac{\phi}{1-\left(\frac{D_{min}}{D_{max}}\right)^{2-D_f}} \left[D_{max}^{2-D_f} - D_{min}^{2-D_f}\right] \tag{3.22}$$

On the basis of fractal theory, Cai et al. (Cai et al. 2012) proposed a fully-analytical equation for spontaneous imbibition of wetting phase into fractal porous media. The main equations of this model are summarized in Appendix A. The authors assumed an average imbibition rate in capillaries with different diameters. As shown in Eqs. (A.4) and (A.5), the straight height (L_s) of the liquid column inside the capillary is assumed to be constant when integrating Eq. (A.4) from the minimum diameter (D_{min}) to the maximum diameter (D_{max}). It means that the liquid column in capillaries with different diameters rises with a similar rate during the imbibition process. In other words, liquid imbibition is piston-like and all capillaries are filled with the same rate. However, Eq. (3.4) or Eq. (3.7) shows that straight height of liquid column (L_s) at a certain time is a function of capillary diameter and the larger the diameter of capillary, the faster the liquid fills the capillary (larger L_s). In this study, we consider faster imbibition in larger capillaries and assume that the liquid imbibition is not piston-like. For the porous media with highly interconnected pores, such as paper and unconsolidated sand, neighboring menisci merge together and form a continuous air-liquid interface. The menisci advancement is spatially correlated, which restricts the menisci advancement beyond the average front and draws forward the menisci falling behind (Buldyrev et al. 1992; Miranda et al. 2010). The piston-like imbibition model may be valid as a uniform imbibition front was observed in such media (Akin and Kovscek 1999). By contrast, for many natural porous media, the elongated pores with limited connectivity commonly exist (Gelb and Gubbins 1998; Yi etal. 2000; Gruener et al. 2012; Sadjadi and Rieger 2013). The menisci cannot merge together in such media which inhibits the formation of a continuous air-liquid interface. In this case, the imbibition front broadening or non-piston-like displacement front was experimentally visualized by neutron imaging and X-ray CT scanning (Schembre et al. 1998, Gruener et al. 2016). These results suggest the importance of considering the effect of pore size on modeling spontaneous imbibition process.

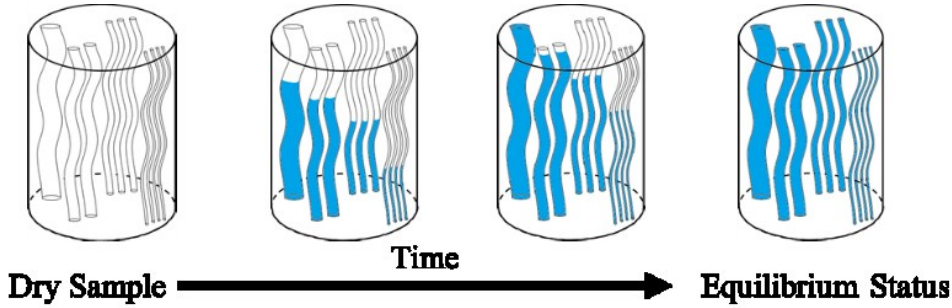

Fig. 3.4. The course of non-piston-like liquid imbibition into the bundle of capillaries with different diameters.

Fig. 3.4 qualitatively illustrates the non-piston-like imbibition into an idealized porous media. As discussed previously, we express the straight height (L_s) as a function of pore size (D) when integrating the imbibed mass in the capillaries from D_{min} to D_{max}. Critical diameter (D_c) is calculated by Eq. (3.20) during the time course of imbibition to determine the diameter of the capillaries that are just filled by liquid. Therefore, we can divide the capillaries into two categories: the capillaries with diameters > D_c that are already filled with liquid and the capillaries with diameters < D_c which are still imbibing the liquid. In addition, D_c is a time-dependent parameter and decreases with time. This is the main difference between our proposed non-piston-like model and the previous piston-like model (Cai et al. 2012).

Moreover, the schematic shown in Fig. 3.4 only represents the spontaneous imbibition process in small scale samples (e.g. less than 10 cm in height). For these small scale samples, the hydrostatic pressure of imbibed liquid is negligible compared with capillary pressure. However, hydrostatic pressure cannot be neglected when modeling the spontaneous imbibition at the field-scale. The height of the natural porous media such as reservoir sections can be several hundreds of meters (Tiab and Donaldson 2015), and the wetting liquid cannot reach the top of the porous media as hydrostatic pressure is comparable to capillary pressure. The equation considering hydrostatic pressure will be derived in the next section.

3.3.2.2 Spontaneous Imbibition in Fractal Porous Media with Considering Hydrostatic Pressure

In this section, we model spontaneous imbibition in a bundle of capillaries with considering hydrostatic pressure. On the basis of Eq. (3.12), the incremental number of pores ($n(D)$) with respect to capillary size is calculate by

$$n(D) = N_f[\geq D] - N_f[\geq (D+\Delta D)] = \frac{4A_f}{\pi D_{max}^{2-D_f}} \frac{2-D_f}{D_f} \frac{\phi'}{1-\left(\frac{D_{min}}{D_{max}}\right)^{2-D_f}} [D^{-Df} - (D+\Delta D)^{-Df}] \tag{3.23}$$

where, $N_f[\geq (D+\Delta D)]$ and $N_f[\geq D]$ are the cumulative numbers of capillaries larger than $D+\Delta D$ and D, respectively. ΔD is the diameter interval. If ΔD is small enough, $n(D)$ can be treated as the incremental number of capillaries with diameter of D. By multiplying the imbibed mass in a single capillary ((m_i) in Eq. (3.8)) by $n(D)$, we can calculate the total imbibed mass of liquid in the capillaries with diameter D at i^{th} time step

$$M_i(D) = m_i \cdot n(D) = \left[(\tau L_{s,i-1})^2 + \left(\frac{D\sigma\, cos\theta}{4\mu} - \frac{\rho g L_{s,i-1} D^2}{16\mu}\right)(t_i - t_{i-1})\right]^{\frac{1}{2}} \times \left[\frac{A_f \rho D^2}{D_{max}^{2-D_f}} \frac{2-D_f}{D_f} \frac{\phi'}{1-\left(\frac{D_{min}}{D_{max}}\right)^{2-D_f}} [D^{-Df} - (D+\Delta D)^{-Df}]\right] \tag{3.24}$$

The total imbibed volume of liquid in a bundle of capillaries with diameter of D is calculated through dividing Eq. (3.24) by the liquid density. It should be mentioned that Eq. (3.24) is valid when the imbibing liquid front has not reached top of the capillary. The equilibrated imbibed mass in a single capillary (m^{eq}) is presented in Eq. (3.16). Similarly, the equilibrated imbibed mass (M^{eq}) in a bundle of capillaries with diameter of D is calculated by

$$M^{eq}(D) = m^{eq} \cdot n(D) = \frac{A_f D^2 H \rho}{D_{max}^{2-D_f}} \frac{2-D_f}{D_f} \frac{\phi}{1-\left(\frac{D_{min}}{D_{max}}\right)^{2-D_f}} [D^{-Df} - (D+\Delta D)^{-Df}] \tag{3.25}$$

Finally, the total imbibed mass of liquid in all capillaries at a certain time (M_T) is calculated by summing $M_i(D)$ and $M^{eq}(D)$ from D_{min} to D_{max} as

$$M_T = \sum_{j=D_{min}}^{j=D_C} M_i(j) + \sum_{j=D_C+\Delta D}^{j=D_{max}} M^{eq}(j)$$

$$= \sum_{j=D_{min}}^{j=D_C} \frac{A_f \rho j^2}{D_{max}^{2-D_f}} \frac{2-D_f}{D_f} \frac{\phi'}{1-\left(\frac{D_{min}}{D_{max}}\right)^{2-D_f}} [j^{-Df} - (j+\Delta D)^{-Df}] \times$$

$$\left[(\tau L_{s,i-1})^2 + \left(\frac{j\sigma\, cos\theta}{4\mu} - \frac{\rho g L_{s,i-1} j^2}{16\mu}\right)(t_i - t_{i-1})\right]^{0.5} \quad (3.26)$$

$$+ \sum_{j=D_C+\Delta D}^{j=D_{max}} \frac{A_f j^2 H \rho}{D_{max}^{2-D_f}} \frac{2-D_f}{D_f} \frac{\phi}{1-\left(\frac{D_{min}}{D_{max}}\right)^{2-D_f}} [j^{-Df} - (j+\Delta D)^{-Df}]$$

Eq. (3.26) is the semi-analytical equation for spontaneous imbibition of wetting phase into fractal porous media with the consideration of hydrostatic pressure. We use MATLAB to solve this equation. The detailed flowchart and procedure are presented in Section 3.4.

In summary, Eqs. (3.19) and (3.26) present the final solutions for the non-piston-like spontaneous imbibition of wetting phase into a bundle of capillaries with ignoring and considering the hydrostatic pressure, respectively. In these two equations, $\rho, \sigma, \theta, \mu, A_f$, H and ϕ are the known physical parameters and D_{max}, D_{min}, D_f and τ are the unknown parameters. In section 3.5, we present a procedure for determining these four unknown parameters.

3.4 Computational Procedure for Calculating the Imbibed Mass with Considering Hydrostatic Pressure

As discussed in previous section, Eq. (3.26) is the final semi-analytical solution for the non-piston-like spontaneous imbibition of wetting phase with considering hydrostatic pressure. The computational procedure for calculating the total imbibed mass (M_T) at the i^{th} time step (t_i) is presented in Fig. 3.5. We implemented this procedure in MATLAB. The pore diameter ranges from D_{min} to D_{max}, and the value of $D_{min}/10$ is chosen as the diameter interval (ΔD). For each time step, we check if the straight liquid column (L_s) for a specific capillary diameter reaches the top of the rock sample (H). Then, we use Eq. (3.24) or (3.25) to calculate the imbibed mass for a specific capillary diameter. Finally, the total imbibed mass (M_T) at i^{th} time step is computed by

summing up the mass of imbibed liquid inside all the capillaries (Eq. (3.26)). Once the unknown parameters of D_{max}, D_{min}, D_f , and τ are specified, total imbibed mass (M_T) versus time can be numerically computed using the flowchart presented in Fig. 3.5.

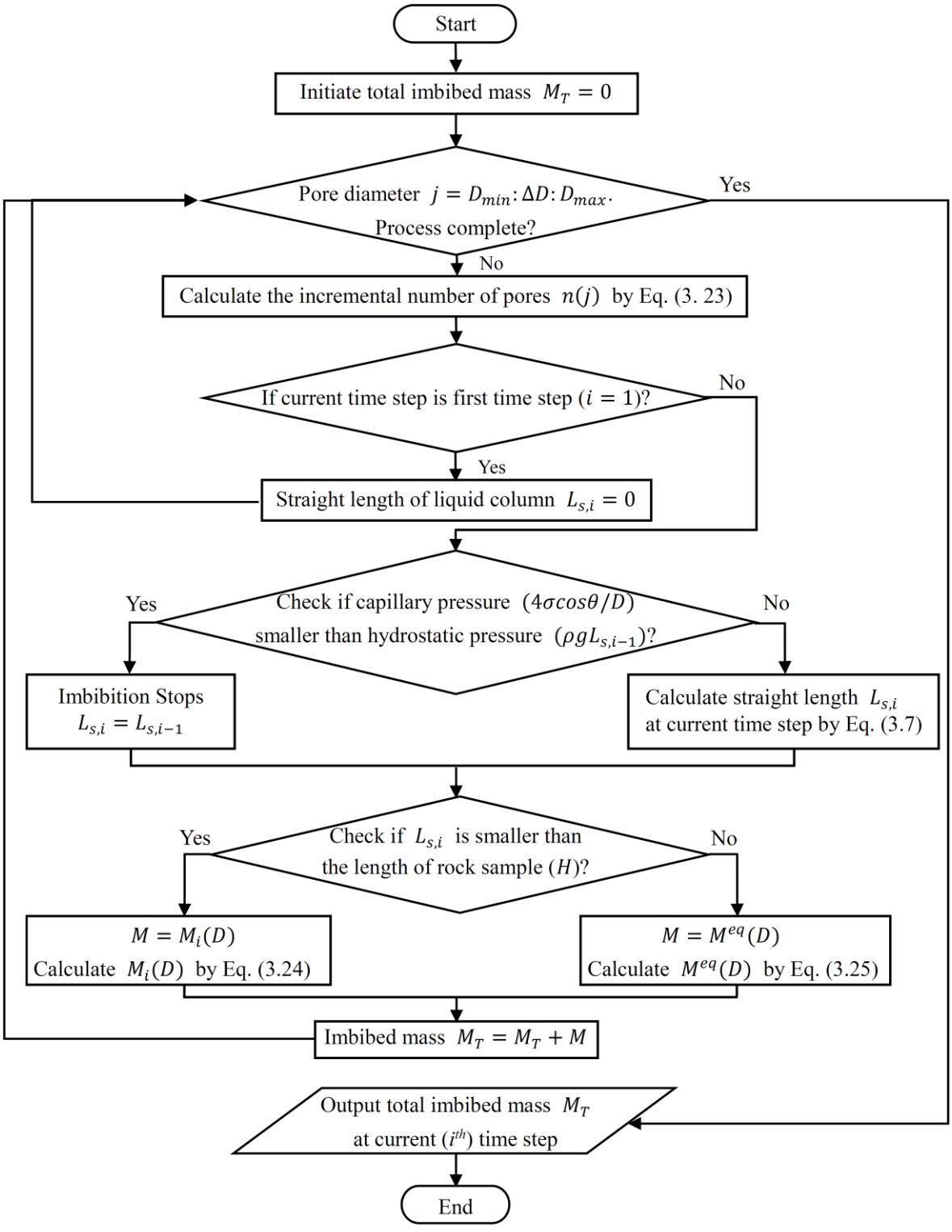

Fig. 3.5. Flowchart for numerical computation of total imbibed mass (M_T) at i^{th} time step.

3.5 Determination of Unknown Parameters

In this section, we introduce the estimation of the unknown parameters: D_{max}, D_{min}, D_f and τ.

D_{max} can be determined by experimental data or mathematical equations. In mercury injection capillary pressure (MICP) test, the pressure corresponding to start of mercury intrusion is converted to maximum pore-throat size by using Young-Laplace equation (Thomas et al. 1968). Mercury is a non-wetting phase in MICP tests, and the mercury intrusion is mainly controlled by the pore-throat size (Wardlaw and Taylor 1976). On the other hand, spontaneous imbibition of wetting phase is mainly controlled by pore-body size (Valvatne and Blunt 2004). Therefore, D_{max} might be underestimated by use of MICP data. In this study, we determine the maximum diameter D_{max} using the following equation (Yu and Cheng 2002; Wu and Yu 2007; Cai et al. 2010; Cai and Yu 2010)

$$D_{max} = \frac{D_S}{4}\left[\sqrt{\frac{2\phi}{1-\phi}} + \sqrt{\frac{\phi}{1-\phi}} + \sqrt{\frac{\pi}{4(1-\phi)}} - 1\right] \tag{3.27}$$

The detailed derivation for Eq. (3.27) is presented in Appendix B. D_S is considered as the mean diameter of the particles in the porous media. Once D_S is specified, D_{max} can be calculated by Eq. (3.27).

Similar to D_{max}, we can use MICP data and determine D_{min}. Pore-throat diameter corresponding to maximum mercury pressure at mercury saturation of 100% pore volume is considered as D_{min}. It should be mentioned that for the tight and shale rock samples with absolute permeability in the order of nanodarcy, the maximum mercury pressure of 400 MPa is not high enough to detect the minimum pore-throat diameter (Clarkson et al. 2012; Lan et al. 2015) and mercury cannot fill more than 60% of pore volume of tight and shale rock samples (Lan et al. 2015; Yassin et al. 2017). Moreover, filling the small micropores with mercury requires applying pressures higher than 400 MPa that may damage the pore structure (Clarkson et al. 2012). Therefore, we need to look for other methods to determine D_{min}. In this chapter, we used the correlation of D_{min}/D_{max}=0.01 to calculate D_{min} (Yu and Cheng 2002; Yu et al. 2009; Cai et al. 2010; Cai et al 2012). Therefore, once D_{max} is determined by using Eq. (3.27), D_{min} can be calculated. In section

3.6.3, we also propose a new method to estimate D_{min} by analyzing the experimental imbibition data.

D_f is an important unknown parameter in Eqs. (3.19) and (3.26), which controls the PSD of fractal porous media. We will discuss the effect of D_f on PSD in the following section. One of the methods for determining D_f is box-counting method (Feder and Aharony 1990). This method is based on the image analysis of the cross section of rock sample. Yu and Li (Yu and Li 2001) also proposed an analytical correlation to approximate D_f, as shown in Eq. (A.12). As D_f is a function of porosity (ϕ) and D_{min}/D_{max}, D_f can be determined once ϕ, D_{min} and D_{max} are specified.

Cai et al. (Cai et al. 2012) assumed an average tortuosity for pores with different diameters and the average tortuosity was calculated by using the following correlation (Comiti and Renaud 1989)

$$\tau = 1 + 0.41 ln \frac{1}{\phi} \tag{3.28}$$

Therefore, once D_S and porosity ϕ are determined, the other unknown parameters can be calculated, and the spontaneous imbibition of wetting phase can be modeled using Eq. (3.19) or (3.26).

3.6 Modeling Results

In this section, we compare the results of our proposed model (Eq. (3.26)) with those of the previous model (Cai et al. 2012). Then, we investigate the effect of hydrostatic pressure by comparing the results of Eq. (3.26) and Eq. (3.19). We also investigate the effect of D_f and D_{min} on the initial imbibition rate and equilibrium time.

3.6.1 Comparing Piston-Like and Non-Piston-Like Imbibition Models

As discussed before, we consider faster imbibition in larger capillaries and assume that the imbibition front is not piston-like. This is the main difference between our proposed model and the one developed by Cai et al. (2012). In this section, we model the co-current spontaneous imbibition of water using Eq. (3.26) and Eq. (A.15). Both equations consider the effect of hydrostatic pressure on the spontaneous imbibition. Eq. (A.15) was derived based on the assumption that the imbibition of wetting phase will never reach top of the rock sample, which is

considered as a no-flow boundary (Cai et al. 2012). This assumption requires the height of the rock sample to be high enough to allow equilibrium of hydrostatic and capillary forces. Thus, in order to compare the proposed model with Eq. (A.15), we assume the rock sample is infinitely long ($H=\infty$) in Eq. (3.26).

Table 3.1: Fluid properties used for modeling co-current spontaneous imbibition.

Fluid	Water
Density, ρ (g/cm^3)	1.0
Viscosity, μ (mPa.s)	1.0
Surface tension, σ (mN/m)	72.7
Contact angle, θ (degree)	30

Table 3.2: Rock properties used for modeling co-current spontaneous imbibition.

Cross sectional area, A_f (cm^2)	3
Porosity in Eq. (A15), ϕ (fraction)	0.2
Surface porosity in Eqs. (3.19) and (3.26), ϕ' (fraction)	0.2
Mean diameter of particles, D_s (cm)	0.02

The parameters used for modelling spontaneous imbibition are listed in Tables 3.1 and 3.2. It is worth to mention that Eq. (A.15) considers porosity (ϕ) equals to the 'surface porosity' (ϕ'). However, in this study we consider ϕ' which is smaller than ϕ based on Eq. (3.13). Since the area open to flow affects the imbibition rate, assuming ϕ' in Eq. (3.26) equal to ϕ in Eq. (A.15) leads to consistent open to flow area for both models. According to the correlations presented in Section 3.5, the unknown parameters are calculated and listed in Table 3.3. The value of D_f in Table 3.3 was calculated by Eq. (A.12) (Cai et al. 2012). As shown in Eq. (A.12), D_{min} and D_{max} would change with D_f for a given ϕ. However, in this chapter we investigate the effect of each parameter on modeling results by keeping the other parameters constant. Therefore, we do not apply Eq. (A.12) into Eq. (3.26) nor Eq. (A.15).

Table 3.3: Unknown parameters calculated by using the fluid and rock properties.

Maximum diameter D_{max} (μm)	59.88
Minimum diameter D_{min} (μm)	0.5988
Fractal dimension D_f	1.65
Average Tortuosity τ	1.66

Figs. 3.6a-c compare the imbibed mass of water versus time by Eq. (3.26) and Eq. (A.15) for a bundle of capillaries with different values of D_f, using the parameters in Tables 3.1-3.3. The results show that the imbibition rate of water modeled by Eq. (3.26) is always higher than that modeled by Eq. (A.15). This can be explained by different displacement patterns in the two models. The imbibition process in Eq. (A.15) is considered as piston-like displacement, which means an average rate of liquid imbibition inside all the capillaries is assumed. However, we assume that the wetting phase imbibes faster in larger capillaries. In other words, straight height (L_s) of the liquid column in larger capillaries is higher than that in smaller capillaries at a certain time. Fig. 3.7 compares the imbibition rates predicted by the previous model (Cai et al. 2012) and the proposed model. We obtain the average imbibition rate for the previous model (Cai, Hu, et al. 2012) through dividing Eq. (A.15) by ($\rho A_f \phi \tau$). For the proposed model, Eq. (3.7) is used to calculate the liquid imbibition rate in maximum (D=D_{max}) and minimum (D=D_{min}) capillaries. The parameters in Tables 3.1-3.3 are also used in Fig.3.7. As shown in Fig. 3.7, Eq. (A.15) overestimates the imbibition rate in small capillaries but underestimates the imbibition rate in large capillaries. As the imbibed mass of liquid in larger capillaries plays a more pronounced role in the total imbibed mass, Eq. (3.26) predicts higher imbibition rate than Eq. (A.15).

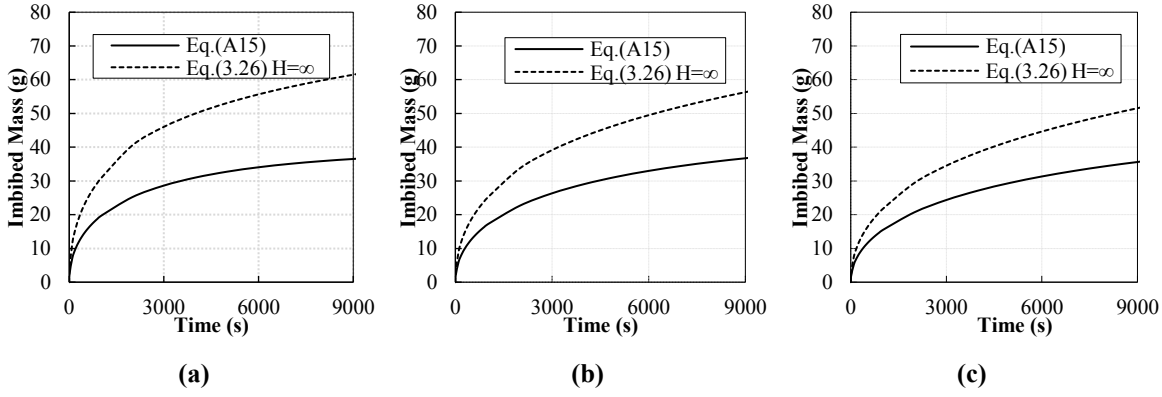

Fig. 3.6. Co-current spontaneous imbibition of water modeled by Eq. (A.15) and Eq. (3.26) for a

bundle of capillary tubes with D_f of (a) 1.1, (b) 1.65 and (c) 1.9. D_{max}=59.88 µm, D_{min}=0.5988 µm and τ=1.66 for all three figures.

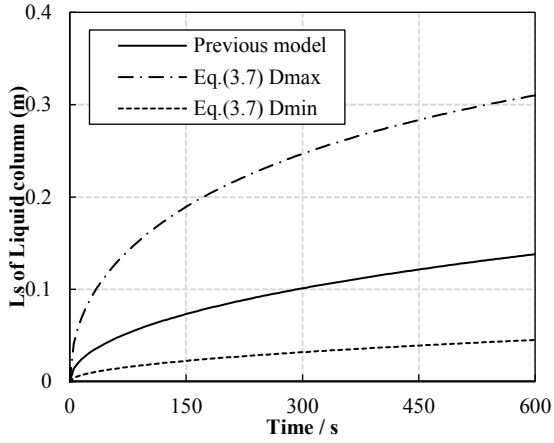

Fig. 3.7. Comparison of imbibition rate predicted by the previous model (Cai, Hu, et al. 2012), Eq. (3.7) with D=D_{max}, and Eq. (3.7) with D=D_{min}.

Figs. 3.6a-c also show the imbibition rate increases with the increasing D_f and Eq. (3.26) is more sensitive to the D_f changes compared with Eq. (A.15). To illustrate the effect of D_f on the pore size distribution of rock sample, we define the fractional number of pores ($f(D)$) as

$$f(D) = \frac{n(D)}{N_f(\geq D_{min})} \tag{3.29}$$

Substituting Eqs. (3.12) and (3.23) into Eq. (3.29) gives

$$f(D) = \frac{D^{-D_f} - (D + \Delta D)^{-D_f}}{D_{min}^{-D_f}} \tag{3.30}$$

We use MATLAB to compute the fractional number of pores with diameter from D_{min} to D_{max} by using Eq. (3.30). ΔD=D_{min}/10 is chosen. Fig. 3.8 is the log-log plot of $f(D)$ versus pore diameter. According to this figure, a porous media with larger D_f has relatively lower number of larger pores. Since imbibed mass in larger pores has significant impact on the total imbibed mass, the samples with higher number of larger pores (smaller D_f) have higher imbibition rate as shown in Figs. 3.6a-c.

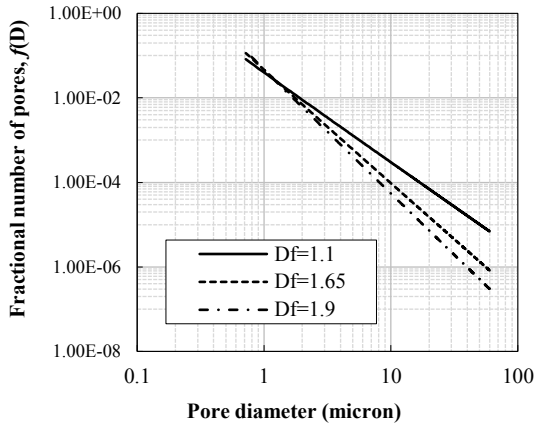

Fig. 3.8. Fractional number of pores ($f(D)$) versus pore diameter (D) in bundle of capillaries for different values of D_f.

Fig. 3.9 shows the imbibed mass of water versus time predicted by Eq. (3.26) for different values of H, using the parameters in Tables 3.1-3.3. As Eq. (A.15) does not account for H, the predicted result remains similar to that presented in Fig. 3.6b. Fig. 3.9 indicates that the value of H in Eq. (3.26) should be as high as 0.45 m to result in an equilibrated imbibed mass close to that predicted by Eq. (A.15). In other words, Eq. (A.15) is valid only if the H of rock sample to be as high as 0.45 m. In addition, the three curves in Fig. 3.9 modeled by Eq. (3.26) show a similar imbibition rate at initial period (< 2000 s), which indicates the insignificant effect of H on the initial imbibition rate.

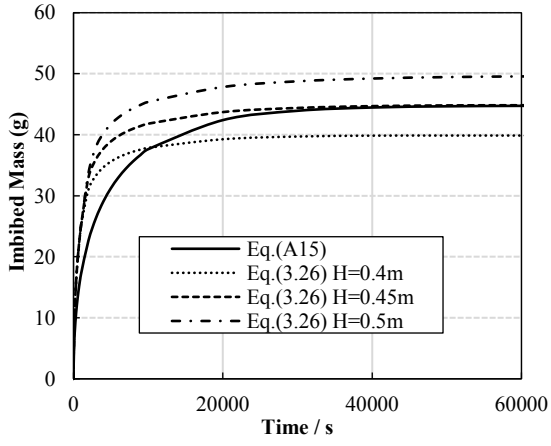

Fig. 3.9. Co-current spontaneous imbibition of water modeled by Eq. (A.15) and the proposed semi-analytical expression Eq. (3.26) for rock samples with different height (H).

3.6.2 Effect of Hydrostatic Pressure on Initial Imbibition Rate and Equilibrated Mass

In order to discuss the effect of hydrostatic pressure on co-current spontaneous imbibition of water, we compare the results modeled by Eq. (3.19) and Eq. (3.26). We use the parameters presented in Tables 3.1-3.3. ϕ' is calculated by Eq. (3.13).

Figs. 3.10a-c show the results of Eq. (3.19) and Eq. (3.26) for values of H equal to 0.5 m, 1 m, and 2 m. The difference between the two curves in each plot is attributed to the hydrostatic pressure and the difference becomes more significant with increasing H. This observation indicates that the hydrostatic pressure not only reduces the imbibition rate but also equilibrates the capillary pressure and ceases the imbibition of liquid before reaching top of the rock sample. The equilibrium height of the liquid column (H^{eq}) inside a capillary under the effect of hydrostatic pressure can be estimated by

$$H^{eq} = \frac{4\sigma cos\theta}{D\rho g} \tag{3.31}$$

When $H^{eq} < H$ for a specific capillary, imbibition stops before reaching top of the capillary. Rearranging Eq. (3.31) gives

$$D^* = \frac{4\sigma cos\theta}{\rho g H} \tag{3.32}$$

Threshold diameter D^* means the wetting phase in the capillaries larger than D^* cannot reach top of the capillaries. For long samples, the effect of hydrostatic pressure is significant and using Eq. (3.19) leads to an overestimation of imbibed volume.

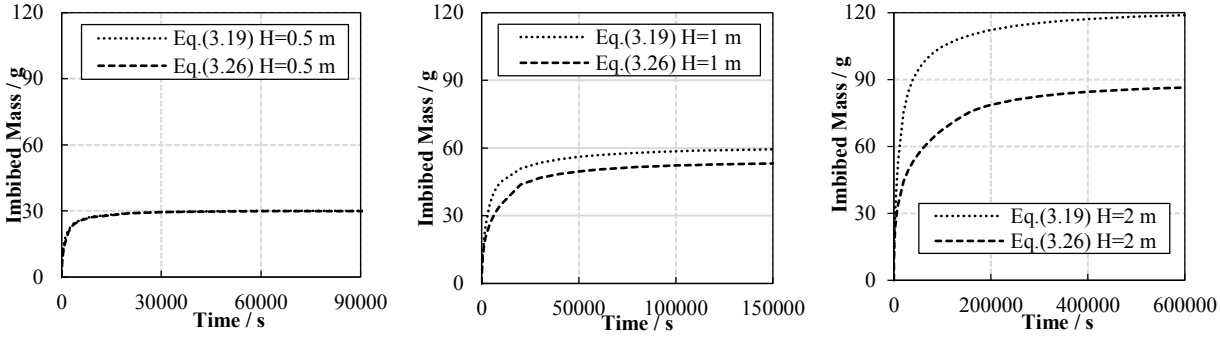

(a) **(b)** **(c)**

Fig. 3.10. Comparing the results of Eq. (3.19) and Eq. (3.26) for (a) *H*=0.5 m, (b) *H*=1 m, and (c) *H*=2 m.

3.6.3 Effect of Minimum Pore Diameter on Equilibrium Time

In this section, we investigate the effect of minimum pore diameter (D_{min}) on the imbibition process by using Eq. (3.19). We use the same parameters presented in Tables 3.1-3.3 except D_{min}. H is assumed to be 0.05 m and ϕ' is calculated by Eq. (3.13). According to Fig. 3.11, we keep the maximum diameter (D_{max}) constant while changing the ratio of D_{max}/D_{min} to study the effect of D_{min} on spontaneous imbibition process. We also keep D_f constant to isolate the effect of D_{min} on imbibition profile. We choose four different ratios of D_{max}/D_{min} (100, 200, 500 and 1000). The four values of D_{min} corresponding to the four ratios are 0.6, 0.3, 0.1 and 0.06 μm. By decreasing D_{min}, the pore size distribution of the porous media becomes wider.

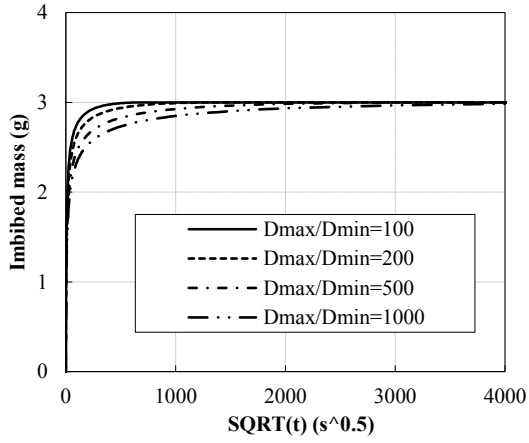

Fig. 3.11. Spontaneous imbibition of water into the porous media for different values of D_{min}.

As shown in Fig. 3.11, D_{min} has a negligible effect on imbibition rate during the initial period ($t <$ 20 s). This is explained by the fact that the initial imbibition rate is mainly controlled by the imbibition of liquid into larger pores and we keep D_{max} constant. However, we can observe that as the pore size distribution becomes wider, the imbibition profiles become more smeared as shown in Fig. 3.11. Specifically, decreasing D_{min} increases the equilibrium time (t_{eq}). The equilibrium time for the four values of D_{min} (0.6, 0.3, 0.1 and 0.06 μm) are 750, 1500, 4500 and 7500 s. The negative relation between D_{min} and t_{eq} can be explained by the fact that the wetting phase imbibes faster into larger capillaries compared with smaller capillaries. As schematically shown in Fig. 3.4, t_{eq} can be interpreted as the time needed for the wetting phase to fill the

capillaries with D_{min}. If we ignore the hydrostatic pressure for samples with small height, t_{eq} can be calculated by rearranging Eq. (3.4)

$$t_{eq} = \frac{4\mu(H\tau)^2}{\sigma cos\theta D_{min}} \tag{3.33}$$

t_{eq} is inversely proportional to D_{min}, which is consistent with the equilibrium times presented in Fig.3.11. Eq. (3.33) can be used to determine D_{min} using experimental imbibition data and t_{eq}. As discussed before, D_{min} for the tight and shale rock samples with ultra-low permeability cannot be detected by MICP test. Eq. (3.33) provides a new solution to estimate D_{min} using experimental imbibition data. Eq. (3.33) for the calculation of D_{min} originally comes from the non-piston-like assumption. In piston-like displacement model, the liquid inside all the capillaries reaches the top of the rock sample at the same time and we cannot use t_{eq} to calculate D_{min}.

3.7 Limitations of the Modified Fractal Model

The proposed model can be extended in future to address the following limitations:

(1) We assume there is no interconnection between capillaries, therefore, the liquid imbibes straight upward. However, the interconnection between pores commonly exists in natural porous media and may lead to backfilling (Chandler et al. 1982; Peters 1990) and meniscus arrest (Gruener et al. 2012; Sadjadi and Rieger 2013; Sadjadi et al. 2015) mechanisms:

(a) One of the mechanisms of fluid imbibition in interconnected pores is backfilling (Chandler et al. 1982; Peters 1990), as shown in Fig. 3.12a. At an early time (t_1), the wetting liquid (blue) imbibes into both large and small pores simultaneously and displaces the air. As the fluid imbibes relatively faster in the large pore, it reaches the junction earlier than the fluid in small pore, and then backfills the small pore. The air inside the small pore will be trapped due to the backfilling (Peters 1990). Thus, assuming elongated pores without any interconnection may overestimate the imbibed volume of wetting liquid in the smaller pores.

(b) Another notable mechanism is meniscus arrest (Gruener et al. 2012; Sadjadi and Rieger 2013; Sadjadi et al. 2015). As shown in Fig. 3.12b, a Y-shaped junction consists of three pores: a feeding pore as the fluid entrance and two branch pores, one wider than the feeding pore and one narrower than the feeding pore. When the liquid invades the feeding pore and reaches the Y-shaped junction,

the meniscus is split into two. The meniscus in the narrow pore immediately propagate while the meniscus in the wide pore is arrested until the pressure in the Y-shaped junction exceeds the pressure in the wide pore. Therefore, the imbibition rate in the larger pores will be overestimated if we do not account for the interconnection between individual pores and possible meniscus arrest.

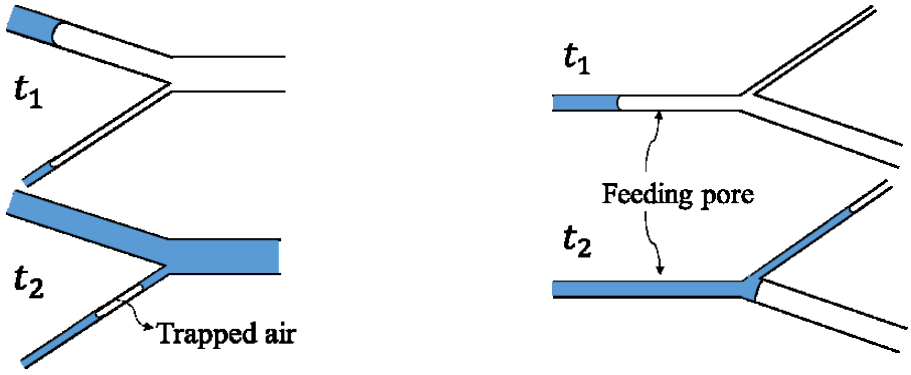

Fig. 3.12. Schematic view of (a) backfilling of smaller pores (Chandler et al. 1982, Peters 1990) and (b) Meniscus arrest in larger pores (Gruener et al. 2012, Sadjadi et al. 2015, Sadjadi and Rieger 2013) due to the interconnection between pores with different diameters (t1<t2).

(2) In order to compare the proposed model with the previous fractal model (Cai et al. 2012), we assumed constant tortuosity for all the pores regardless of pore diameters. However, the tortuosity was found to depend on (1) pore diameter and (2) pore length based on the fractal theory (Cai and Yu 2011; Schopf et al. 2017). Specifically, the pores with smaller diameter usually have higher degrees of tortuosity. Using an average value of tortuosity might underestimate tortuosity of small pores, which in turn underestimates the minimum pore diameter calculated by Eq. (3.33).

3.8 Summary

In this chapter, we derived a new model for spontaneous imbibition of wetting phase into the fractal porous media. The significant difference between the proposed model with the previous model (Cai et al. 2012) is that we assume imbibition front is not uniform, which means the liquid inside capillaries with different diameters reaches the top of the rock sample at different times if hydrostatic pressure can be neglected. Compared with the previous model (Cai et al. 2012), the proposed model is still valid after the wetting phase reaches top of the rock sample, which makes the model more applicable in analyzing the experimental data.

An analytical equation without considering hydrostatic pressure and a semi-analytical equation with considering hydrostatic pressure were derived. The proposed model is highly sensitive to the pore size distribution (PSD) of the porous media. This feature can help us to characterize the pore network of the rock samples by analyzing spontaneous imbibition data. Moreover, the sensitivity analysis indicates the minimum pore diameter (D_{min}) controls the equilibrium time (t_{eq}) in the spontaneous imbibition process. On the basis of this finding, we proposed a new solution to calculate D_{min} of rock samples by analyzing spontaneous imbibition data.

Chapter 4: Characterizing the Dual-Wettability Pore Network by Using Modified Fractal Model

4.1 Introduction

The objective of this chapter is to compute the water-wet and water-repellant pore size distributions (PSDs) of the unconventional rocks by analyzing the comparative oil and brine imbibition data. A previously-proposed fractal model which considers the non-piston-like imbibition front is used to achieve this objective. We use a history matching technique to match the measured imbibition data with the proposed fractal model, and determine the parameters such as fractal dimension (D_f) and minimum pore diameter (D_{min}) that controlling imbibition profile. The determined parameters are then used to calculate PSD. The PSD of oil-wet pores (PSD_{oil}) is calculated by oil imbibition data and the PSD of water-wet pores (PSD_{water}) is calculated by brine imbibition data. The PSD of water-repellant pores ($PSD_{water\text{-}repellant}$) is calculated by decoupling of PSD_{oil} and PSD_{water}.

In this chapter, we propose the hypothesis in sections 4.2. Section 4.3 introduces the detailed theory and procedure for analyzing the comparative imbibition data and calculating PSD_{water} and $PSD_{water\text{-}repellant}$. The results of PSD_{water} and $PSD_{water\text{-}repellant}$ for the Montney rock samples are presented in section 4.4. Sections 4.5 and 4.6 present the limitations and primary conclusions of this work.

4.2 Assumptions and Hypotheses

By analyzing the comparative imbibition data as well as the petrophysical properties of unconventional rock samples, the following assumptions were proposed and qualitatively validated in the previous studies (Lan et al. 2015; Yassin et al. 2016):

(a) High imbibed volume of oil suggests that oil can imbibe into most of the pores, including inorganic and organic pores.

(b) Low imbibed volume of brine suggests that brine can only imbibe into the inorganic pores.

(c) The size of organic pores is generally smaller than the size of inorganic pores.

It is evident that the imbibition process is strongly related to the pore network of porous media (Akin and Kovscek 1999; Blunt 2001; Cai et al. 2010; Gruener et al. 2016). For instance, the

maximum pore diameter significantly affect the initial imbibition rate. In this study, we expect that the PSD can be calculated by analyzing the imbibition data. As mentioned in the assumptions, we can calculate PSD_{water} by analyzing the brine imbibition data and calculate PSD_{oil} by analyzing oil imbibition data. Then, $PSD_{water\text{-}repellant}$ can be calculated by the decoupling of PSD_{oil} and PSD_{water}.

4.3 Theory of Imbibition Transient Analysis (ITA) Method

In this section, we propose a new Imbibition Transient Analysis (ITA) method to characterize the dual-wettability pore network based on oil and brine imbibition data. We analyze the imbibition data with our proposed fractal model (Shi et al. 2017) and determine the unknown parameters such as fractal dimension (D_f) and minimum pore diameter (D_{min}) that control the imbibition process. Then, the determined parameters are utilized to calculate PSD_{water} and $PSD_{water\text{-}repellant}$. Section 4.3.1 reviews our previously-proposed fractal model (Shi et al. 2017) and Section 4.3.2 presents the procedure for determining the unknown parameters, such as D_f and D_{min}, in the fractal model. Section 4.3.3 introduces the equations for calculating PSD_{water} and $PSD_{water\text{-}repellant}$ by using the determined values of the unknown parameters.

In this study, we consider the pore network of rock samples as an idealized bundle of capillaries with different diameters, as shown in Figs. 4.1a-b. The idealized pore network is considered as a dual-wettability system, where larger pores are hydrophilic inorganic pores while smaller pores are hydrophobic organic pores. According to the assumptions in Section 4.2, oil (green colored) can imbibe into both large inorganic and small organic pores, while brine (blue colored) only imbibes into larger inorganic pores.

All the pores are exposed to liquid at the bottom of the sample and imbibition process in all the pores starts simultaneously. The spontaneous imbibition of wetting fluid into the capillaries can be considered as laminar flow described by the Lucas-Washburn (L-W) equation (Lucas 1918; Washburn 1921). On the basis of the L-W equation, the imbibition rate of wetting phase is positively proportional to the square root of pore diameter. As different capillaries have different imbibition rates, imbibition process is not piston-like and imbibition front is not uniform, as shown in Figs. 4.1a-b. The non-piston-like imbibition front has also been experimentally observed by neutron imaging and x-ray computerized tomography scanning (Schembre et al. 1998; Gruener et al. 2012; Gruener et al. 2016).

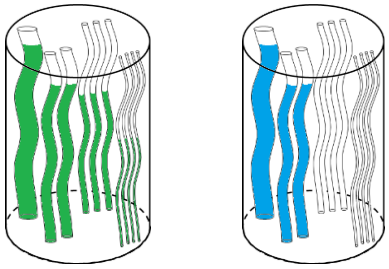

Fig. 4.1. Schematic illustration of co-current spontaneous imbibition of (a) oil and (b) brine into a bundle of dual-wet capillaries with different diameters.

Figs. 4.2a shows the measured profiles of oil and brine imbibition into one pair of Montney rock samples (UMT3), and Fig.4.2b schematically illustrates the corresponding distribution of oil and brine imbibing into the idealized bundle of capillaries. The rock sample is initially saturated with air (initial water saturation, S_{wi}=0) and the imbibed volume of liquid is zero at Stage 1. Stage 2 represents the initial period of imbibition process. On the basis of the aforementioned assumptions, oil imbibes into most of the pores while brine only imbibes into larger inorganic pores. The higher initial imbibition rate of oil compared with brine (Fig. 4.2a) is explained by the fact that more pores are available for oil uptake. Stage 3 represents the late period of imbibition process. Since the imbibition rate is higher in larger pores, oil has reached the top of larger pores and continues to imbibe into smaller pores. Therefore, the oil imbibition rate decreases dramatically as the larger pores are already filled with the oil. For brine imbibition, as brine can only imbibe into the larger pores, the equilibrated state has been already reached at Stage 3. The earlier equilibrium of brine compared with oil supports the presence of small water-repellant pores inaccessible for brine imbibition (Yassin et al. 2017). At Stage 4, all pores have been filled with the oil and the oil imbibition profile has reached the equilibrated state. In summary, non-piston-like liquid imbibition along with the assumptions explain the results of the imbibition tests for the Montney rock samples reasonably well.

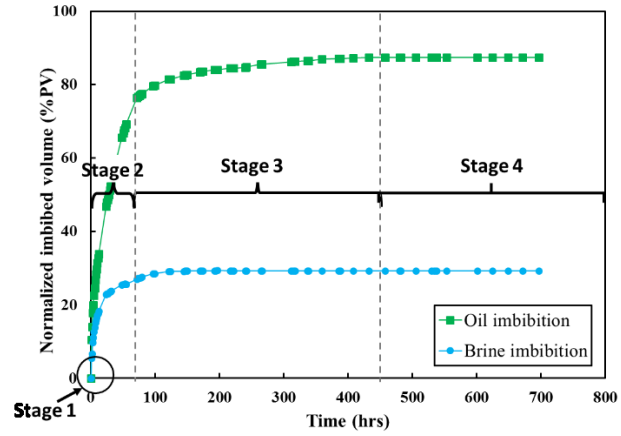

(a)

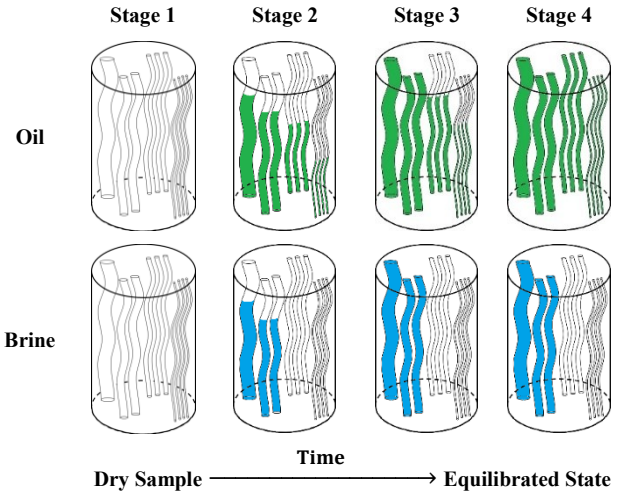

(b)

Fig. 4.2. (a) Experimental data of oil and brine imbibition into one pair of Montney rock samples (UMT3) and (b) schematic illustration of non-piston-like oil and brine imbibition into the idealized bundle of capillaries with dual-wettability characteristics.

4.3.1 Review of the Proposed Fractal Model for Co-current Spontaneous Imbibition

In this section, we review our proposed fractal model for non-piston-like co-current spontaneous imbibition (Shi et al. 2017).

Since the introduction of fractal theory by Mandelbrot (Mandelbrot 1967; Mandelbrot and Pignoni 1983), fractal theory has been widely used for characterizing the complex pore structure of rocks (Krohn 1988a; Yang et al. 2014; Lai et al. 2017). On the basis of fractal theory (Mandelbrot 1967;

Krohn 1988b; Yu and Cheng 2002), the number of pores with a particular diameter is a function of (1) pore diameter and (2) fractal dimension:

$$N(\geq D) = (\frac{D_{max}}{D})^{D_f} \tag{4.1}$$

Here, N is the total number of pores with diameter equal to or larger than D, D_{max} is the maximum pore diameter in a self-similar unit or porous media, and D_f is the fractal dimension which controls the PSD. In two-dimensional space, D_f lies in $1<D_f<2$ (Cai et al. 2012). According to Eq. (4.1), the number of pores increases with decreasing pore diameter, which is also qualitatively illustrated in Figs. 4.1-4.2. Shi et al. (2017) proposed a modified fractal model for co-current spontaneous imbibition of wetting liquid into the bundle of capillaries. The model is derived from spontaneous imbibition in a single capillary (Poiseuille 1844):

$$L_s = \sqrt{\frac{D\sigma\ cos\theta}{4\mu\tau^2}}\sqrt{t} \tag{4.2}$$

L_s is the straight length of the liquid column inside a capillary. D is the capillary diameter. σ is the air-liquid surface tension. θ is the air-liquid contact angle and μ is the liquid viscosity. τ is the tortuosity which is defined as the ratio of the tortuous length over straight length (Carman 1937):

$$\tau = \frac{L_f}{L_s} \tag{4.3}$$

L_f is tortuous length of the liquid column inside a capillary. Eq. (4.2) is similar to Lucas-Washburn (L-W) equation (Lucas 1918; Washburn 1921) except the tortuosity term, and indicates that the larger the diameter of the capillary (D), the faster the liquid fills the capillary. Therefore, instead of assuming a piston-like displacement, we considered a non-piston-like imbibition front (Shi et al. 2017). In other words, the liquid inside larger capillaries reaches the top of the rock sample faster than that in smaller capillaries.

To model the spontaneous imbibition process, we developed an analytical equation without considering hydrostatic pressure and a semi-analytical equation with considering the hydrostatic pressure (Shi et al. 2017). The role of hydrostatic pressure is usually negligible compared with that of capillary pressure, especially for the small scale rock samples (less than 10 cm in height).

Therefore, in this paper, we use the following equation without considering the hydrostatic pressure:

$$M_T = \frac{A_f \rho}{2D_{max}^{2-D_f}} \frac{\phi_a'}{1-\left(\frac{D_{min}}{D_{max}}\right)^{2-D_f}} \sqrt{\frac{\sigma cos\theta}{\mu}} \left(\frac{2-D_f}{2.5-D_f}\right) \left[D_C^{2.5-D_f} - D_{min}^{2.5-D_f}\right] \sqrt{t} + \frac{A_f \rho H}{D_{max}^{2-D_f}} \frac{\phi_a}{1-\left(\frac{D_{min}}{D_{max}}\right)^{2-D_f}} \left[D_{max}^{2-D_f} - D_C^{2-D_f}\right] \quad (4.4)$$

M_T is total imbibed mass of wetting liquid at a certain time. A_f and H are cross-sectional area and height of the rock sample. D_{max} and D_{min} are the maximum and minimum pore diameters, respectively. ρ is the density of wetting liquid. Wetting porosity (ϕ_a) is the ratio of the equilibrated volume of imbibed oil or brine (V_{io} or V_{iw}) to V_B and wetting surface porosity (ϕ_a') is the ratio of effective pore area open to oil or brine imbibition (A_o or A_w) to A_f. Figs. 4.3a and 4.3b schematically show the relationship between ϕ_a and ϕ_a' for oil imbibition (ϕ_{ao} and ϕ_{ao}') and brine imbibition (ϕ_{aw} and ϕ_{aw}'), respectively.

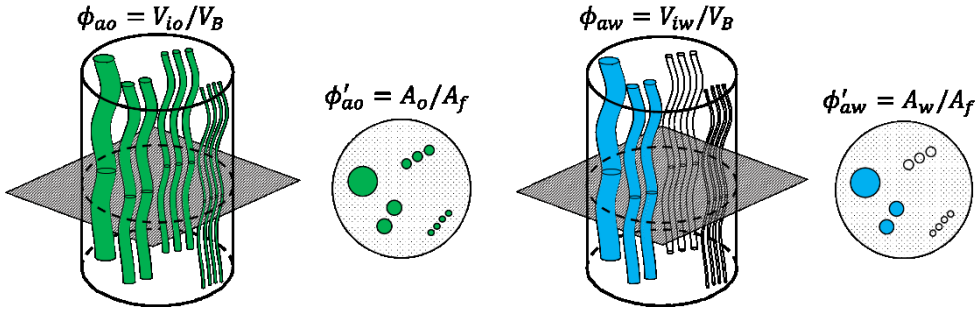

Fig. 4.3. Schematic diagram illustrating the relationship between ϕ_a and ϕ_a' for (a) oil imbibition (ϕ_{ao} and ϕ_{ao}') and (b) brine imbibition (ϕ_{aw} and ϕ_{aw}').

In the original version of Eq. (4.4), we use effective porosity (ϕ) and surface porosity (ϕ') because Eq. (4.4) was used for the case where the imbibition liquid is wetting phase for all pores. In this dual-wettability study, we use ϕ_a and ϕ_a' to account for the case where the imbibition liquid is non-wetting phase for some of the pores. D_C is the diameter of the capillaries that are just filled by the liquid at time t

$$D_C = \frac{4\mu\tau^2 H^2}{\sigma cos\theta t} \quad (4.5)$$

D_C is a time-dependent parameter and should lie in the range of D_{min} to D_{max}. As described in Fig. 4.2, D_C decreases with time as smaller pores are filled later than larger pores.

In Eqs. (4.4) and (4.5), ρ, θ, σ, μ, A_f and H are the known physical parameters and ϕ_a, ϕ_a', τ, D_f, D_{max} and D_{min} are the unknown parameters. In section 4.3.2, a detailed procedure for determining these unknown parameters will be presented.

4.3.2 Determination of the Unknown Parameters

In this section, we introduce the methods for determining the unknown parameters in Eq. (4.4). The determined parameters will be used for calculating the PSD_{water} and $PSD_{water\text{-}repellant}$, which will be discussed in Section 4.3.3.

D_{max} and D_{min}

We obtain the value of D_{max} using the available MICP data. In MICP test, the pressure corresponding to the start of mercury intrusion is converted to maximum pore-throat size using Young-Laplace equation (Thomas et al. 1968). Mercury is a non-wetting phase, and the mercury intrusion is a drainage process which is mainly controlled by the pore-throat size (Wardlaw and Taylor 1976). On the other hand, spontaneous imbibition of wetting phase is mainly controlled by pore-body size (Valvatne and Blunt 2004). Therefore, D_{max} might be underestimated by use of MICP data.

Similar to D_{max}, MICP data can be used for determining D_{min}. Pore-throat diameter corresponding to mercury pressure at mercury saturation of 100% pore volume (PV) is considered as D_{min}. However, for some of the tight Montney rock samples with absolute permeability in the order of nanodarcy (Lan et al. 2015), mercury fills less than 60% of the pore volume (Lan et al. 2015; Yassin et al. 2017) at maximum mercury pressure of 400 MPa. In other words, mercury pressure may not be high enough to detect D_{min}. Therefore, we need to look for other methods to determine D_{min}. As schematically shown in Fig. 4.2, the equilibrated time (t_{eq}) of the imbibition profile can be interpreted as the time needed for the wetting phase to fill the capillaries with D_{min}. In our previous study (Shi et al. 2017), we developed an equation to calculate D_{min} using t_{eq}:

$$D_{min} = \frac{4\mu(H\tau)^2}{\sigma cos\theta t_{eq}} \tag{4.6}$$

Then only unknown parameter in Eq. (4.6) is τ. Once τ is specified, D_{min} can be calculated using Eq. (4.6).

ϕ_a and ϕ_a'

According to Fig. 4.3a-b, wetting porosity (ϕ_a) and wetting surface porosity (ϕ_a') are not necessarily the same. For oil imbibition case, V_{io} can be calculated by

$$V_o = (A_f \phi_a')\tau H \tag{4.7}$$

According to the definition of ϕ_a, V_o can also be determined by

$$V_o = V_B \phi_a = A_f H \phi_a \tag{4.8}$$

Thus, ϕ_a and ϕ_a' follow

$$\phi_a = \phi_a' \tau \tag{4.9}$$

For brine imbibition, ϕ_{aw} is also equal to $\tau\phi_{aw}'$.

ϕ_a is equal to ϕ_a' only when the capillaries are straight (τ=1). Schopf et al. (2017) also applied Eq. (4.9) for developing a model of spontaneous imbibition into highly porous layers of aggregated particles. ϕ_a can be determined from experimental imbibition data. According to Eq. (4.9), once τ is specified, ϕ_a' can be determined accordingly.

τ and D_f

For a fixed value of ϕ_a, larger τ results in smaller value of ϕ_a' (Eq. (4.9)), leading to smaller area open for liquid imbibition. Thus, τ is one of the parameters that controling the imbibition rate. τ, firstly introduced by Carman (1937), has different definitions (geometrical, hydraulic, electrical, and diffusional tortuosity) for different transport processes in porous media. Thus, the values of tortuosity varies from one to another due to different definitions (Cornell and Katz 1953; Van et al 1974; Clennell 1997; Ziarani and Aguilera 2012). In this study, we use hydraulic tortuosity which is defined by Eq. (4.3). Matyka et al. (2008) conducted a comprehensive review of the

empirical correlations for hydraulic tortuosity as a function of effective porosity (ϕ) and indicated that Eq. (4.10) gives the best matching results:

$$\tau = 1 - p\ln(\phi) \tag{10}$$

Here, p is a fitting parameter with the values ranging from 0.49 to 1.00 (Weissberg 1963; Ho and Striender 1981; TSAI and STRIEDER 1986; Comiti and Renaud 1989; Barrande et al. 2007). Using the effective porosity of the Montney rock samples (Lan et al. 2015) in Eq. (4.10), the calculated value of tortuosity lies between 2.0 and 4.5.

Fractal dimension, D_f, affects the imbibition rate by controling the pore size distribution of the porous media. To illustrate the effect of D_f on the pore size distribution, we define the fractional number of pores ($f(D)$) as

$$f(D) = \frac{n(D)}{N_f(\geq D_{min})} \tag{4.11}$$

where $n(D)$ is the incremental number of pores with diameter of D and $N_f(\geq D_{min})$ is the total number of pores. The equations for $n(D)$ and $N_f(\geq D)$ are presented in Section 4.3.3. Fig. 4.4a presentes $f(D)$ calcualted by Eq. (4.11) versus D for diferent values of D_f. Fig. 4.4b shows the total imbibed mass (M_T) of water versus time calculated by Eq. (4.4) for different values of D_f. According to Fig. 4.4a, the porous media with larger D_f has relatively lower number of larger pores (Katz and Thompson 1985; Tyler and Wheatcraft 1990). Since the imbibed mass of liquid in larger pores plays a more pronounced role in M_T, larger D_f shows slower imbibition rate, as shown in Fig. 4.4b.

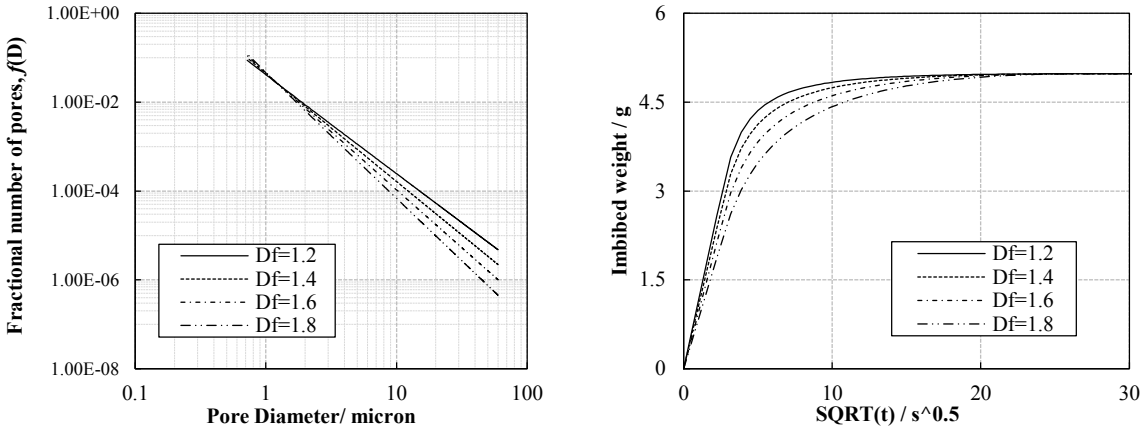

(a) **(b)**

Fig. 4.4. (a) $f(D)$ (Eq. (4.11)) versus D using D_{max}=60 µm and D_{min}=0.6 µm. (b) Total imbibed mass of water (Eq. (4.4)) versus time using σ =72.7 mN/m, μ =1 mP·S, ρ =1 g/cm^3, θ =30°, A_f= 3 cm^2, H =5 cm, ϕ_a=0.2, D_{max}=60 µm and D_{min}=0.6 µm.

In this paper, we use history matching technique and determine τ and D_f by matching Eq. (4.4) with the experimental imbibition data. The history matching process is implemented using MATLAB software (Peters et al. 2010). We use Genetic Algorithm (GA) as an optimaztion tool to get the best match between experimental imbibition data and Eq. (4.4). GA, firstly introdueced by John Holland (1975), is a search method that inspired by natural evolution (Sen et al. 1995; Harding et al. 1998; Patel et al. 2005). GA does not need the objective function (*OF*) to be continuous and differentiable and can avoid local optima (Guerreiro et al. 1998). τ and D_f are two variables with the search space of 2.0 to 4.5 and 1 to 2, respectively. The search space of τ is estimated by Eq. (4.10). $1<D_f<2$ is used as we consider fractal geometry in a two-dimensional space (Cai et al. 2012). *OF* is defined as

$$OF = \frac{1}{N_{exp}} \cdot \sum_{i=1}^{N_{exp}} \left| \frac{M_i - M_i^{exp}}{M_i^{exp}} \right| \tag{4.12}$$

where N is the number of experimental imbibition data points before reaching the equilibrated state. M_i is calculated by Eq. (4.4) and M_i^{exp} is the imbibed mass of wetting liquid from imbibition tests. *OF* is minimized by GA. Fig. 4.5 presents the detailed procedure for determining τ and D_f by minimization of *OF*.

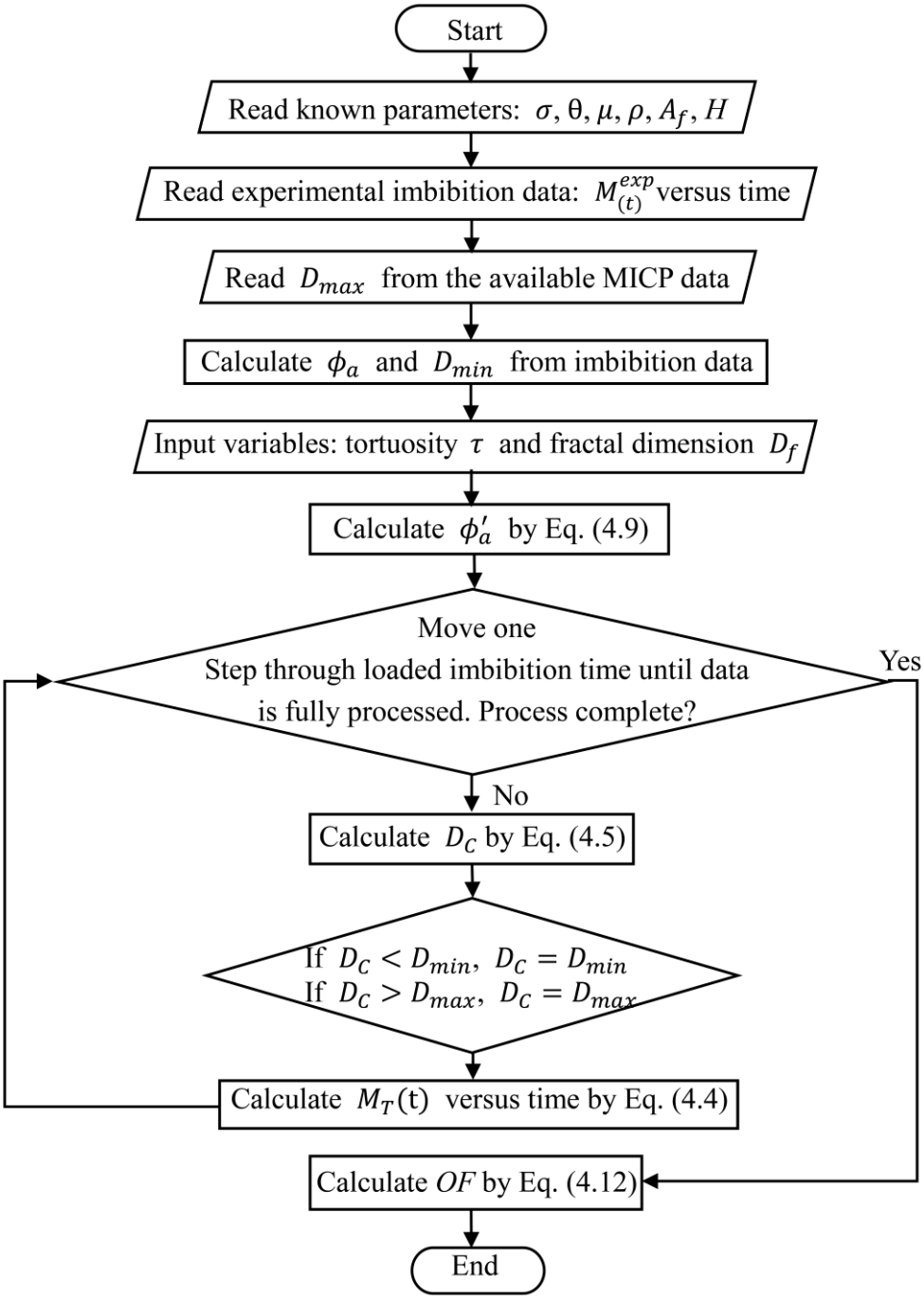

Fig. 4.5. The procedure for determining the τ and D_f by minimization of the objective function (*OF*).

In summary, D_{max} is obtained from the available MICP data; D_{min} is determined from equilibrated time of imbibition test using Eq. (4.6); ϕ_a is calculated from equilibrated imbibed volume of liquid;

ϕ_a' is calculated by Eq. (4.9); and τ and D_f are determined by minimization of the *OF*. Once D_{min} and D_f are determined from oil and brine imbibition data and D_{max} are obtained from MICP data, the PSD_{oil} and PSD_{water} can be calculated.

4.3.3 Calculation of PSD

In this section, we derive the equation for computing the PSD by using the parameters determined in Section 4.3.2.

The number of capillaries with diameter larger than D in the rock sample (N_f) is calculated by (Wu and Yu 2007; Yu et al. 2009)

$$N_f(\geq D) = \frac{A_f \times \phi_a'}{A_{pu}} N(\geq D) = \frac{4A_f}{\pi D_{max}^{2-D_f}} \frac{2-D_f}{D_f} \frac{\phi_a'}{1-\left(\frac{D_{min}}{D_{max}}\right)^{2-D_f}} D^{-Df} \tag{4.13}$$

Here, A_{pu} is the cross-sectional area of unit cell. By differentiating Eq. (4.13) with respect to D, we can calculate the incremental number of capillaries ($n(D)$) with diameters in the range of D to $D+dD$ (Cai et al. 2012):

$$n(D) = -dN_f = \frac{4A_f}{\pi D_{max}^{2-D_f}} \frac{(2-D_f)\phi_a'}{1-\left(\frac{D_{min}}{D_{max}}\right)^{2-D_f}} D^{-(D_f+1)} dD \tag{4.14}$$

In Eq. (4.14), $dN_f < 0$ implies that the number of capillaries decreases with increasing the pore diameter (Yu et al. 2009). Then, we calculate the incremental volume of the capillaries ($V(D)$) with diameters between D_1 and D_2 by integrating Eq. (4.14) from D_1 to D_2:

$$V(D) = \int_{D_1}^{D_2} v(D)\, n(D) = \int_{D_1}^{D_2} \left(\frac{\pi D^2}{4} \tau H\right) \cdot n(D) \tag{4.15}$$

D_1 and D_2 are the two pore diameters that satisfy $D_{min}<D_1<D_2<D_{max}$. Inserting Eq. (4.14) into Eq. (4.15) gives

$$V(D) = \frac{A_f H \phi_a}{D_{max}^{2-D_f} - D_{min}^{2-D_f}} \left(D_2^{2-D_f} - D_1^{2-D_f}\right) \tag{4.16}$$

According to Eq. (4.16), once D_{max}, D_{min} and D_f are specified, we can calculate the volume of the capillaries with diameters between D_1 and D_2. Similarly, we use Eq. (4.16) to calculate the total accessible pore volume (V_T) with $D_1 = D_{min}$ and $D_2 = D_{max}$

$$V_T = \int_{D_{min}}^{D_{max}} v(D)\, n(D) = \frac{A_f H \phi_a}{D_{max}^{2-D_f} - D_{min}^{2-D_f}} \left(D_{max}^{2-D_f} - D_{min}^{2-D_f} \right) = A_f H \phi_a \tag{4.17}$$

The pore volume fraction of the capillaries with the diameter from D_1 to D_2 is calculated by dividing Eq. (4.16) by Eq. (4.17)

$$F(D)\% = \frac{V(D)}{V_T} = \frac{\left(D_2^{2-D_f} - D_1^{2-D_f} \right)}{\left(D_{max}^{2-D_f} - D_{min}^{2-D_f} \right)} \times 100 \tag{4.18}$$

$F(D)$ is normalized frequency. Eq. (4.18) is the primary equation for calculation of the PSD. The parameters controlling the PSD are D_f, D_{max}, and D_{min}. As presented in section 4.3.2, these three parameters can be determined by analyzing the oil and brine imbibition data. Therefore, the PSD_{oil} and PSD_{water} can be calculated by Eq. (4.18). Finally, the PSD of organic pores ($PSD_{water\text{-}repellant}$) can be calculated by the decoupling of PSD_{oil} and PSD_{water} (2017)

$$PSD_{water-repellant} = \frac{PV_{oil} PSD_{oil} - PV_{water} PSD_{water}}{PV_{water-repellant}} \tag{4.19}$$

where, PV is the pore volume. It is worth noting that Eq. (4.19) is based on the assumption that oil can imbibe into both hydrophilic inorganic and hydrophobic organic pores but brine cannot imbibe into hydrophobic organic pores.

4.4 Results and Discussions

In this section, we apply the ITA method to characterize the pore network of the Montney rock samples (Lan et al. 2015). Five samples are from the upper Montney Formation (UMT) and four samples are from the lower Montney Formation (LMT). Compared with UMT rock samples, LMT rock samples have relatively lower porosity and permeability (Lan et al. 2015). Table 4.1 summarizes the depth, dimensions, and petrophysical properties of the rock samples. The effective porosity of the rock samples is measured by helium porosimetry method. The absolute

permeability (K) is measured by pulse-decay technique on the offset rock samples. The air-liquid contact angle is obtained by measuring the contact angle of oil and brine droplets on dry surface of the rock samples before starting the imbibition tests. This contact angle is not necessarily the same as the contact angle at the pore scale. D_{max} and D_{min} of the rock samples are obtained from the MICP tests (Lan et al. 2015). We name the D_{min} obtained from MICP data as $D_{min\text{-}MICP}$. According to Table 4.1, D_{max} of the LMT rock samples is much smaller than that of UMT rock samples, which is in agreement with the relatively-lower porosity and permeability of the LMT rock samples.

Table 4.2 lists the physical properties of oil and brine used in the imbibition tests. Dodecane and 2 Wt% KCl are used as the oil and brine in the imbibition and contact angle measurement tests. Figs. 4.6a and 4.6b present the results of MICP test for UMT4 and LMT3 rock samples, respectively. The y-axis represents the fraction of PV invaded by mercury. The cumulative mercury saturations at the maximum pressure of 400 MPa for UMT4 and LMT3 samples are 90% and 60% of PV, respectively. The reason for the low cumulative mercury saturation of LMT3 rock samples is that mercury cannot access the nanopores with diameters less than 3-5 nm. MICP data for the other Montney rock samples were presented in the previous study (Lan et al. 2015).

Table 4.1: Depth, cross-sectional area, height, effective porosity, absolute permeability, air-liquid contact angle, maximum diameter, and minimum diameter for upper Montney and lower Montney samples. Subscripts *o* and *w* represent dodecane and brine, respectively (Lan et al. 2015).

Sample ID	Depth (m)	Cross-Sectional Area (cm^2)	Height (cm)	Porosity (fraction)	Permeability (mD)	Air-Liquid Contact Angle (°)	Maximum Diameter (nm)	Minimum Diameter (nm)
UMT 1_o	2127.21	10.752	6.60	0.051	–	0	131.0	4.50
UMT 1_w	2127.55	10.752	6.60	0.047	–	45.2	131.0	4.50
UMT 2_o	2130.20	10.752	6.80	0.057	3.89×10^{-3}	0	131.0	4.50
UMT 2_w	2130.57	10.752	6.90	0.049	3.89×10^{-3}	46.5	131.0	4.50
UMT 3_o	2137.45	10.752	6.60	0.064	2.35×10^{-2}	0	368.0	4.88
UMT 3_w	2137.83	10.752	6.70	0.069	2.35×10^{-2}	36.7	368.0	4.88
UMT 4_o	2144.01	10.752	6.70	0.072	1.05×10^{-1}	0	262.0	4.70
UMT 4_w	2144.37	10.752	6.95	0.078	1.05×10^{-1}	41.6	262.0	4.70
UMT 5_o	2150.74	10.752	6.75	0.057	4.42×10^{-3}	0	131.0	3.72
UMT 5_w	2151.17	10.752	6.50	0.051	4.42×10^{-3}	44.5	131.0	3.72

LMT 1_o	2323.20	10.752	6.75	0.036	1.50×10^{-2}	0	14.6	3.72
LMT 1_w	2323.53	10.752	6.70	0.040	1.50×10^{-2}	37.0	14.6	3.72
LMT 2_o	2329.80	10.752	6.90	0.029	2.33×10^{-3}	0	37.8	3.72
LMT 2_w	2330.22	10.752	6.95	0.032	2.33×10^{-3}	40.0	37.8	3.72
LMT 3_o	2340.29	10.752	6.55	0.036	2.04×10^{-3}	0	21.6	3.72
LMT 3_w	2340.61	10.752	6.60	0.040	2.04×10^{-3}	45.0	21.6	3.72
LMT 4_o	2346.98	10.752	6.75	0.041	1.01×10^{-2}	0	57.6	3.72
LMT 4_w	2347.28	10.752	6.60	0.045	1.01×10^{-2}	37.0	57.6	3.72

Table 4.2. Properties of oil and brine used for co-current spontaneous imbibition and contact angle tests (Lan et al. 2015).

Fluid	Density (g/cm^3)	Viscosity (cP)	Surface Tension (dynes/cm)
Dodecane	0.749	1.374	25.35
2 wt% of KCl	1.02	0.89	72.7

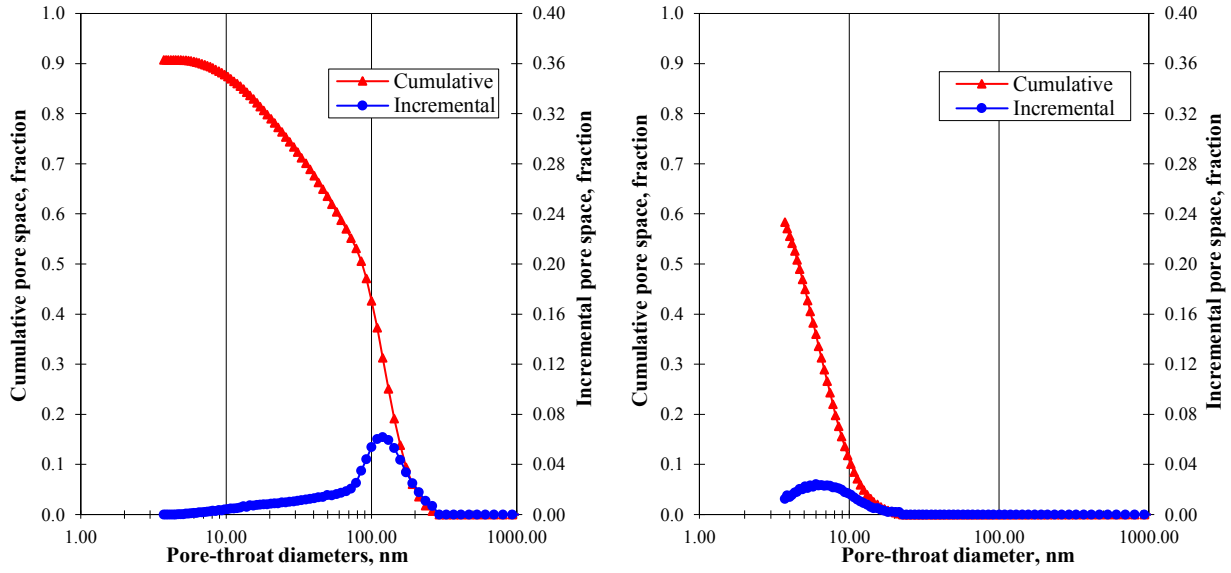

(a) **(b)**

Fig. 4.6. The results of MICP test for (a) UMT4 and (b) LMT3 (Lan et al. 2015). The maximum mercury pressure is 400 Mpa. The cumulative mercury saturations at 400 Mpa for UMT4 and LMT3 Samples are 90% and 60 % of PV, respectively.

4.4.1 Determined unknown parameters by analyzing imbibition data

In this section, we discussed the determined unknown parameters in Eq. (4.4) and these parameters will be used for calculating the PSD_{water} and $PSD_{water\text{-}repellant}$. As presented in section 4.3.2, we calculate ϕ_a through dividing V_o or V_w by V_B. t_{eq} along with Eq. (4.6) are used to calculate D_{min} from experimental imbibition data. D_{max} is obtained from the MICP data (Table 4.1). To determine τ and D_f, we match the experimental imbibition data with Eq. (4.4) by minimizing the OF. Figs 4.7 and 4.8 compare the measured imbibition profiles with those predicted by Eq. (4.4) for five UMT and four LMT rock samples, respectively. Table 4.3 summarizes the parameters used in Eq. (4.4).

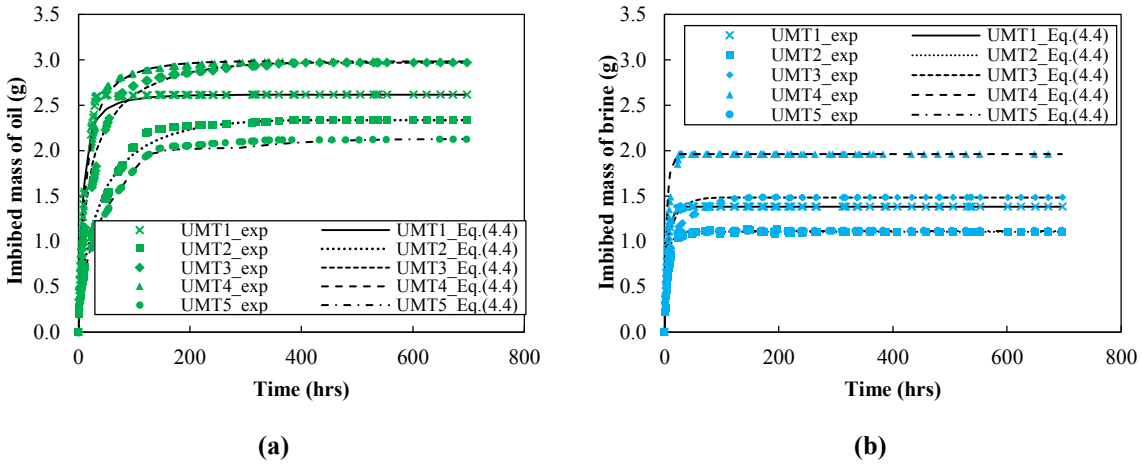

(a) (b)

Fig. 4.7. Comparison between modeling (Eq. (4.4)) and experimental results of (a) oil and (b) brine imbibition tests for the upper Montney rock samples.

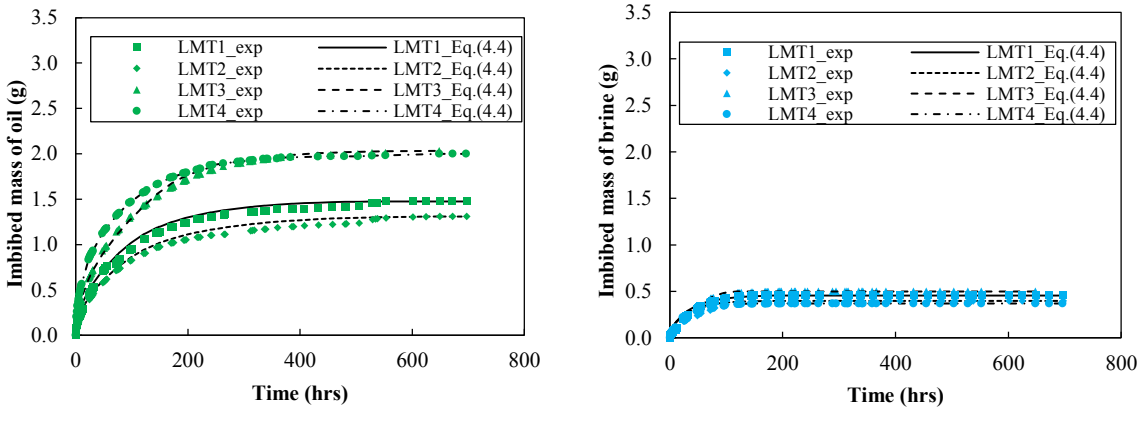

(a) (b)

Fig. 4.8. Comparison between modeling (Eq. (4.4)) and experimental results of (a) oil and (b) brine imbibition tests for the lower Montney rock samples.

Table 4.3. The values of unknown parameters used in Eq. (4.4).

Sample ID	Accessible porosity ϕ_a (fraction)	Maximum diameter D_{max} (nm)	Equilibrium time t_{eq} (hrs)	Minimum diameter D_{min} (nm)	Tortuosity τ	Fractal dimension D_f
UMT 1_o	0.049	131.0	313.80	5.34	2.50	1.55
UMT 1_w	0.019	131.0	32.50	12.50	2.19	1.52
UMT 2_o	0.043	131.0	408.00	6.36	3.01	1.80
UMT 2_w	0.015	131.0	2.45	28.00	2.72	1.78
UMT 3_o	0.056	368.0	433.00	6.30	3.02	1.88
UMT 3_w	0.020	368.0	97.25	10.50	2.81	1.90
UMT 4_o	0.055	262.0	358.50	3.02	2.02	1.72
UMT 4_w	0.026	262.0	23.83	14.70	1.99	1.68
UMT 5_o	0.039	131.0	647.83	3.08	2.51	1.92
UMT 5_w	0.016	131.0	96.33	4.35	2.28	1.42
LMT 1_o	0.027	14.6	553.33	1.75	2.14	1.92
LMT 1_w	0.006	14.6	22.20	2.19	2.52	1.94
LMT 2_o	0.024	37.8	672.00	1.73	2.31	1.96
LMT 2_w	0.005	37.8	192.50	2.15	2.19	1.92
LMT 3_o	0.039	21.6	696.00	1.85	2.40	1.88
LMT 3_w	0.007	21.6	98.33	5.18	2.28	1.87
LMT 4_o	0.037	57.6	647.83	1.82	2.16	1.92
LMT 4_w	0.005	57.6	170.33	2.02	2.14	1.90

t_{eq} and D_{min}

As listed in Table 4.3, for both LMT and UMT rock samples, t_{eq} for oil imbibition ($t_{eq(o)}$) is significantly higher than t_{eq} for brine imbibition ($t_{eq(w)}$). Consequently, D_{min} determined from oil imbibition test ($D_{min(o)}$) is lower than D_{min} determined from brine imbibition test ($D_{min(w)}$). For instance, $t_{eq(o)}$ and $t_{eq(w)}$ of UMT1 are 313.8 and 32.5 hours, respectively. Using Eq. (4.6), $D_{min(o)}$ and $D_{min(w)}$ for UMT1 are 5.34 nm and 12.5 nm, respectively. In other words, late equilibrium of oil compared with brine suggests the abundance of hydrophobic small pores with low wetting affinity towards brine, and high wetting affinity towards oil. Yassin et al. (2016, 2017) used the results of SEM/ESD analyses and proposed that the small hydrophobic pores within the organic

matter may be responsible for the late equilibrium of oil compared with brine in spontaneous imbibition tests.

Furthermore, $t_{eq(o)}$ of UMT samples is generally lower than $t_{eq(o)}$ of LMT samples and consequently $D_{min(o)}$ of UMT samples is higher than $D_{min(o)}$ of LMT samples. The lower value of permeability of the LMT samples compared with that of the UMT samples (Table 4.1) supports the presence of smaller pores in the LMT samples, which means $D_{min(o)}$ (LMT)< $D_{min(o)}$ (UMT) . In addition, by comparing the values of $D_{min\text{-}MICP}$ in Table 4.1 and D_{min} calculated by t_{eq} in Table 4.3 for LMT rock samples, one can find that oil imbibition results give smaller values of D_{min} compared with MICP test results. This suggests that oil can imbibe into small nanpores inaccessible for mercury intrusion. The results of SEM/EDS analyses (Yassin et al. 2016) show the abundance of nanpores within organic matter. The hydrophobic organic pores have high wetting affinity for spontaneous oil uptake. However, mercury is a non-wetting phase and cannot fill a significant fraction of these nanopores even at high pressure of 400 MPa.

τ

τ determined from oil imbibition test (τ_o) is generally larger than τ determined from brine imbibition (τ_w), as listed in Table 4.3. For instance, τ_o and τ_w for UMT1 rock sample are 2.50 and 2.19, respectively. As previously discussed, oil can imbibe into organic small pores that have strong wetting affinity towards oil, but low wetting affinity towards brine. Previous studies (Cai and Yu 2011, Cai, Yu, Zou, and Mei 2010, Cai et al. 2014, Yu, Cai, and Zou 2009) demonstrated that the rocks with smaller pore sizes have generally higher degrees of tortuosity. Therefore, the higher value of τ_o compared with τ_w is due to the imbibition of oil into relatively-smaller organic pores inaccessible for brine imbibition.

4.4.2 Results of $PSD_{inorg+org}$, PSD_{inorg} and PSD_{org}

In this section, first, we use the parameter determined from oil imbibition data (Table 4.3) along with Eq. (4.18) and calculate the $PSD_{inorg+org}$. The $PSD_{inorg+org}$ is compared with the PSD obtained from MICP test (PSD_{MICP}). Then, we use the parameters determined from brine imbibition data (Table 4.3) along with Eq. (4.18) and calculate the PSD_{inorg}. Finally, we calculate PSD_{org} using Eq. (4.19).

4.4.2.1 $PSD_{inorg+org}$ and comparison with PSD_{MICP}

Fig. 4.9a-b compares the final mercury and oil saturations for the UMT and LMT plugs, respectively. The final mercury and oil saturations are calculated by dividing the total invaded volume of mercury and oil by the effective pore volume. It is worth noting that the rock samples were analyzed as received without any cleaning process. So the pore space which are not accessible to oil imbibition may by occupied by the original oil or formation brine. For the LMT samples, the final mercury saturation at 400 MPa is around 30-70% PV, while the final oil saturation is around 80-100% PV. In conclusion, PSD calculated by oil imbibition data should cover 20% to 40% PV that is not accessible for mercury. Yassin et al. (Yassin et al. 2016) concluded that the Montney rock samples have significant fraction of small pores within organic matter. The hydrophobic organic pores can imbibe the oil phase spontaneously. However, mercury is a non-wetting phase and cannot intrude into most of the organic nanopores even at high pressure of 400 MPa. The organic pore volume inaccessible by mercury may explain the lower cumulative mercury saturation compared with the cumulative oil saturation for the LMT plugs (Fig. 4.9b).

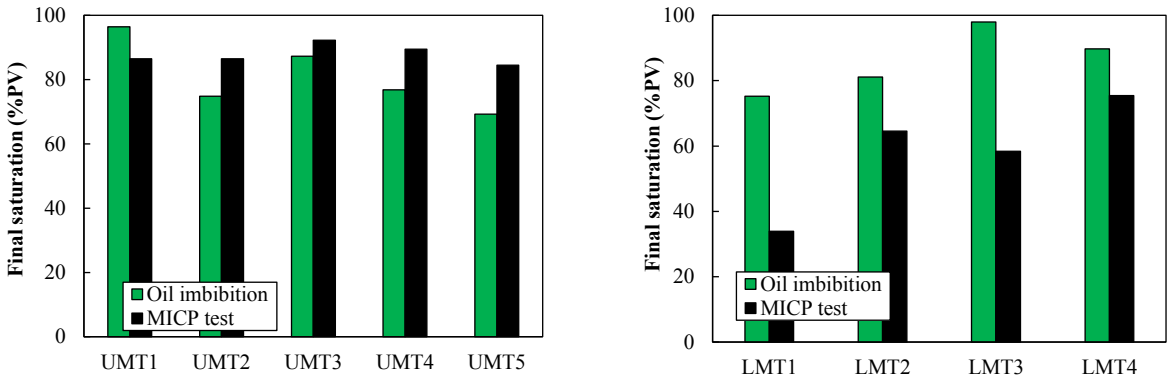

Fig. 4.9. A comparison between final mercury and oil saturations for (a) UMT rock samples and (b) LMT rock samples.

We use the parameters determined from oil imbibition data (Table 4.3) along with Eq. (4.18) and calculate $PSD_{inorg+org}$. Figs. 4.10 and 4.11 compare $PSD_{inorg+org}$ and PSD_{MICP} for UMT and LMT samples, respectively. For UMT samples, $PSD_{inorg+org}$ and PSD_{MICP} generally show similar trends for larger pores (> 100 nm in diameter). However, $PSD_{inorg+org}$ gives higher fraction of smaller nanopores (< 40 nm in diameter) compared with PSD_{MICP}, as shown in Fig. 4.10. This is in

agreement with the previous observations (Yassin et al. 2016) regarding the presence of nanopores within solid bitumen/pyrobitumen with hydrophobic characteristics. Similarly, for LMT samples, a significant fraction of small pores are detected by oil imbibition which are missed by the PSD_{MICP} (Fig. 4.11). In other words, oil imbibition data can detect small nanopores (< 3.75 nm in diameter) which are not accessible by mercury even at the maximum mercury pressure of 400 MPa. Therefore, oil imbibition can detect an additional 20-40% PV compared with MICP test as discussed in Fig. 4.9. Comparing $PSD_{inorg+org}$ and PSD_{MICP} (Figs 4.10-4.11) shows that the proposed ITA method can complement the conventional MICP technique for pore-size characterization of unconventional tight rocks.

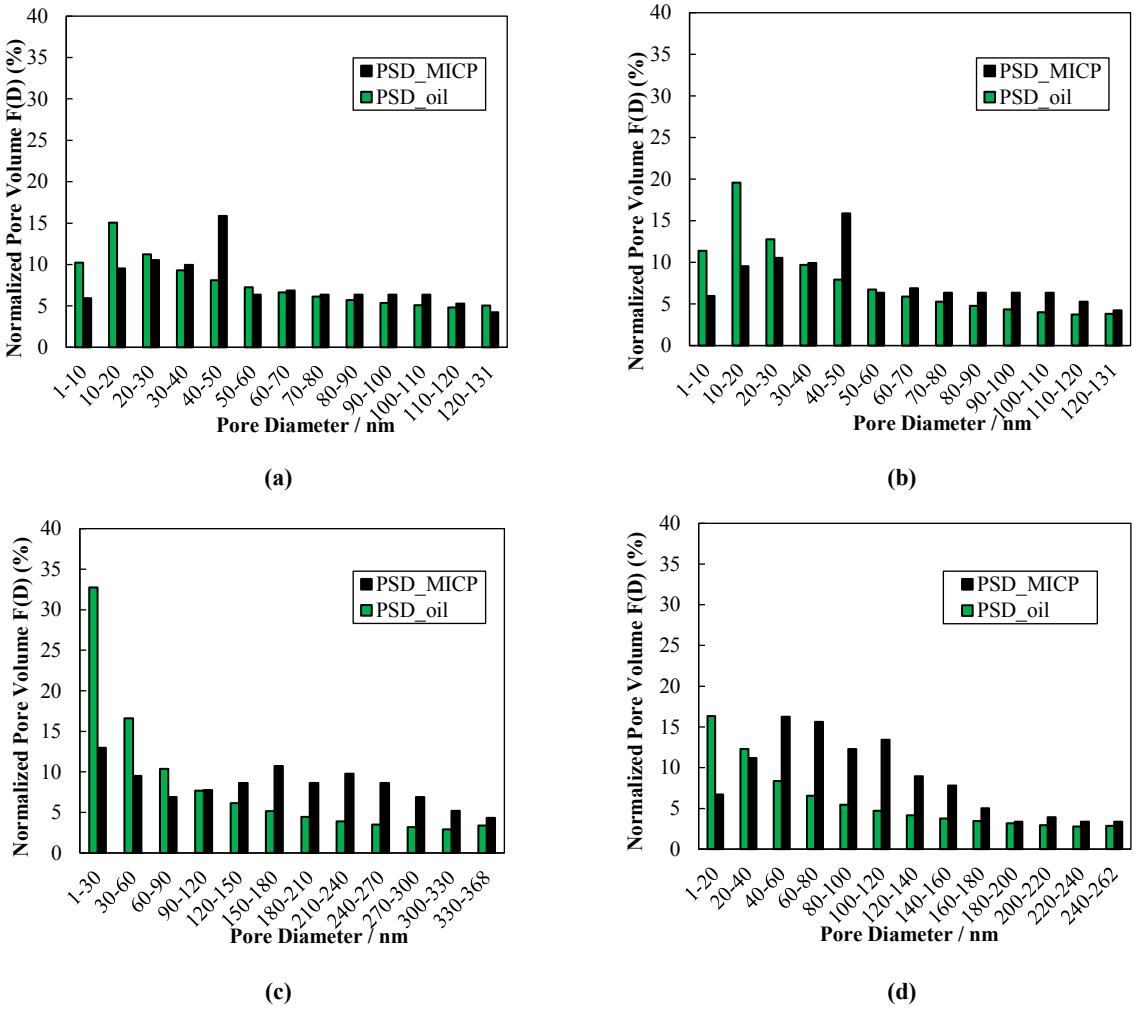

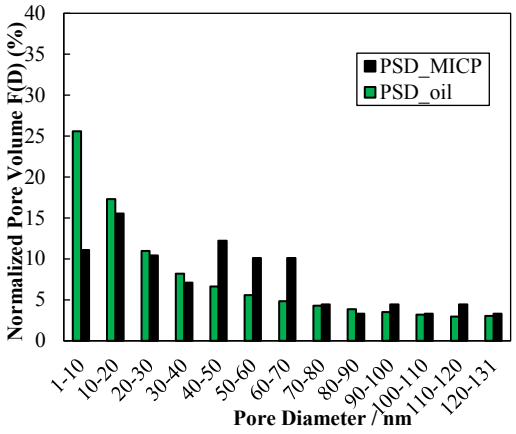

(e)

Fig. 4.10. Comparison of $PSD_{inorg+org}$ with PSD_{MICP} for (a) UMT1, (b) UMT2, c) UMT3, (d) UMT4, and (e) UMT5 rock samples.

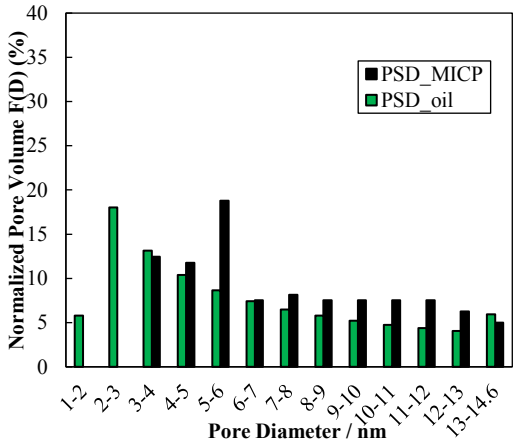

(a)

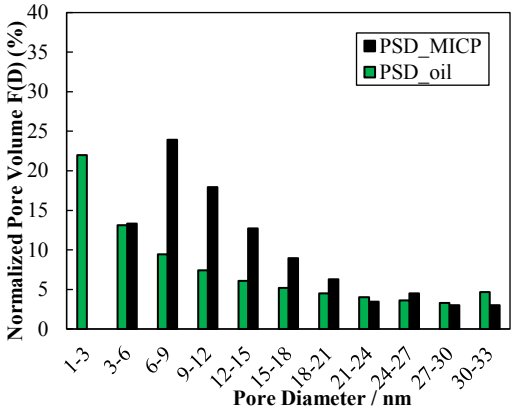

(b)

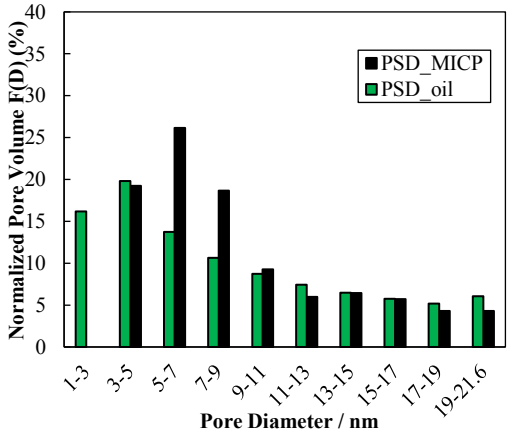

(c)

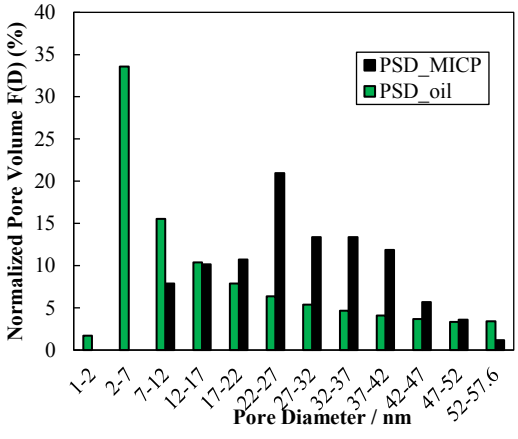

(d)

Fig. 4.11. Comparison of $PSD_{inorg+org}$ with PSD_{MICP} for (a) LMT1, (b) LMT2, (c) LMT3, and (d) LMT4 rock samples.

We also calculate the average pore diameter (D^{avg}) for UMT and LMT rock samples by

$$D^{avg} = \sum_{D=D_{min}}^{D=D_{max}} \{D \cdot F(D)\} \tag{4.20}$$

Figs. 4.12a and 4.12b compares D^{avg} calculated by oil imbibition and MICP test for UMT and LMT samples, respectively. For both cases, D^{avg} calculated by $PSD_{inorg+org}$ is lower than D^{avg} calculated by PSD_{MICP}. This result can be explained by that fact that oil can be imbibed spontaneously into organic nanopores which cannot be accessed by mercury even at high pressures of 400 MPa.

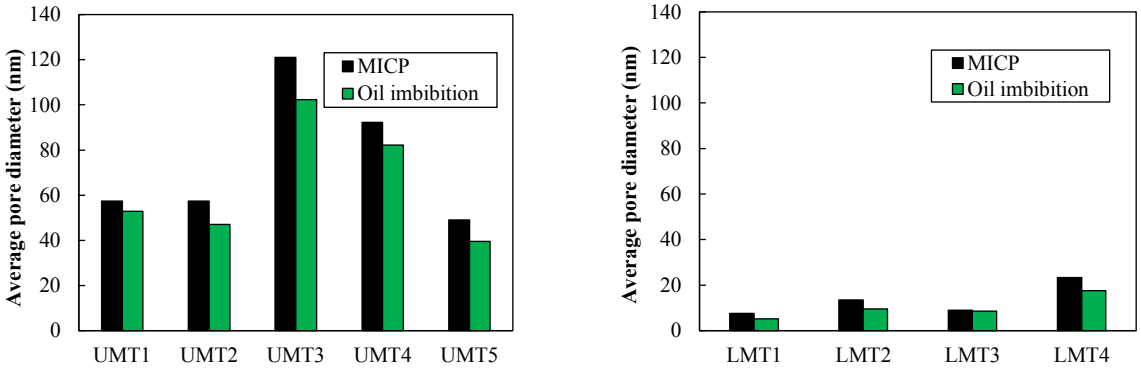

Fig. 4.12. A comparison between average pore diameters (D^{avg}) calculated by $PSD_{inorg+org}$ and PSD_{MICP} for (a) UMT and (b) LMT rock samples.

4.2.2.2 PSD_{inorg} and PSD_{org}

In this section, we use the parameters determined from brine imbibition data (Table 4.3) along with Eq. (4.18) and calculate the PSD_{inorg}. Then, we calculate PSD_{org} using Eq. (4.19). PSD_{org} may represent the organic pores that are within the solid bitumen/pyrobitumen with little or no wetting affinity towards the aqueous phase. Figs. 4.13 and 4.14 present the calculated $PSD_{inorg+org}$ from oil imbibition, PSD_{inorg} from brine imbibition and PSD_{org} by Eq. (4.19), for UMT and LMT samples, respectively. For UMT samples (Fig. 4.13), PSD_{inorg} (blue bars) shows that more than 80% of inorganic pores have diameters > 40 nm; while around 60% of organic pores (yellow bars) have

diameters < 30 nm. PSD_{inorg} of LMT rock samples (Fig. 4.14) shows that more than 80% of inorganic pores are > 7 nm; while around 70% of the organic pores are < 7 nm. We also use Eq. (4.20) to calculate the D^{avg} of inorganic and organic pores for UMT and LMT rock samples, as shown in Figs. 4.15a-b. D^{avg} of inorganic pores is larger than D^{avg} of organic pores for both UMT and LMT samples.

According to the results in Figs. 4.13-4.15, the pore network of the samples generally consists of larger inorganic pores and smaller organic pores, which is in agreement with the assumptions presented in Section 4.2. In addition, PSD_{org} shows the abundance of organic nanopores for both UMT and LMT rock samples. This result is in agreement with the SEM images showing that small nanopores are primarily within solid bitumen/pyrobitumen (Yassin et al. 2016).

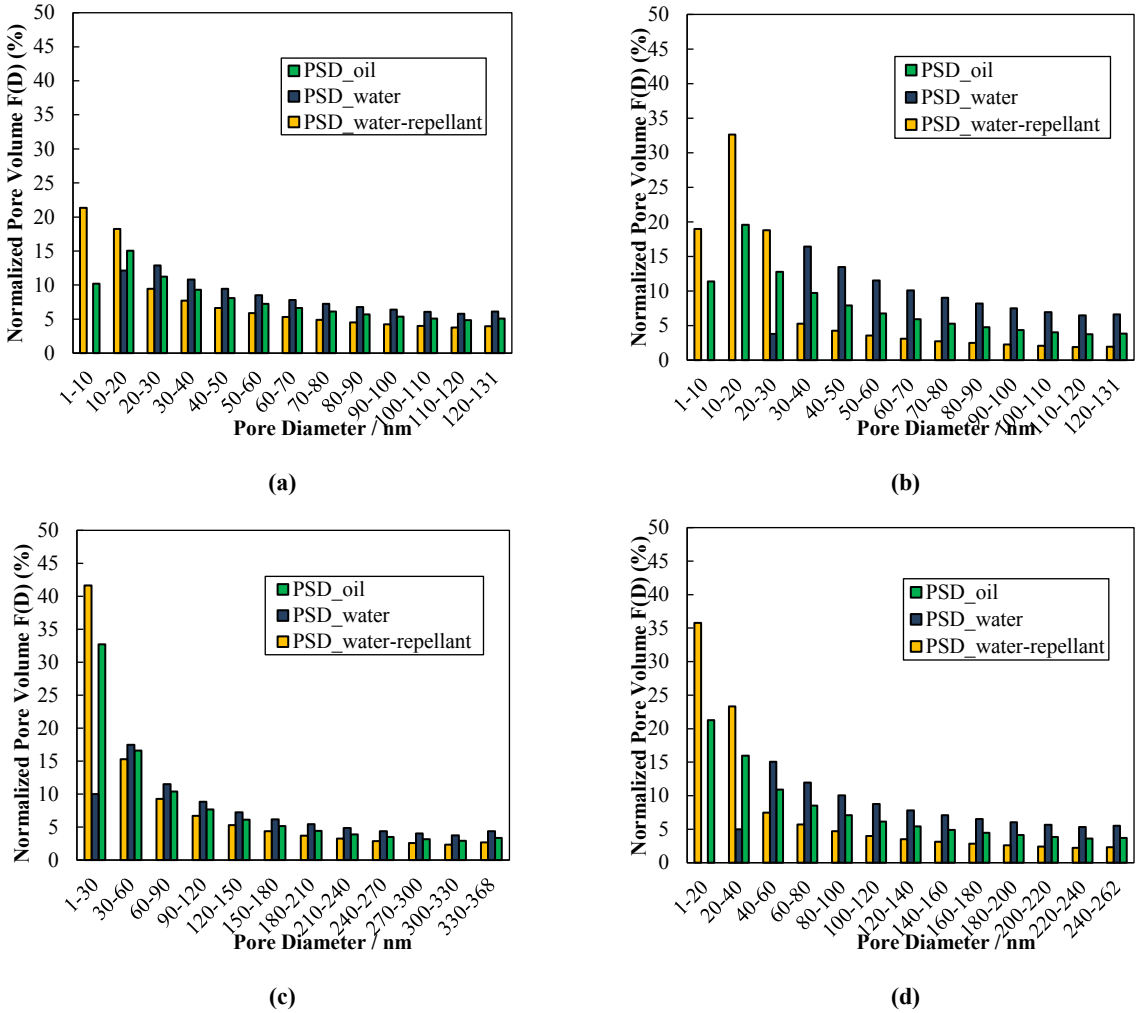

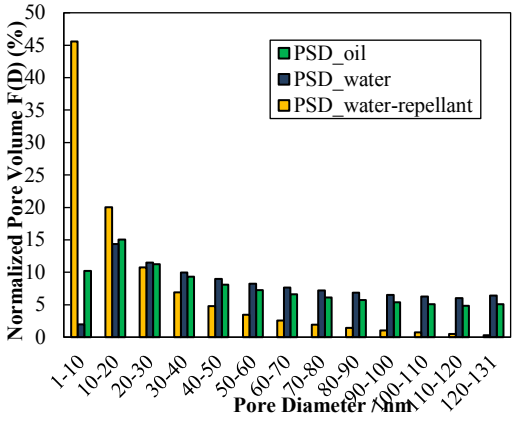

(e)

Fig. 4.13. $PSD_{inorg+\ org}$, PSD_{org}, and PSD_{inorg} for (a) UMT1, (b) UMT2, (c) UMT3, (d) UMT4 and (e) UMT5 rock samples.

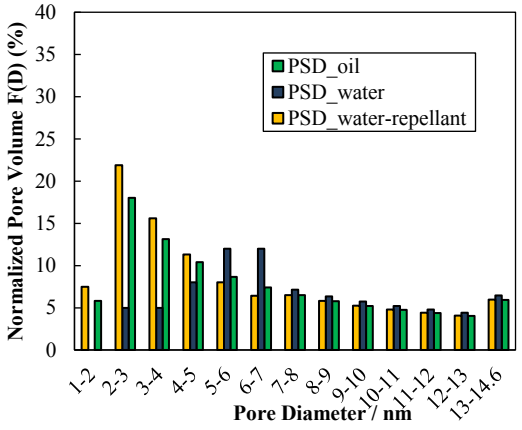

(a)

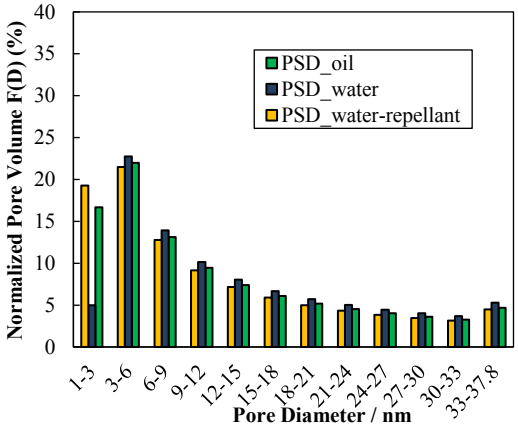

(b)

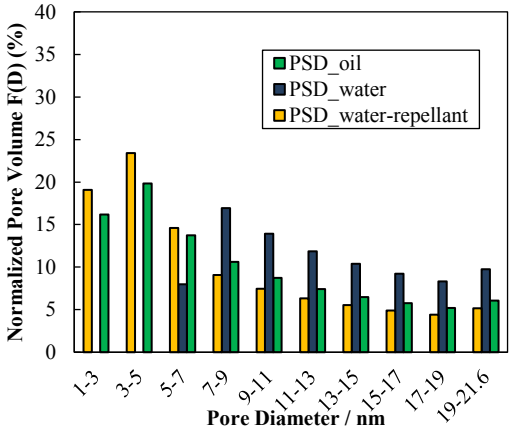

(c)

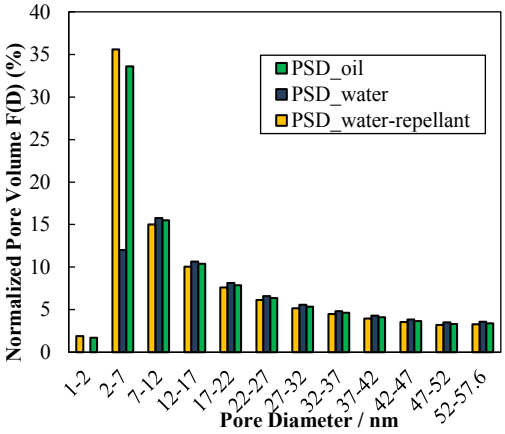

(d)

Fig. 4.14. $PSD_{inorg+\ org}$, PSD_{org}, and PSD_{inorg} for (a) LMT1, (b) LMT2, (c) LMT3, and (d) LMT4 rock samples.

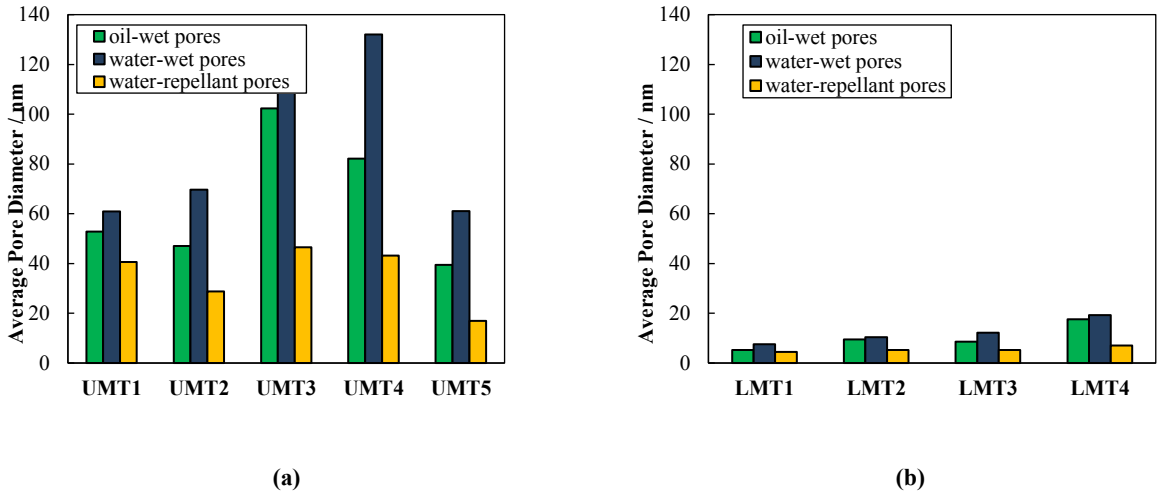

Fig. 4.15. Comparison of D^{avg} obtained from $PSD_{inorg+org}$, PSD_{inorg} and PSD_{org} of (a) UMT and (b) LMT rock samples.

4.5 Limitations

In this section, we present the limitations of the proposed fractal model and ITA method as follows:

a. In this study, we considered the capillary pressure as the driving mechanism for liquid imbibition, and ignored other driving mechanisms such as water adsorption by clay minerals (Bernard 1967), osmotic effect (Chenevert 1989, Neuzil 2000, Bai, Guo, and Jin 2008, Chen, Ewy, and Yu 2010), or electrical double layer expansion (Holmberg, Shah, and Schwuger 2002, Nasralla and Nasr-El-Din 2014). For instance, the Montney rock samples generally have more than 10 wt% of clay content (Lan et al. 2015). Clay particles may adsorb water and induce micro-fractures triggered by clay expansion (Ghanbari and Dehghanpour 2015, Dehghanpour et al. 2013). In case of inducing micro-fractures, calculating PSD_{inorg} by brine imbibition may overestimate the PV_{inorg}. In addition, we assume the pore network of rock samples does not change during the time course of imbibition process and we neglect the pore size alterations that may be induced by clay swelling.

b. The proposed fractal model idealizes the pore network of porous media as the bundle of capillaries without interconnection. However, natural porous media with considerable pore connectivity makes the imbibition process more complicated. For example, the interconnection between pores may lead to backfilling (Chandler et al. 1982, Peters 1990) in small pores. Assuming wetting liquid in small pores can be continuously imbibed from the bottom to the top may lead to erroneous calculation of PSD.

c. This study assumed that water can only detect inorganic pores driven by capillary pressure. However, water molecules may condense in extremely small organic nanopores (~0.3 nm) as a result of strong solid-fluid attractions (Zolfaghari, Dehghanpour, and Xu 2017, Liu and Monson 2005). Therefore, inaccuracy may occur in the calculation of PSD_{inorg} and PSD_{org} if we ignore the possible condensation of water in the organic pores.

d. As discussed before, mercury intrusion is a drainage process, which is controlled by the size of pore-throat (Wardlaw and Taylor 1976). However, spontaneous imbibition of wetting phase is mainly controlled by the size of pore bodies (Valvatne and Blunt 2004). As we use the D_{max} from MICP data for the proposed ITA method, D_{max} might be underestimated. Moreover, the MICP results are obtained from the offset rock samples near tested Montney rock samples. In this study, we assume the D_{max} of the offset rock samples is similar to D_{max} of the studied rock samples, which may not be the case for the Montney rocks with high degree of heterogeneity (Duenas 2014).

e. The contact angle we used in our model is measured on the polished surface of the rock sample, however the value of contact angle in Eq. (4.4) should be at the pore scale. In this study, we simply assume that the contact angle on the surface of rock sample is similar to pore-scale contact angle.

4.6 Summary

In this chapter, we proposed an ITA method to characterize the pore network of the Montney rock samples by comparative analysis of the oil and brine imbibition data. The previously-proposed fractal model (Shi, Yassin, and Dehghanpour 2017) with considering non-piston like imbibition front was used. On the basis of the assumptions, $PSD_{inorg+org}$ was calculated using oil imbibition data PSD_{inorg} was calculated using brine imbibition. PSD_{org} was calculated by the decoupling of $PSD_{inorg+org}$ and PSD_{inorg}.

The modeling results show that the pore network of Montney rock samples can be generally divided into larger inorganic pores and smaller organic pores, which is in agreement with the previous observation and assumptions (Yassin et al. 2016, Lan et al. 2015). Moreover, the proposed ITA method is beneficial for characterizing the pore network of extremely tight rocks.

Chapter 5: Conclusions and Recommendations for Future Work

5.1 Main Results and Contributions

In this study, we proposed an analytical fractal model for co-current spontaneous imbibition with considering non-piston-like imbibition front. In the proposed model, first the larger pores are filled by wetting phase, followed by smaller pores. Considering non-piston-like imbibition, we used available imbibition data and proposed a novel Imbibition Transient Analysis (ITA) to calculate pore size distribution (PSD) of Montney rock samples. We applied history matching technique to match the experimental imbibition data with the proposed fractal model, and obtain the unknown parameters controlling imbibition profile. The determined parameters are then used to calculate PSD. The PSD of inorganic and organic pores ($PSD_{inorg+org}$) is calculated by oil imbibition data and PSD of inorganic pores (PSD_{inorg}) is calculated by brine imbibition data. The PSD of organic pores (PSD_{org}) is calculated by decoupling of $PSD_{inorg+org}$ and PSD_{inorg}. Followings are the main conclusions of this study:

(1) The proposed fractal model is still valid after the wetting phase reaches top of the rock sample, which makes the model more applicable in analyzing the experimental data. The imbibition tests are usually performed on the rock samples with limited size (e.g. < 10 cm in height). In these cases, the top of the rock sample is considered as a no-flow boundary and the advancement of imbibition front can be stopped before the hydrostatic and capillary pressure are equilibrated.

(2) We derived analytical equation without considering hydrostatic pressure and semi-analytical equation with considering hydrostatic pressure. Comparing the results predicted by these two equations helps us to evaluate the role of hydrostatic pressure on the spontaneous imbibition process.

(3) The proposed fractal model is highly sensitive to the PSD of the porous media. The proposed model considered higher imbibition rate in larger pores compared with the piston-like imbibition model. In other words, the role of larger pores on the imbibition is more pronounced in the propsoed model. As the imbibed mass in larger pores dominates the total imbibed mass, the imbibition rate predicted by the proposed model is more sensitive to the PSD changes. This feature

can help us to characterize the pore network of the rock samples by analyzing spontaneous imbibition data.

(4) We found that the minimum pore diameter (D_{min}) controls the equilibrium time (t_{eq}) in the spontaneous imbibition process. t_{eq} increases as D_{min} decreases and the imbibition profiles become more smeared as PSD becomes wider. Moreover, we proposed a new solution to calculate D_{min} of rock samples by analyzing spontaneous imbibition data. The proposed solution comes from non-piston-like displacement assumption and cannot be derived from piston-like models.

(5) Compared with the existing piston-like model, the proposed non-piston-like model can better explain the comparative oil and brine imbibition profiles for the unconventional rock samples. Compared with oil imbibition, brine imbibition shows earlier equilibrated time. Early equilibrium of brine together with the proposed fractal model suggests that brine cannot imbibe into small hydrophobic pores. This result is in agreement with the SEM images showing that that larger pores are predominantly hydrophilic and smaller pores are primarily hydrophobic (Yassin et al. 2016).

(6) The proposed ITA technique provides a new way for separate characterization of PSD_{inorg} and PSD_{org}. For dual-wettability porous media such as the Montney rock samples, the traditional MICP test fails to distinguish between organic and inorganic pore networks as mercury is the non-wetting phase towards both inorganic and organic pores. Using ITA method, we calculated the PSD_{inorg} and PSD_{org} and proved the feasibility of calculating PSD based on imbibition data. Moreover, oil can imbibe into very small pores (< 3 nm) which are not accessible by mercury even at high pressure of 400 MPa. The ITA technique can complement the conventional MICP technique for a more comprehensive characterization of the pore network of unconventional tight rocks.

5.2 Recommendations for Future Work

(1) For the fractal model, we assumed there is no interconnection between capillaries, therefore, the liquid imbibes straight upward. However, the interconnection between pores commonly exists in natural porous media and may lead to backfilling (Chandler et al. 1982, Peters 1990) and meniscus arrest (Gruener et al. 2012, Sadjadi et al. 2015, Sadjadi and Rieger 2013) mechanisms. As mentioned above, those mechanisms could make the fluid flow more complex. Therefore, it is

recommended to extend the proposed model by considering the interconnection between pores in the future work.

(2) In this study, we considered the capillary pressure as the only driving mechanism for liquid uptake, and ignored other driving mechanisms such as water adsorption by clay minerals (Bernard 1967), osmotic effect (Chenevert 1989, Neuzil 2000, Bai, Guo, and Jin 2008, Chen, Ewy, and Yu 2010), or electrical double layer expansion (Holmberg, Shah, and Schwuger 2002, Nasralla and Nasr-El-Din 2014). For example, unconventional rocks such as shales have high clay content which could strongly affect the brine uptake. For the future work, a more comprehensive model with considering aforementioned mechanisms is demanded.

(3) For the proposed ITA, we obtained the maximum diameter (D_{max}) from the MICP data. As discussed before, MICP test gives the pore-throat diameters rather than pore-body diameters and D_{max} could be overestimated by using MICP data. D_{max} can also be estimated by Eq. (3.27) (Yu and Cheng 2002, Wu and Yu 2007, Cai, Yu, Zou, and Luo 2010, Cai and Yu 2010) but it requires the mean pore diameter, which is hard to determine in the natural porous media. As D_{max} is one of essential parameters in PSD and imbibition modeling, a more accurate method is required to determine D_{max} for the future work.

Bibliography

Adler, PM, J-F Thovert. 1993. Fractal porous media. *Transport in porous media* **13** (1): 41-78.

Akin, S, AR Kovscek. Imbibition studies of low-permeability porous media. Society of Petroleum Engineers.

Al Hinai, Adnan, Reza Rezaee, Lionel Esteban et al. 2014. Comparisons of pore size distribution: A case from the Western Australian gas shale formations. *Journal of Unconventional Oil and Gas Resources* **8**: 1-13.

Alotaibi, Mohammed B, Ramez A Nasralla, Hisham A Nasr-El-Din. 2011. Wettability studies using low-salinity water in sandstone reservoirs. *SPE Reservoir Evaluation & Engineering* **14** (06): 713-725.

Amott, Earl. 1959. Observations relating to the wettability of porous rock.

Bai, M, Q Guo, Z-H Jin. Study of Wellbore Stability due to Drilling Fluid/Shale Interactions. American Rock Mechanics Association.

Barrande, M, R Bouchet, R Denoyel. 2007. Tortuosity of porous particles. *Analytical Chemistry* **79** (23): 9115-9121.

Bear, Jacob. 2013. *Dynamics of fluids in porous media*, Courier Corporation (Reprint).

Bell, James Munsie, FK Cameron. 1906. The flow of liquids through capillary spaces. *The Journal of Physical Chemistry* **10** (8): 658-674.

Benavente, David, Peter Lock, M Ángeles García Del Cura et al. 2002. Predicting the capillary imbibition of porous rocks from microstructure. *Transport in porous media* **49** (1): 59-76.

Berg, Robert R. 1975. Capillary pressures in stratigraphic traps. *AAPG bulletin* **59** (6): 939-956.

Bernard, George G. Effect of floodwater salinity on recovery of oil from cores containing clays. Society of Petroleum Engineers.

Blunt, Martin J. 2001. Flow in porous media—pore-network models and multiphase flow. *Current opinion in colloid & interface science* **6** (3): 197-207.

Bo-Ming, Yu. 2005. Fractal character for tortuous streamtubes in porous media. *Chinese Physics Letters* **22** (1): 158.

Brunauer, Stephen, Paul Hugh Emmett, Edward Teller. 1938. Adsorption of gases in multimolecular layers. *Journal of the American chemical society* **60** (2): 309-319.

Buldyrev, SV, A-L Barabási, F Caserta et al. 1992. Anomalous interface roughening in porous media: Experiment and model. *Physical Review A* **45** (12): R8313.

Bustin, R Marc, Amanda MM Bustin, Albert Cui et al. Impact of shale properties on pore structure and storage characteristics. Society of Petroleum Engineers.

Cai, Jianchao, Xiangyun Hu, Dag Chun Standnes et al. 2012. An analytical model for spontaneous imbibition in fractal porous media including gravity. *Colloids and Surfaces A: Physicochemical and Engineering Aspects* **414**: 228-233.

Cai, Jianchao, Liang Luo, Ran Ye et al. 2015. Recent advances on fractal modeling of permeability for fibrous porous media. *Fractals* **23** (01): 1540006.

Cai, Jianchao, Edmund Perfect, Chu-Lin Cheng et al. 2014. Generalized modeling of spontaneous imbibition based on Hagen–Poiseuille flow in tortuous capillaries with variably shaped apertures. *Langmuir* **30** (18): 5142-5151.

Cai, Jianchao, Lijun You, Xiangyun Hu et al. 2012. Prediction of effective permeability in porous media based on spontaneous imbibition effect. *International Journal of Modern Physics C* **23** (07): 1250054.

Cai, Jianchao, Boming Yu. 2010. Prediction of maximum pore size of porous media based on fractal geometry. *Fractals* **18** (04): 417-423.

Cai, Jianchao, Boming Yu. 2011. A discussion of the effect of tortuosity on the capillary imbibition in porous media. *Transport in porous media* **89** (2): 251-263.

Cai, Jianchao, Boming Yu, Mingqing Zou et al. 2010. Fractal characterization of spontaneous co-current imbibition in porous media. *Energy & Fuels* **24** (3): 1860-1867.

Cai, Jianchao, Boming Yu, Mingqing Zou et al. 2010. Fractal analysis of invasion depth of extraneous fluids in porous media. *Chemical Engineering Science* **65** (18): 5178-5186.

Carman, Philip Crosbie. 1937. Fluid flow through granular beds. *Transactions-Institution of Chemical Engineeres* **15**: 150-166.

Chalmers, Gareth R, R Marc Bustin, Ian M Power. 2012. Characterization of gas shale pore systems by porosimetry, pycnometry, surface area, and field emission scanning electron microscopy/transmission electron microscopy image analyses: Examples from the Barnett, Woodford, Haynesville, Marcellus, and Doig units. *AAPG bulletin* **96** (6): 1099-1119.

Chandler, Richard, Joel Koplik, Kenneth Lerman et al. 1982. Capillary displacement and percolation in porous media. *Journal of Fluid Mechanics* **119**: 249-267.

Chen, Guizhong, Russell T Ewy, Mengjiao Yu. 2010. Analytic solutions with ionic flow for a pressure transmission test on shale. *Journal of Petroleum Science and Engineering* **72** (1): 158-165.

Chenevert, ME. Diffusion of water and ions into shales.

Chilingar, George V, TF Yen. 1983. Some notes on wettability and relative permeabilities of carbonate reservoir rocks, II. *Energy Sources* **7** (1): 67-75.

Clarkson, Christopher R, M Freeman, L He et al. 2012. Characterization of tight gas reservoir pore structure using USANS/SANS and gas adsorption analysis. *Fuel* **95**: 371-385.

Clennell, M Ben. 1997. Tortuosity: a guide through the maze. *Geological Society, London, Special Publications* **122** (1): 299-344.

Comiti, Jacques, Maurice Renaud. 1989. A new model for determining mean structure parameters of fixed beds from pressure drop measurements: application to beds packed with parallelepipedal particles. *Chemical Engineering Science* **44** (7): 1539-1545.

Cornell, David, Donald L Katz. 1953. Flow of gases through consolidated porous media. *Industrial & Engineering Chemistry* **45** (10): 2145-2152.

Cui, Albert, Raphael Wust, Brent Nassichuk et al. A nearly complete characterization of permeability to hydrocarbon gas and liquid for unconventional reservoirs: a challenge to conventional thinking. 1716-1732: Society of Exploration Geophysicists, American Association of Petroleum Geologists, Society of Petroleum Engineers.

Curtis, Mark Erman, Raymond Joseph Ambrose, Carl H Sondergeld et al. Transmission and scanning electron microscopy investigation of pore connectivity of gas shales on the nanoscale. Society of Petroleum Engineers.

Davies, Graham R. 1997. The Triassic of the Western Canada Sedimentary Basin: tectonic and stratigraphic framework, paleogeography, paleoclimate and biota. *Bulletin of Canadian Petroleum Geology* **45** (4): 434-460.

Dehghanpour, H, Q Lan, Y Saeed et al. 2013. Spontaneous imbibition of brine and oil in gas shales: effect of water adsorption and resulting microfractures. *Energy & Fuels* **27** (6): 3039-3049.

Dehghanpour, H, HA Zubair, A Chhabra et al. 2012. Liquid intake of organic shales. *Energy & Fuels* **26** (9): 5750-5758.

Dehghanpour, Hassan, Mingxiang Xu, Ali Habibi. 2015. Wettability of gas shale reservoirs. *Fundamentals of Gas Shale Reservoirs*: 341-359.

Duenas, Claudia. 2014. *Understanding rock quality heterogeneity of montney shale reservoir, pouce coupe field, Alberta, Canada*, Colorado School of Mines (Reprint).

Feder, J, A Aharony. Fractals in physics. 1-3.

Garrouch, Ali A, Liaqat Ali, Fuad Qasem. 2001. Using diffusion and electrical measurements to assess tortuosity of porous media. *Industrial & Engineering Chemistry Research* **40** (20): 4363-4369.

Gauss, CF. 1830. On a new general principle of mechanics. *Philosophical Magazine* **8**: 137-140.

Gelb, Lev D, KE Gubbins. 1998. Characterization of porous glasses: Simulation models, adsorption isotherms, and the Brunauer− Emmett− Teller analysis method. *Langmuir* **14** (8): 2097-2111.

Ghanbari, Ebrahim, Hassan Dehghanpour. 2015. Impact of rock fabric on water imbibition and salt diffusion in gas shales. *International Journal of Coal Geology* **138**: 55-67.

Ghanbari, Ebrahim, Hassan Dehghanpour. 2016. The fate of fracturing water: A field and simulation study. *Fuel* **163**: 282-294.

Gidley, John L. 1989. Recent advances in hydraulic fracturing.

Gruener, Simon, Helen E Hermes, Burkhard Schillinger et al. 2016. Capillary rise dynamics of liquid hydrocarbons in mesoporous silica as explored by gravimetry, optical and neutron imaging: Nano-rheology and determination of pore size distributions from the shape of imbibition fronts. *Colloids and Surfaces A: Physicochemical and Engineering Aspects* **496**: 13-27.

Gruener, Simon, Zeinab Sadjadi, Helen E Hermes et al. 2012. Anomalous front broadening during spontaneous imbibition in a matrix with elongated pores. *Proceedings of the National Academy of Sciences* **109** (26): 10245-10250.

Guerreiro, JNC, Helio JC Barbosa, ELM Garcia et al. 1998. Identification of reservoir heterogeneities using tracer breakthrough profiles and genetic algorithms. *SPE Reservoir Evaluation & Engineering* **1** (03): 218-223.

Habibi, Ali, Hassan Dehghanpour, Mojtaba Binazadeh et al. 2016. Advances in Understanding Wettability of Tight Oil Formations: A Montney Case Study. *SPE Reservoir Evaluation & Engineering* **19** (04): 583-603.

Hamm, Se‐Yeong, Pascal Bidaux. 1996. Dual‐porosity fractal models for transient flow analysis in fissured rocks. *Water resources research* **32** (9): 2733-2745.

Handy, LL. 1960. Determination of effective capillary pressures for porous media from imbibition data.

Hansen, JP, AT Skjeltorp. 1988. Fractal pore space and rock permeability implications. *Physical review B* **38** (4): 2635.

Harding, TJ, NJ Radcliffe, PR King. 1998. Hydrocarbon production scheduling with genetic algorithms. *SPE Journal* **3** (02): 99-107.

Hirasaki, George J, Chein-Chung Huang, Gigi Qian Zhang. 2000. Interpretation of wettability in sandstones with NMR analysis. *Petrophysics* **41** (03).

Hirasaki, George, Danhua Leslie Zhang. 2004. Surface chemistry of oil recovery from fractured, oil-wet, carbonate formations. *Spe Journal* **9** (02): 151-162.

Ho, Fun-gau, William Striender. 1981. A variational calculation of the effective surface diffusion coefficient and tortuosity. *Chemical Engineering Science* **36** (2): 253-258.

Holland, John H. 1975. Adaptation in natural and artificial systems. An introductory analysis with application to biology, control, and artificial intelligence. *Ann Arbor, MI: University of Michigan Press*.

Holmberg, Krister, Dinesh Ochhavlal Shah, Milan J Schwuger. 2002. *Handbook of applied surface and colloid chemistry*, Vol. 1, John Wiley & Sons (Reprint).

Hurst, Andrew, Paul H Nadeau. 1995. Clay microporosity in reservoir sandstones: an application of quantitative electron microscopy in petrophysical evaluation. *AAPG bulletin* **79** (4): 563-573.

Jacquin, Ch G, PM Adler. 1987. Fractal porous media II: geometry of porous geological structures. *Transport in Porous Media* **2** (6): 571-596.

Johnson, Elizabeth G, Laura A Johnson. 2012. Hydraulic fracture water usage in northeast British Columbia: Locations, volumes and trends. *Geoscience Reports*: 41-63.

Katz, A_J, AH Thompson. 1985. Fractal sandstone pores: implications for conductivity and pore formation. *Physical Review Letters* **54** (12): 1325.

Keneti, SAR, RCK Wong. Investigation of bimodularity in the Montney shale using the Brazilian test. American Rock Mechanics Association.

Khlaifat, Abdelaziz Lafi, Hani Qutob, Naiem Barakat. Tight gas sands development is critical to future world energy resources. Society of Petroleum Engineers.

Krohn, Christine E. 1988a. Fractal measurements of sandstones, shales, and carbonates. *Journal of Geophysical Research: Solid Earth* **93** (B4): 3297-3305.

Krohn, Christine E. 1988b. Sandstone fractal and Euclidean pore volume distributions. *Journal of Geophysical Research: Solid Earth* **93** (B4): 3286-3296.

Kuila, Utpalendu, Manika Prasad. 2013. Specific surface area and pore‐size distribution in clays and shales. *Geophysical Prospecting* **61** (2): 341-362.

Labani, Mohammad Mahdi, Reza Rezaee, Ali Saeedi et al. 2013. Evaluation of pore size spectrum of gas shale reservoirs using low pressure nitrogen adsorption, gas expansion and mercury porosimetry: A case study from the Perth and Canning Basins, Western Australia. *Journal of Petroleum Science and Engineering* **112**: 7-16.

Lai, Jin, Guiwen Wang, Zhuoying Fan et al. 2017. Fractal analysis of tight shaly sandstones using nuclear magnetic resonance measurements. *AAPG Bulletin* (20,170,522).

Lan, Qing, Hassan Dehghanpour, James Wood et al. 2015. Wettability of the Montney tight gas formation. *SPE Reservoir Evaluation & Engineering* **18** (03): 417-431.

Leyva-Gomez, Hector, Tayfun Babadagli. 2017. High-Temperature Solvent Injection for Heavy-Oil Recovery From Oil Sands: Determination of Optimal Application Conditions Through Genetic Algorithm. *SPE Reservoir Evaluation & Engineering* **20** (02): 372-382.

Li, Jing, Xiangfang Li, Xiangzeng Wang et al. 2016. Water distribution characteristic and effect on methane adsorption capacity in shale clay. *International Journal of Coal Geology* **159**: 135-154.

Li, Kewen. 2010a. Analytical derivation of Brooks–Corey type capillary pressure models using fractal geometry and evaluation of rock heterogeneity. *Journal of Petroleum Science and Engineering* **73** (1): 20-26.

Li, Kewen. 2010b. More general capillary pressure and relative permeability models from fractal geometry. *Journal of contaminant hydrology* **111** (1): 13-24.

Li, Kewen, Roland N Horne. 2006. Fractal modeling of capillary pressure curves for The Geysers rocks. *Geothermics* **35** (2): 198-207.

Li, Kewen, Haiyang Zhao. 2012. Fractal prediction model of spontaneous imbibition rate. *Transport in porous media* **91** (2): 363-376.

Li, Xiao-Yan, Bruce E Logan. 2001. Permeability of fractal aggregates. *Water research* **35** (14): 3373-3380.

Liu, J-C, PA Monson. 2005. Does water condense in carbon pores? *Langmuir* **21** (22): 10219-10225.

Liu, Xiangjun, Jian Xiong, Lixi Liang. 2015. Investigation of pore structure and fractal characteristics of organic-rich Yanchang formation shale in central China by nitrogen adsorption/desorption analysis. *Journal of Natural Gas Science and Engineering* **22**: 62-72.

Liu, Xuefeng, Jianfu Wang, Lin Ge et al. 2017. Pore-scale characterization of tight sandstone in Yanchang Formation Ordos Basin China using micro-CT and SEM imaging from nm-to cm-scale. *Fuel* **209**: 254-264.

Lucas, R. 1918. Rate of capillary ascension of liquids. *Kolloid Z* **23** (15): 15-22.

Lundblad, Anders, Bill Bergman. 1997. Determination of Contact Angle in Porous Molten‐Carbonate Fuel‐Cell Electrodes. *Journal of the Electrochemical Society* **144** (3): 984-987.

Majumdar, Arunava, Bharat Bhushan. 1990. Role of fractal geometry in roughness characterization and contact mechanics of surfaces. *ASME J. Tribol* **112** (2): 205-216.

Mandelbrot, Benoit B. 1967. How long is the coast of Britain. *science* **156** (3775): 636-638.

Mandelbrot, Benoit B, Roberto Pignoni. 1983. *The fractal geometry of nature*, Vol. 173, WH freeman New York (Reprint).

Matyka, Maciej, Arzhang Khalili, Zbigniew Koza. 2008. Tortuosity-porosity relation in porous media flow. *Physical Review E* **78** (2): 026306.

Miranda, AM, IL Menezes-Sobrinho, MS Couto. 2010. Spontaneous imbibition experiment in newspaper sheets. *Physical review letters* **104** (8): 086101.

Nasralla, Ramez A, Hisham A Nasr-El-Din. 2014. Double-layer expansion: is it a primary mechanism of improved oil recovery by low-salinity waterflooding? *SPE Reservoir Evaluation & Engineering* **17** (01): 49-59.

NEB, AER, BC OGC, BC MNGD. 2013. The Ultimate Potential for Unconventional Petroleum from the Montney Formation of British Columbia and Alberta. *Energy Briefing Note*.

Neuzil, CE. 2000. Osmotic generation of'anomalous' fluid pressures in geological environments. *Nature* **403** (6766): 182.

Nieto, John, Robert Bercha, Jim Chan. Shale Gas Petrophysics-Montney and Muskwa, Are They Barnett Look-Alikes? : Society of Petrophysicists and Well-Log Analysts.

Odusina, EO, CH Sondergeld, CS Rai. 2011. NMR study of shale wettability. Canadian Unconventional Resources Conference, 15–17 November, Alberta, Canada. *Society of Petroleum Engineers, doi* **10**.

Pape, Hansgeorg, Christoph Clauser, Joachim Iffland. 1999. Permeability prediction based on fractal pore-space geometry. *Geophysics* **64** (5): 1447-1460.
Patel, Anil N, David Davis, Charles Foster Guthrie et al. Optimizing cyclic steam oil production with genetic algorithms. Society of Petroleum Engineers.
Perfect, E, BD Kay. 1995. Applications of fractals in soil and tillage research: a review. *Soil and Tillage Research* **36** (1-2): 1-20.
Peters, Ekwere J. 1990. Petrophysics. *The University of Texas at Austin, Austin*.
Peters, Lies, Rob Arts, Geert Brouwer et al. 2010. Results of the Brugge benchmark study for flooding optimization and history matching. *SPE Reservoir Evaluation & Engineering* **13** (03): 391-405.
Pia, Giorgio, Ulrico Sanna. 2013. A geometrical fractal model for the porosity and thermal conductivity of insulating concrete. *Construction and Building Materials* **44**: 551-556.
Pittman, Edward D. 1972. Diagenesis of quartz in sandstones as revealed by scanning electron microscopy. *Journal of Sedimentary Research* **42** (3).
Poiseuille, Jean Leonard. 1844. *Recherches expérimentales sur le mouvement des liquides dans les tubes de très-petits diamètres*, Imprimerie Royale (Reprint).
Power, William L, Terry E Tullis. 1991. Euclidean and fractal models for the description of rock surface roughness. *Journal of Geophysical Research: Solid Earth* **96** (B1): 415-424.
Rieu, Michel, Edith Perrier. 1998. Fractal models of fragmented and aggregated soils.
Sadjadi, Zeinab, Michael Jung, Ralf Seemann et al. 2015. Meniscus arrest during capillary rise in asymmetric microfluidic pore junctions. *Langmuir* **31** (8): 2600-2608.
Sadjadi, Zeinab, Heiko Rieger. 2013. Scaling theory for spontaneous imbibition in random networks of elongated pores. *Physical review letters* **110** (14): 144502.
Sahimi, Muhammad. 1993. Flow phenomena in rocks: from continuum models to fractals, percolation, cellular automata, and simulated annealing. *Reviews of modern physics* **65** (4): 1393.
Saraji, Soheil, Mohammad Piri. 2015. The representative sample size in shale oil rocks and nano-scale characterization of transport properties. *International Journal of Coal Geology* **146**: 42-54.
Schembre, JM, S Akin, LM Castanier et al. Spontaneous water imbibition into diatomite. Society of Petroleum Engineers.
Schopf, Sven O, Andreas Hartwig, Udo Fritsching et al. 2017. Imbibition into Highly Porous Layers of Aggregated Particles. *Transport in Porous Media*: 1-23.
Sen, Mrinal K, Akhil Datta-Gupta, PL Stoffa et al. 1995. Stochastic reservoir modeling using simulated annealing and genetic algorithm. *SPE Formation Evaluation* **10** (01): 49-56.
Shi, Yue, Mahmood Reza Yassin, Hassan Dehghanpour. 2017. A Modified Model for Spontaneous Imbibition of Wetting Phase into Fractal Porous Media. *Colloids and Surfaces A: Physicochemical and Engineering Aspects*.
Sigal, Richard Frederick. 2015. Pore-size distributions for organic-shale-reservoir rocks from nuclear-magnetic-resonance spectra combined with adsorption measurements. *SPE Journal* **20** (04): 824-830.
Smith, Derrell A. 1966. Theoretical considerations of sealing and non-sealing faults. *AAPG Bulletin* **50** (2): 363-374.

Thomas, LK, DL Katz, MR Tek. 1968. Threshold pressure phenomena in porous media. *Society of Petroleum Engineers Journal* **8** (02): 174-184.

Tiab, Djebbar, Erle C Donaldson. 2015. *Petrophysics: theory and practice of measuring reservoir rock and fluid transport properties*, Gulf professional publishing (Reprint).

TSAI, DAH SHYANG, WILLIAM STRIEDER. 1986. Effective conductivities of random fiber beds. *Chemical Engineering Communications* **40** (1-6): 207-218.

Tyler, Scott W, Stephen W Wheatcraft. 1990. Fractal processes in soil water retention. *Water Resources Research* **26** (5): 1047-1054.

Valvatne, Per H, Martin J Blunt. 2004. Predictive pore‐scale modeling of two‐phase flow in mixed wet media. *Water Resources Research* **40** (7).

Van Brakel, Jaap, PM Heertjes. 1974. Analysis of diffusion in macroporous media in terms of a porosity, a tortuosity and a constrictivity factor. *International Journal of Heat and Mass Transfer* **17** (9): 1093-1103.

Vengosh, Avner, Robert B Jackson, Nathaniel Warner et al. 2014. A critical review of the risks to water resources from unconventional shale gas development and hydraulic fracturing in the United States. *Environmental science & technology* **48** (15): 8334-8348.

Wang, Yang, Yanming Zhu, Shangbin Chen et al. 2014. Characteristics of the nanoscale pore structure in Northwestern Hunan shale gas reservoirs using field emission scanning electron microscopy, high-pressure mercury intrusion, and gas adsorption. *Energy & Fuels* **28** (2): 945-955.

Wardlaw, Norman C, RP Taylor. 1976. Mercury capillary pressure curves and the intepretation of pore structure and capillary behaviour in reservoir rocks. *Bulletin of Canadian Petroleum Geology* **24** (2): 225-262.

Washburn, Edward W. 1921. The dynamics of capillary flow. *Physical review* **17** (3): 273.

Weissberg, Harold L. 1963. Effective diffusion coefficient in porous media. *Journal of Applied Physics* **34** (9): 2636-2639.

Wheatcraft, Stephen W, Scott W Tyler. 1988. An explanation of scale‐dependent dispersivity in heterogeneous aquifers using concepts of fractal geometry. *Water Resources Research* **24** (4): 566-578.

Wu, Jinsui, Boming Yu. 2007. A fractal resistance model for flow through porous media. *International journal of heat and mass transfer* **50** (19): 3925-3932.

Xie, Heping, Jin-An Wang, Wei-Hong Xie. 1997. Fractal effects of surface roughness on the mechanical behavior of rock joints. *Chaos, Solitons & Fractals* **8** (2): 221-252.

Xu, M, H Dehghanpour. 2014. Advances in understanding wettability of gas shales. *Energy & Fuels* **28** (7): 4362-4375.

Xu, Peng, Boming Yu. 2008. Developing a new form of permeability and Kozeny–Carman constant for homogeneous porous media by means of fractal geometry. *Advances in water resources* **31** (1): 74-81.

Xuefei, Sun, Kishore K Mohanty. Estimation of flow functions during drainage using genetic algorithm. Society of Petroleum Engineers.

Yang, Feng, Zhengfu Ning, Huiqing Liu. 2014. Fractal characteristics of shales from a shale gas reservoir in the Sichuan Basin, China. *Fuel* **115**: 378-384.

Yassin, Mahmood Reza, Momotaj Begum, Hassan Dehghanpour. 2017. Organic shale wettability and its relationship to other petrophysical properties: A Duvernay case study. *International Journal of Coal Geology* **169**: 74-91.

Yassin, Mahmood Reza, Hassan Dehghanpour, James Wood et al. 2016. A theory for relative permeability of unconventional rocks with dual-wettability pore network. *SPE Journal*.

Yarveicy, Hamidreza, Ali Haghtalab. 2017. Effect of amphoteric surfactant on phase behavior of hydrocarbon-electrolyte-water system-an application in enhanced oil recovery. *Journal of Dispersion Science and Technology* **8**: 0193-2691.

Yi-Qiao, Song, Seungoh Ryu, Pabitra N Sen. 2000. Determining multiple length scales in rocks. *Nature* **406** (6792): 178.

Young, Thomas. 1805. An essay on the cohesion of fluids. *Philosophical Transactions of the Royal Society of London* **95**: 65-87.

Yu, Boming, Jianchao Cai, Mingqing Zou. 2009. On the physical properties of apparent two-phase fractal porous media. *Vadose Zone Journal* **8** (1): 177-186.

Yu, Boming, Ping Cheng. 2002. A fractal permeability model for bi-dispersed porous media. *International Journal of Heat and Mass Transfer* **45** (14): 2983-2993.

Yu, Boming, Jianhua Li. 2001. Some fractal characters of porous media. *Fractals* **9** (03): 365-372.

Zhang, D Leslie, Shunhua Liu, Maura Puerto et al. 2006. Wettability alteration and spontaneous imbibition in oil-wet carbonate formations. *Journal of Petroleum Science and Engineering* **52** (1): 213-226.

Zhang, Peimao, Tor Austad. 2006. Wettability and oil recovery from carbonates: Effects of temperature and potential determining ions. *Colloids and Surfaces A: Physicochemical and Engineering Aspects* **279** (1): 179-187.

Ziarani, Ali S, Roberto Aguilera. 2012. Pore-throat radius and tortuosity estimation from formation resistivity data for tight-gas sandstone reservoirs. *Journal of Applied Geophysics* **83**: 65-73.

Zolfaghari, Ashkan, Hassan Dehghanpour, Mike Noel et al. 2016. Laboratory and field analysis of flowback water from gas shales. *Journal of Unconventional Oil and Gas Resources* **14**: 113-127.

Zolfaghari, Ashkan, Hassan Dehghanpour, Mingxiang Xu. 2017. Water sorption behaviour of gas shales: II. Pore size distribution. *International Journal of Coal Geology*.

Appendix A: Derivation of Cai's model (Cai, Hu, et al. 2012)

The cumulative size number (N) of pores in a unit cell follows the fractal scaling law (Yu and Cheng 2002)

$$N(\geq D) = \left(\frac{D_{max}}{D}\right)^{D_f} \tag{A.1}$$

The number of capillaries with diameter larger than D in the rock sample (N_f) is derived by scaling up from unit cell to rock sample (Yu, Cai, and Zou 2009)

$$\begin{aligned} N_f(\geq D) &= \frac{A_f \times \phi}{A_p} N(\geq D) \\ &= \frac{4A_f}{\pi D_{max}^{2-D_f}} \frac{2-D_f}{D_f} \frac{\phi}{1-\left(\frac{D_{min}}{D_{max}}\right)^{2-D_f}} D^{-Df} \end{aligned} \tag{A.2}$$

where A_f and ϕ are the total cross-sectional area and porosity of the rock sample. Differentiating Eq. (A.2) with respect to D, the number of pores of sizes lying between D and $D + dD$ in the area A_f is

$$-dN_f = \frac{4A_f}{\pi D_{max}^{2-D_f}} \frac{(2-D_f)\phi}{1-\left(\frac{D_{min}}{D_{max}}\right)^{2-D_f}} D^{-(D_f+1)} dD \tag{A.3}$$

The flow rate of imbibition in a single capillary

$$q(D) = \frac{\pi}{128} \frac{D^4}{\mu L_f} \left(\frac{4\sigma cos\theta}{D} - \rho g L_s\right) \tag{A.4}$$

The total flow rate through the bottom cross-sectional area is obtained by integrating Eq. (A.4) over the minimum (D_{min}) to maximum (D_{max}) pores

$$\begin{aligned} Q = -\int_{D_{min}}^{D_{max}} q(D)\, dN_f &= \frac{\sigma cos\theta}{8\mu\tau L_s} \frac{2-D_f}{3-D_f} \frac{A_f \phi D_{max}\left[1-\left(\frac{D_{min}}{D_{max}}\right)^{3-D_f}\right]}{1-\left(\frac{D_{min}}{D_{max}}\right)^{2-D_f}} - \\ &\frac{A_f \rho g}{32\mu\tau} \frac{2-D_f}{4-D_f} \frac{\phi D_{max}^2\left[1-\left(\frac{D_{min}}{D_{max}}\right)^{4-D_f}\right]}{1-\left(\frac{D_{min}}{D_{max}}\right)^{2-D_f}} \end{aligned} \tag{A.5}$$

As in general $D_{min}/D_{max}<10^{-2}$ and $0<D_f<2$ in two dimension, Eq. (A.5) can be reduced as

$$Q = \frac{\sigma cos\theta}{8\mu\tau L_s}\frac{2-D_f}{3-D_f}\frac{A_f\phi D_{max}}{1-\left(\frac{D_{min}}{D_{max}}\right)^{2-D_f}} - \frac{A_f\rho g}{32\mu\tau}\frac{2-D_f}{4-D_f}\frac{\phi D_{max}^2}{1-\left(\frac{D_{min}}{D_{max}}\right)^{2-D_f}} \quad \text{(A.6)}$$

Dividing Eq. (A.6) by the ($A_f\phi\tau$) yields the average imbibition rate

$$v = \frac{\sigma cos\theta}{8\mu\tau^2 L_s}\frac{2-D_f}{3-D_f}\frac{D_{max}}{1-\left(\frac{D_{min}}{D_{max}}\right)^{2-D_f}} - \frac{\rho g}{32\mu\tau^2}\frac{2-D_f}{4-D_f}\frac{D_{max}^2}{1-\left(\frac{D_{min}}{D_{max}}\right)^{2-D_f}} \quad \text{(A.7)}$$

The mass increase (M) due to the imbibition action is given as

$$M = \rho A_f \phi L_0 \quad \text{(A.8)}$$

Differentiating Eq. (A.8) with respect to time and inserting Eq. (A.7) into it give

$$\frac{dM}{dt} = \frac{a}{M} - b \quad \text{(A.9)}$$

where

$$a = \frac{\sigma cos\theta(2-D_f)D_{max}(A_f * \phi * \rho)^2}{8\mu\tau^2(3-D_f)\left[1-\left(\frac{D_{min}}{D_{max}}\right)^{2-D_f}\right]} \quad \text{(A.10)}$$

$$b = \frac{A_f\rho^2 g(2-D_f)\phi D_{max}^2}{32\mu\tau^2(4-D_f)\left[1-\left(\frac{D_{min}}{D_{max}}\right)^{2-D_f}\right]} \quad \text{(A.11)}$$

Yu and Li (Yu and Li 2001) developed a relationship between the fractal dimension (D_f), porosity (ϕ) and D_{min}/D_{max}

$$D_f = 2 - \frac{ln\phi}{ln\frac{D_{min}}{D_{max}}} \quad \text{(A.12)}$$

Rearranging Eq. (A12) gives

$$\phi = \left(\frac{D_{min}}{D_{max}}\right)^{2-D_f} \quad \text{(A.13)}$$

If we followed the Eq. (A.12) deduced by Yu and Li (Yu and Li 2001), $\left(\frac{D_{min}}{D_{max}}\right)^{2-D_f}$ term in Eqs. (A.10) and (A.11) can be simply replaced by porosity (ϕ).

Cai et al. (Cai, Hu, et al. 2012) introduce the Lambert W function $W(x)$ defined by an inverse exponential function

$$x = W(x)e^{W(x)} \tag{A.14}$$

And the final full analytical expression for wetting phase spontaneous imbibition into porous media is obtained as:

$$M(t) = \frac{a}{b}\left\{1 + W\left(-e^{-1-\left(\frac{b^2}{a}\right)t}\right)\right\} \tag{A.15}$$

where

$$W(x) = \frac{2ex - 10.7036 + 7.56859\sqrt{2 + 2ex}}{12.7036 + 5.13501\sqrt{2 + 2ex}} \tag{A.16}$$

Appendix B. Derivation of Eq. (3.27) (Yu and Cheng 2002, Wu and Yu 2007, Cai, Yu, Zou, and Luo 2010, Cai and Yu 2010)

Yu and Cheng (2002) proposed a bi-dispersed model and calculated the maximum pore diameter Dmax based on an equilateral-triangle arrangement of circular particles

$$D_{max1} = \frac{D_s}{2}\sqrt{\frac{2\phi}{1-\phi}} \tag{B.1}$$

Wu and Yu (2007) calculated D_{max} based on a square arrangement of circular particles

$$D_{max2} = \frac{D_s}{2}\sqrt{\frac{\phi}{1-\phi}} + \sqrt{\frac{\pi}{4(1-\phi)}} - 1 \tag{B.2}$$

Cai and Yu (2010) took the average of two above equations as an approximation for D_{max}

$$D_{max} = \frac{D_S}{4}\left[\sqrt{\frac{2\phi}{1-\phi}} + \sqrt{\frac{\phi}{1-\phi}} + \sqrt{\frac{\pi}{4(1-\phi)}} - 1\right] \tag{B.3}$$